NTNU – Trondheim
Norwegian University of
Science and Technology

Power plant with CO$_2$ capture based on adsorption

Snorre Foss Westman

NTNU

Norwegian University
of Science and Technology

Department of Energy
and Process Engineering

EPT-M-2012-94

MASTER THESIS

for

Student Snorre Foss Westman

Spring 2012

Power plant with CO_2 capture based on adsorption

Kraftverk med CO_2-fangst basert på adsorpsjonsprosess

Background and objective

The main objective of this master thesis is to develop a process flowsheet model to study the performance of a coal fired power plant when integrated with a novel technology so-called Sorption Enhanced Water Gas Shift (SEWGS) for pre-combustion CO_2 capture. The SEWGS technology considered in this work is based on a Pressure Swing Adsorption (PSA) process which operates in a cyclic manner. In this process carbon dioxide is removed from a synthesis gas at elevated temperature by adsorption. Simultaneously, carbon monoxide is converted to carbon dioxide by the water-gas shift reaction. The periodic adsorption and desorption of carbon dioxide is induced by a pressure swing cycle, and the cyclic capacity can be amplified by purging with steam. The separation of CO_2 across a WGS reactor with sorbents eliminates the need for a separate downstream CO_2 control process. Moreover, it would result in a purified CO_2 stream at an appreciably higher temperature and pressure than obtained with existing capture processes, thus reducing the energy requirement for CO_2 compression. When it comes to an integration of a process island and power production island in an Integrated Gasification Combined Cycle (IGCC) incorporating SEWGS technology, it is greatly important to study the performance of the units operating within the process island and investigate how they impact the efficiency penalty and power production rate. Due to the chemical reactions take place in the SEWGS, it is one of the important components in the process island which can affect the performance and efficiency of the power production process. Therefore it was defined for this work to carry out a dynamic modeling and simulation of the cyclic operation of the PSA-based SEWGS to evaluate the behaviour of the system and its capabilities over the conventional WGS reactors.

The following tasks are to be considered:

1. Literature review
2. Dynamic simulation of the whole cyclic operation of the Sorption Enhanced Water Gas Shift (SEWGS) system as a Pressure Swing Adsorption process in the simulation software gPROMS, using a dynamic reactor model for the reaction/adsorption mode.

Within 14 days of receiving the written text on the master thesis, the candidate shall submit a research plan for his project to the department.

When the thesis is evaluated, emphasis is put on processing of the results, and that they are presented in tabular and/or graphic form in a clear manner, and that they are analyzed carefully.

The thesis should be formulated as a research report with summary both in English and Norwegian, conclusion, literature references, table of contents etc. During the preparation of the text, the candidate should make an effort to produce a well-structured and easily readable report. In order to ease the evaluation of the thesis, it is important that the cross-references are correct. In the making of the report, strong emphasis should be placed on both a thorough discussion of the results and an orderly presentation.

The candidate is requested to initiate and keep close contact with his/her academic supervisor(s) throughout the working period. The candidate must follow the rules and regulations of NTNU as well as passive directions given by the Department of Energy and Process Engineering.

Risk assessment of the candidate's work shall be carried out according to the department's procedures. The risk assessment must be documented and included as part of the final report. Events related to the candidate's work adversely affecting the health, safety or security, must be documented and included as part of the final report.
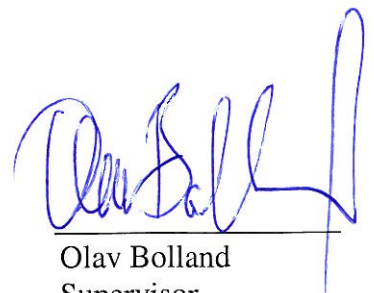
Pursuant to "Regulations concerning the supplementary provisions to the technology study program/Master of Science" at NTNU §20, the Department reserves the permission to utilize all the results and data for teaching and research purposes as well as in future publications.

The final report is to be submitted digitally in DAIM. An executive summary of the thesis including title, student's name, supervisor's name, year, department name, and NTNU's logo and name, shall be submitted to the department as a separate pdf file. Based on an agreement with the supervisor, the final report and other material and documents may be given to the supervisor in digital format.

Department of Energy and Process Engineering, 16. January 2012

Lars Erik Bakken
Coordinator

Olav Bolland
Supervisor

Co-Supervisor: Bita Najmi, NTNU

Preface

This master's thesis concludes my five years at Energy and Environmental Engineering at NTNU.

I would like to thank my main supervisor, Olav Bolland at NTNU and my co-supervisor, Bita Najmi at NTNU, for patience and significant amounts of help and guidance during the work process. Also, a thanks is directed to Hugo Jakobsen at the Department of Chemical Engineering at NTNU and Carlos Grande at SINTEF in Oslo, for significant help.

Trondheim, June 7, 2012

Snorre Foss Westman

Abstract

A dynamic one-dimensional homogeneous model for a packed bed sorption-enhanced water-gas shift (SEWGS) reactor has been developed, describing the non-isothermal, non-adiabatic and non-isobaric operation of this type of reactor. The model was developed to describe a SEWGS reactor designed to work under operating conditions and syngas feeds encountered in a coal-fed Integrated Gasification Combined Cycle power plant utilizing an oxygen-fed gasifier. Different from previous integration designs reported in literature, the feasibility of leaving out the conventional high-temperature water-gas shift (WGS) reactor upstream of the SEWGS reactor has been investigated. The reactor was assumed to be packed with a mixture of K_2CO_3-promoted hydrotalcite CO_2 adsorbent and commercial high-temperature FeCr-based water-gas shift catalyst pellets.

Utilizing the reactor model, a mathematical modelling framework for the operation of eight SEWGS reactors in a SEWGS cycle has been developed. This system model accounts for all the necessary interactions between the reactors during the SEWGS cycle, including the exchange of mass in the feed, rinse, equalization and repressurization steps. In contrast to available open literature, the mathematical framework describes in detail how the necessary switches in the boundary conditions for the reactors have been realized.

Simulations of several SEWGS cycles were carried out. The results were compared with experimental and modelling data from literature. Due to inconsistencies in the parameters and implementation of the model in the simulation software employed, results were in most aspects quantitatively not comparable to results from literature. However, the qualitative trends and physical mechanisms expected were observed and confirmed by the model. The temperatures in the reactors reached an unacceptable high level with respect to the tolerable operating conditions of the catalyst and adsorbent. It is planned to continue the work on the model, and implementing it within a full power plant model to investigate the effects of changes in the power production and thus the required amount of syngas to be treated.

Sammendrag

En dynamisk endimensjonal homogen modell for en adsorpsjons-forfremmet vann-gass skiftreaksjonsreaktor "sorption-enhanced water-gas shift" (SEWGS) har blitt utviklet, som beskriver den ikke-isoterme, ikke-adiabatiske og ikke-isobare driften av denne typen reaktor. Modellen ble utviklet for å beskrive en SEWGS-reaktor konstruert for å fungere under de driftsforhold og fødestrømmer av syntesegass som finnes i et kull-matet Integrated Gasification Combined Cycle kraftverk, som benytter en oksygen-matet gasifiseringsreaktor. Forskjellig fra tidligere integreringsdesign fra litteraturen, har muligheten for å utelate den konvensjonelle høytemperaturs vann-gass skiftreaktoren "water-gas shift" (WGS) oppstrøms for SEWGS-reaktoren, blitt undersøkt. Reaktoren ble antatt å være pakket med en blanding av en K_2CO_3-promotert hydrotalsitt CO_2 adsorbent og kommersiell høytemperaturs FeCr-basert WGS katalysator.

Med denne reaktormodellen som grunnlag, har et matematisk modelleringsrammeverk for driften av åtte SEWGS-reaktorer i en SEWGS syklus blitt utviklet. Denne systemmodellen tar høyde for alle nødvendige interaksjoner mellom reaktorene i løpet av SEWGS-syklusen, herunder utveksling av masse i matetrinnet, rensetrinnet, trinnene for trykkutjevning og trinnet for trykkøkning. I motsetning til tilgjengelig åpen litteratur, beskriver det matematiske rammeverket i detalj hvordan de nødvendige forandringene i grensebetingelsene for reaktorene har blitt gjennomført.

Simuleringer av flere SEWGS-sykluser ble gjennomført. Resultatene ble sammenlignet med eksperimentell data og modelleringsdata fra litteraturen. På grunn av uoverensstemmelser i parametere og implementering av modellen i det benyttede simuleringsprogrammet, var resultatene i de fleste aspekter kvantitativt ikke sammenlignbare med resultater fra litteraturen. Imidlertid ble de forventede kvalitative trender og fysiske mekanismer observert og bekreftet av modellen. Temperaturen i reaktorene nådde et uakseptabelt høyt nivå med hensyn til de tolerable driftsforhold for katalysatoren og adsorbenten. Det er planlagt å fortsette arbeidet med modellen, og implementere den i en modell for hele kraftverket for å undersøke effekten av endringer i kraftproduksjon og dermed den nødvendige mengden av syntesegass som skal behandles.

Contents

Nomenclature

Abbreviations

ASU	Air separation unit
ATR	Autothermal reforming
CFDM	Centered finite difference method
CL750	Commercial sodium oxides
DS	Double salt adsorbents
GT	Gas turbine
HRSG	Heat recovery steam generator
HTC	Hydrotalcite, $Mg_6Al_2(OH)_{16}[CO_3] \cdot 4(H_2O)$
IGCC	Integrated gasification combined cycle
IRCC	Integrated reforming combined cycle
K-HTC	K_2CO_3-promoted hydrotalcite
LDF	Linear driving force
LDH/Os	Layered double hydroxides/oxides
PbO	Lead oxide adsorbents
PDAE	Partial differential algebraic equation
PSA	Pressure-swing adsorption
SE-SMR	Sorption-enhanced steam-methane reforming
SEWGS	Sorption-enhanced water-gas shift
Syngas	Synthesis gas
TSA	Temperature-swing adsorption
VPSA	Vacuum pressure-swing adsorption
WGS	Water-gas shift

Greek symbols

β_1	Constant in Eq.(27)	(-)
ε_b	Void fraction of reactor bed (inter-particle gas volume/reactor volume)	
		(m^3 gas in bed/m^3 reactor)

XV

$\varepsilon_{p,ads}$	Adsorbent particle void fraction (intra-particle gas volume/particle volume)	
		(m^3 gas in particle/m^3 particle)
$\varepsilon_{p,cat}$	Catalyst particle void fraction (intra-particle gas volume/particle volume)	
		(m^3 gas in particle/m^3 particle)
ε_t	Total void fraction of reactor bed (total gas volume/reactor volume)	
		(m^3 gas/m^3 reactor)
η_{cap}	CO_2 capture ratio	(mol/mol)
η_i	Catalyst efficiency (including stoichiometric coefficient) for component i (-)	
$\eta_{Recovery}$	H_2 and CO recovery factor	(mol/mol)
Φ	Constant in Eq.(27)	(-)
γ	Constant in Eq.(27)	(-)
λ_s	Shape factor of the catalyst and adsorbent particles	(-)
μ	Gas-phase dynamic viscosity	(Pa · s)
$\rho_{b,ads}$	Adsorbent bulk density in reactor bed	(kg adsorbent/m^3 reactor)
$\rho_{b,cat}$	Catalyst bulk density in reactor bed	(kg catalyst/m^3 reactor)
$\rho_{p,ads}$	Adsorbent particle density	(kg adsorbent/m^3 adsorbent particle)
ρ_{gas}	Gas-phase density	(kg gas/m^3 gas)

Roman symbols

a	Langmuir isotherm parameter	(-)
a_{k_z}	Constant of the empirical correlation of the effective thermal conductivity (-)	
$\bar{c}$	Total gas-phase concentration	(mol gas/m^3 gas)
$\bar{c}_i$	Gas-phase concentration of component i in gas mixture	(mol i/m^3 gas)
$\bar{c}_{i,inlet,j}$	Gas-phase concentration of component i in gas mixture at reactor j inlet	
		(mol i/m^3 gas)
$\bar{c}_{i,outlet,j}$	Gas-phase concentration of component i in gas mixture at reactor j outlet	
		(mol i/m^3 gas)
$\bar{C}_{p,i}$	Gas-phase molar specific heat capacity of component i at constant pressure	
		(J/(mol i · K))
$\bar{C}_{p,gas}$	Gas-phase molar specific heat capacity at constant pressure (J/(mol gas · K))	

$C_{p,gas}$	Gas-phase mass specific heat capacity at constant pressure	(J/(kg gas · K))
$C_{p,ads}$	Adsorbent specific heat capacity at constant pressure	(J/(kg adsorbent · K))
$C_{p,cat}$	Catalyst specific heat capacity at constant pressure	(J/(kg catalyst · K))
D_{ax}	Axial dispersion coefficient	(m^2/s)
D_m	Molecular diffusion coefficient	(m^2/s)
d_p	Catalyst and adsorbent particle diameter	(m)
D_p	Effective pore diffusivity	(m^2/s)
d_t	Internal diameter of reactor	(m)
e	Emissivity of the solid particles	(-)
F_{press}	Pressure scale-up factor	(-)
$\bar{h}_i$	Enthalpy of component i at temperature T	(J/mol i)
$\bar{h}_{f,i}^{\circ}$	Enthalpy of formation of component i at standard state	(J/mol i)
ΔH_{298}	Heat of WGS reaction at 298 K	(J/mol)
$\Delta \bar{h}_{ads,\mathrm{CO_2}}$	Isoteric heat of adsorption of CO_2	(J/mol CO_2 adsorbed)
ΔH_R	Heat of additional surface chemical reaction	(J/mol)
h_{rs}	Solid-solid radiative heat transfer coefficient	(-)
h_{rv}	Void-void radiative heat transfer coefficient	(-)
K_C	Langmuir parameter K_C	(1/Pa)
K_C^0	Langmuir parameter K_C pre-exponential factor	(1/Pa)
k_g	Gas-phase thermal conductivity	(J/(m·K))
k_{LDF}	LDF mass transfer coefficient	(1/s)
K_R	Langmuir parameter K_R	(1/Pa$^{2.5}$)
K_R^0	Langmuir parameter K_R pre-exponential factor	(1/Pa$^{2.5}$)
k_s	Solid-phase thermal conductivity	(J/(m·K))
K_{WGS}	Equilibrium constant for WGS reaction	(-)
k_z	Effective axial, thermal conductivity	(W/(m · K)
L	Reactor length	(m)
m	Monolayer capacity for CO_2 chemisorption	(mol/kg)

M_i	Molar mass of component i	(kg i/mol i)
$moles_{in}$	Moles that has been sent into the SEWGS train system from time $t = 0$ to t	(mol)
$moles_{out}$	Moles that has gone out of the SEWGS train system from time $t = 0$ to t	(mol)
$moles_{reactors}$	Sum of moles in all reactors at time t	(mol)
$moles_{single\ reactor}$	Moles in single reactor at time t	(mol)
$moles_{system}$	Moles in SEWGS train system at time t	(mol)
N	Number of components i in the model	(-)
$\dot{n}$	Molar flow rate	(mol/s)
$\dot{n}_{inlet,j}$	Molar flow rate at reactor j inlet	(mol/s)
$\dot{n}_{outlet,j}$	Molar flow rate at reactor j outlet	(mol/s)
p	Total pressure	(Pa)
Δp	Valve pressure difference	(Pa)
$p_{inlet,j}$	Total pressure at reactor j inlet	(Pa)
$p_{outlet,j}$	Total pressure at reactor j outlet	(Pa)
p_i	Partial pressure of component i	(Pa)
p_{ref}	Pressure at standard reference state = 101325 Pa	(Pa)
Pr	Prandtl number	(-)
q_C	Heat of CO_2 chemisorption	(J/mol)
q_{CO_2}	Adsorbent loading of CO_2	(mol CO_2 adsorbed/kg adsorbent)
$q^*_{CO_2}$	Equilibrium adsorbent loading of CO_2	(mol CO_2 adsorbed/kg adsorbent)
r	Reaction rate of forward WGS reaction, i.e. conversion of CO	(mol/(kg catalyst $\cdot$ s))
$\bar{R}$	Universal gas constant = 8.314	(J/(mol $\cdot$ K))
Re_p	Reynolds number	(-)
S/CO	Steam-to-CO ratio	(mol H_2O/mol CO)
t	Time	(s)
T	Temperature	(K)

$T_{inlet,j}$	Temperature at reactor j inlet	(K)
$T_{outlet,j}$	Temperature at reactor j outlet	(K)
T_{ref}	Temperature at standard reference state = 298.15 K	(K)
T_{wall}	Temperature of reactor wall	(K)
u	Superficial gas velocity	(m/s)
U	Overall bed-to-wall heat transfer coefficient	(W/(m$^2 \cdot$ K))
$u_{inlet,j}$	Superficial gas velocity at reactor j inlet	(m/s)
$u_{outlet,j}$	Superficial gas velocity at reactor j outlet	(m/s)
x_{valve}	Valve opening (stem position)	(-)
y_i	Gas-phase gas molar fraction of component i	(mol i/mol gas)
$y_{i,inlet,j}$	Gas-phase gas molar fraction of component i at reactor j inlet (mol i/mol gas)	
$y_{i,outlet,j}$	Gas-phase gas molar fraction of component i at reactor j outlet (mol i/mol gas)	
z	Axial position in reactor	(m)

1. Introduction

The operation of power plants using fossil fuels as feedstock for combustion results in production of CO_2 in the combustion flue gas. The influence of the contribution of CO_2 emissions to climate change has been thoroughly established. As a consequence, the emission of CO_2 to the atmosphere will have to be paid for through the CO_2 emission quota system. Therefore, it is desirable to in some way capture the CO_2 and transport and store this, to not have to pay for the emission quotas.

In principle, there are three different routes for CO_2 capture: pre-combustion capture, post-combustion capture and oxy-combustion. These can be illustrated as in Figure 1. In post-combustion capture, CO_2 is removed from combustion flue gas, which might come from a power plant, or from the off-gas from industrial processes such as the production of cement. Different methods for post-combustion capture have been investigated, and some of the methods, such as the amine-absorption setups have been used for decades for CO_2 removal with the intention of for example enhanced oil recovery purposes [8].
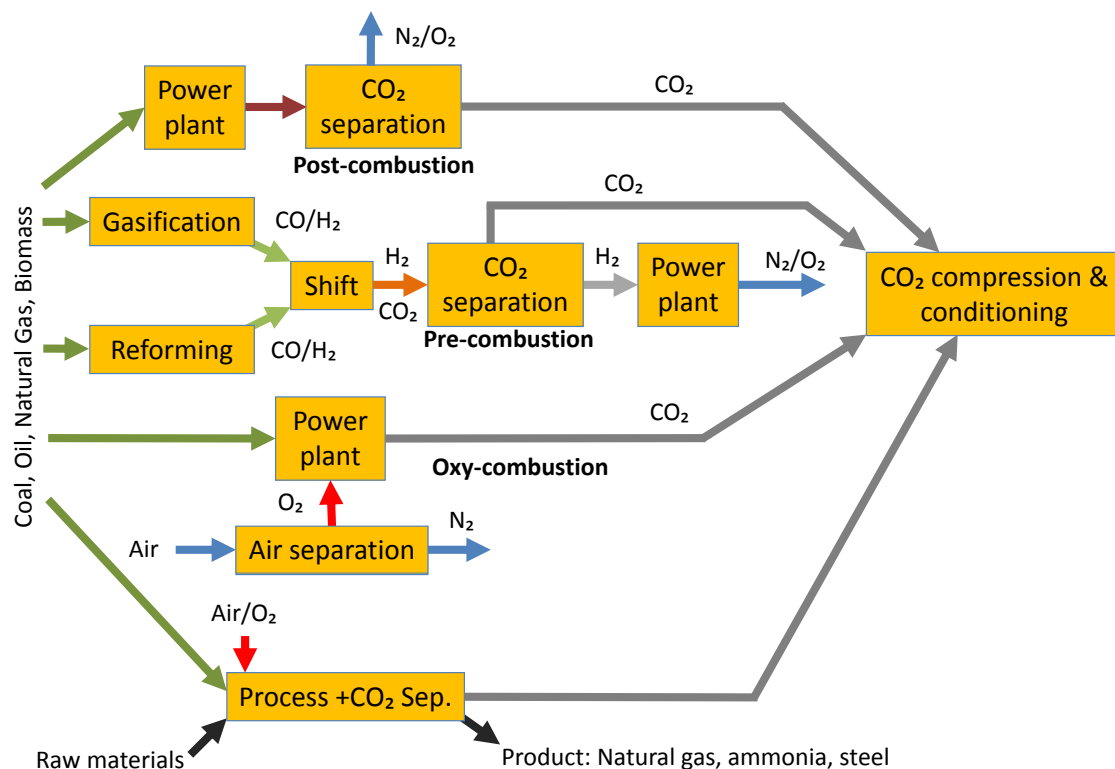

Figure 1: Three different routes for CO_2 capture [6]

In oxy-combustion, another approach to CO_2 removal is made. In ordinary combustion of fossil fuels, air is used to provide oxygen for the combustion. As air contains mostly nitrogen, the combustion flue gas will contain CO_2, but also significant amounts of N_2. In

the perspective of avoiding CO_2 emissions, this flue gas cannot be sent directly to transport and storage as the storage volume required would be significantly larger than if only the CO_2 was to be stored. This is the motivation for oxy-combustion, which avoids the dilution of the flue gas with nitrogen by using almost pure oxygen O_2 in the combustion. The flue gas will then contain mostly CO_2. The oxygen can for example be provided by an air separation unit (ASU).
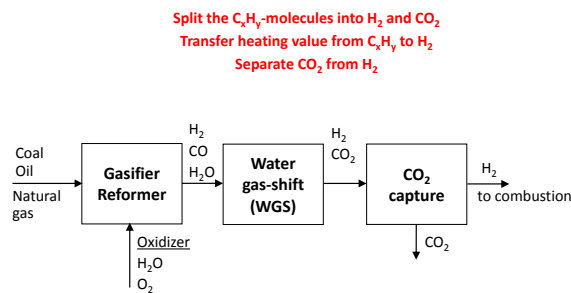
Figure 2: Conceptual flow sheet for pre-combustion CO_2 capture [6]

One novel route for power production from fossil fuels with low to no CO_2 emission is to remove the CO_2 before the combustion takes place. This family of CO_2 capture technologies is called pre-combustion capture. The basic stages employed in pre-combustion CO_2 capture can be illustrated by Figure 2. Instead of combusting hydrocarbons C_nH_m, forming CO_2 in the flue gas, the fuel is converted into a gas mixture consisting of mainly hydrogen H_2 and CO_2. The CO_2 is then removed from the gas mixture, and the H_2 can be combusted in for example a gas turbine. As a result, only water vapour and air are being emitted to the atmosphere as the combustion flue gas [6]. However, there are several configurations of these three basic steps. Several such configurations are currently under development.

Methods using the basic configuration in Figure 2 employs separate downstream reactors involving for example absorption processes or membranes to remove CO_2 before the gas is sent to combustion. Other configurations are mostly based on the integration of CO_2 removal with existing unit operations in the power plant, such as sorption-enhanced or membrane-enhanced reforming of natural gas or coal, and sorption-enhanced or membrane-enhanced water-gas shift reactors. However, these pre-combustion methods have not yet reached the advanced stages of post-combustion capture methods, such as the previously mentioned amine-absorption setups.
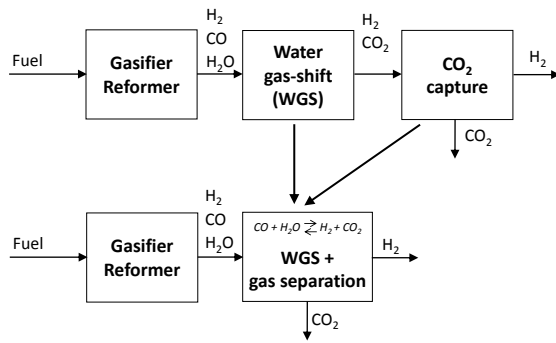
Figure 3: Sorption-enhanced water-gas shift reaction [6]

One such integrated configuration is illustrated in Figure 3. This arrangement is called sorption-enhanced water-gas shift (SEWGS), and combines the step of the water-gas shift (WGS) reaction with the step of CO_2 capture on a solid adsorbent material.

There are several types of feedstock fuel which can be used as input to a power plant with this type of pre-combustion CO_2 capture. However, the focus of the present work will be on the power plant system called integrated gasification combined cycle (IGCC) with the integrated pre-combustion CO_2 capture method SEWGS. The power plant is assumed to use coal as feedstock. The power plant can conceptually be illustrated with the flow sheet in Figure 4, where a distinction has been made between the process island and the power island. In the process island, all unit operations required to process the fuel are included. Please refer to Figure 5 for a flow sheet of the process island. The power island consists of the power-generating units, such as the gas and steam turbines and the heat recovery steam generator (HRSG).
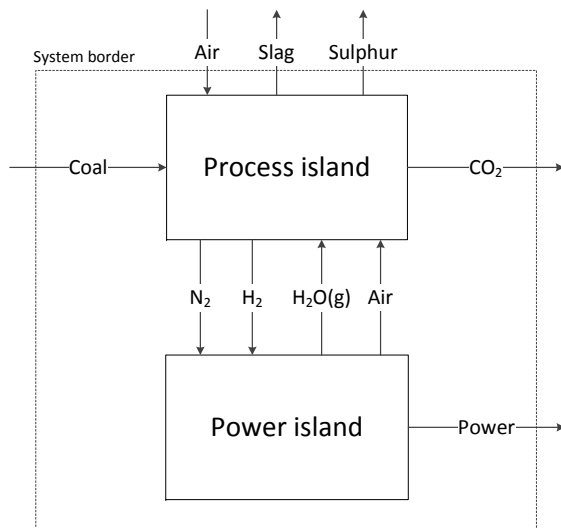
Figure 4: IGCC power plant conceptual flow sheet

The envisioned method starts with the power plant receiving coal, which is gasified through a gasification reactor. Gasification is a partial oxidation of a solid fuel, and the purpose of the gasification is to convert the solid fuel, coal, into a gas mixture consisting mainly of carbon monoxide CO and hydrogen H_2, called syngas (synthesis gas). The gas mixture usually consist of other compounds, the main ones being H_2O, CO_2 and small amounts of H_2S and COS. This gasification can either be carried out by using air, consisting mainly of nitrogen N_2 and oxygen O_2, or by using almost pure oxygen O_2 from an ASU [6].

Several reactions take place during gasification, but the main reactions are [6]

$$C + H_2O(g) \rightleftharpoons CO + H_2 \tag{1}$$
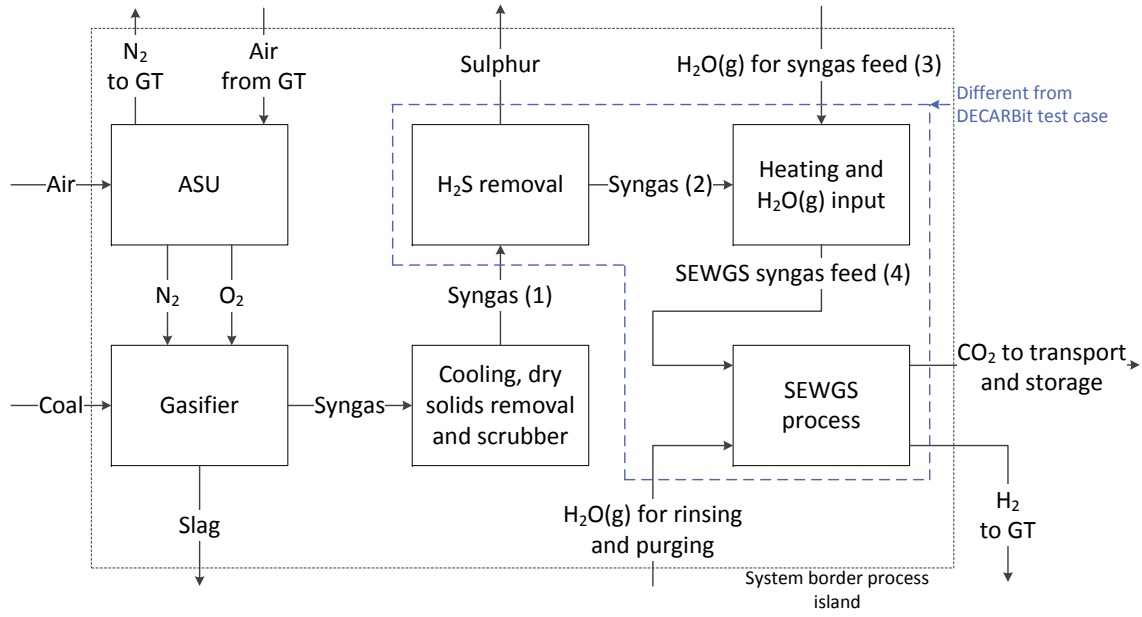
Figure 5: Process island conceptual flow sheet. Based on [16]

$$C + \frac{1}{2}O_2 \rightleftharpoons CO \tag{2}$$

Since the fuel contains hydrogen, the total reaction can be formulated as [6]

$$C_nH_m + \frac{n}{2}O_2 \rightleftharpoons nCO_2 + \frac{m}{2}H_2 \tag{3}$$
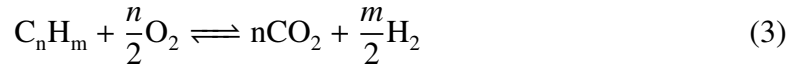
Through the partial oxidation in the gasifier, the energy contained in the coal is converted into heat and a gas mixture, syngas, which can be further oxidized in combustion reactions.

From this point on, the SEWGS concept illustrated in Figure 3 differs from the conventional IGCC power plants with downstream CO_2 capture. In an IGCC power plant with downstream CO_2 capture as shown in Figure 2, the syngas leaving the gasifier is typically cooled and mixed with high-pressure steam. After this, the syngas mixture is typically sent to a high-temperature water-gas shift reactor to convert most of the CO into CO_2 through the water-gas shift (WGS) reaction, thus producing more H_2 [45, 23, 6].

The exothermic WGS reaction [6, 13]

$$CO + H_2O \rightleftharpoons CO_2 + H_2 \qquad \Delta H_{298} = -41 \text{ kJ/mol} \tag{4}$$
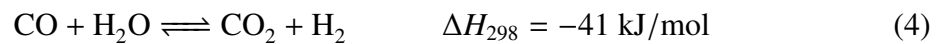
After the high-temperature shift reactor the syngas is typically sent to a low-temperature shift reactor to convert even more CO. However, complete conversion of CO is not possible due to the thermodynamic equilibrium between the reactants and products in the WGS reaction [20].

A possible composition and state of IGCC-produced syngas after leaving the low-temperature shift reactor is given as stream ref1 in Table 2 [16]. It can be seen that there is still a significant amount of carbon monoxide CO in the gas, 1.22 mol-%.

If one were to remove CO_2 from the gas during the WGS reaction, one would shift the equilibrium of the WGS reaction towards the products, and thus be able to approach almost complete conversion of CO [20, 23].

This can be seen from the equilibrium constant for the WGS reaction [1, 40]

$$K_{WGS} = \exp\left(\frac{4577.8}{T} - 4.33\right) = \frac{p_{CO_2}p_{H_2}}{p_{CO}p_{H_2O}} \tag{5}$$

At a given temperature T, if one were to decrease the partial pressure of CO_2, then either the partial pressure of H_2 must increase, the partial pressure of CO must decrease or the partial pressure of H_2O must decrease.

This is the motivation for the use of the sorption-enhanced water-gas shift reactor. A SEWGS reactor will combine the function of the WGS reactors with the process of removing CO_2 from the gas mixture. The SEWGS reactor consists of a packed bed of a suitable adsorbent material and a high-temperature WGS catalyst material. The adsorbent in this case is a solid material onto which CO_2 can be adsorbed, that is, removed from the gas-phase and physically or chemically bonded to the adsorbent material. The function of the reactor is to adsorb the CO_2 onto the adsorbent and thus shift the equilibrium of the WGS reaction towards the product side, such that the CO is almost completely converted into CO_2 and H_2 [45]. By doing this, the WGS reaction is "enhanced" by the adsorption of CO_2.

As the syngas passes through the SEWGS reactor, the adsorbent in the SEWGS reactor will adsorb the CO_2 and the catalyst will catalyse the WGS reaction such that the effluent gas exiting the reactor will consist mainly of H_2 and steam H_2O. This will continue until the reactor column reaches breakthrough, which is the point when the adsorbent are not able to adsorb enough CO_2 per time compared to the inlet feed flow rate, such that the effluent gas exiting the reactor contains CO_2 above a desired level. This period of time when the reactor is receiving feed syngas is usually called the feed step of the reactor cycle.

The effluent gas mixture can be diluted with nitrogen N_2 from the ASU and sent to a gas turbine for combustion and power production, with the main combustion reaction being

$$H_2 + \frac{1}{2}O_2 \longrightarrow H_2O \tag{6}$$

At the point of break-through, this SEWGS reactor cannot be used further for CO_2 removal until regeneration has taken place, and the syngas must be redirected to another SEWGS

reactor [23].

Regeneration is the process of desorbing the CO_2 from the adsorbent and removing the CO_2 from the reactor. The equilibrium adsorption capacity of the adsorbent is a function of temperature and pressure. If the temperature is increased, the equilibrium adsorption capacity decreases, and the CO_2 will be desorbed. Also, if the pressure is decreased, the equilibrium adsorption capacity decreases, giving the same result. The regeneration can therefore in theory be carried out in two ways. Either by increasing the temperature of the reactor, called temperature-swing adsorption (TSA), or by decreasing the pressure in the reactor, called pressure-swing adsorption (PSA). The actual regeneration sequence of most SEWGS setups is a series of steps that are based the principles of PSA.

The operation of a single SEWGS reactor is in effect a batch unit operation. However, by using several SEWGS reactors operating in parallel, one or several being fed syngas and capturing CO_2 while the other CO_2-saturated reactors are being regenerated, the total system of SEWGS reactors are able to operate in a semi-continuous process. Please refer to Figure 6, which shows a simplified flow diagram. This means that, in effect, the effluent gas exiting the system of SEWGS reactors contains close to no CO_2, only combustible H_2, and H_2O and other residual components. This is continuously fed to the gas turbines in the power island. The operation of this system of SEWGS reactors, called the SEWGS cycle, can be illustrated as in Figure 7, where 8 reactors are operating in parallel.
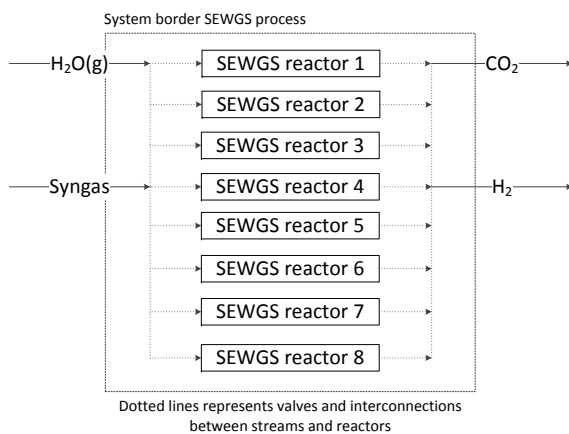
Figure 6: SEWGS process conceptual flow sheet, based on Figure 1 in [2]

There are several possibilities when choosing which type of PSA cycle to utilize for a given purpose. A PSA cycle generally consists of a feed step, and an unknown number and type of steps required to regenerate the reactor, making it ready for starting the cycle once more. In the work by Wright et al. [45], the authors tries to identify the number of reactors required and an appropriate cycle consisting of a sequence of steps for a SEWGS system. They propose a cycle consisting of the steps shown in Figure 7, utilizing 8 reactors. They claim that this cycle and reactor configuration consists of the basic steps which can be expected in a commercial design of this type of process. The SEWGS cycle in Figure 7 is one of the possible PSA cycles that could be utilized to achieve the desired operation of the system of reactors. Within the available literature on the SEWGS process and the cycles employed, this specific cycle is considered the one with best potential, although improvements could possibly be made [45, 44, 2].

Pressure (bar)

26.8900
20.4430
13.9950
7.5475
1.1000

H$_2$-rich product

Rinse H$_2$O

Purge H$_2$O

| F | R | Eq1 | Eq2 | Eq3 | D | P | REq3 | REq2 | REq1 | RP |

Syngas feed

CO$_2$ product

System state	1	2	1	2	1	2	1	2	1	2	1	2	1	2	1	2
Cycle state	1	2	3	4	5	6	7	8	9	10	11	12	13	14	15	16
SEWGS reactor 1	F				R		Eq1	Eq2	Eq3	D	P		REq3	REq2	REq1	RP
SEWGS reactor 2	REq1	RP	F				R		Eq1	Eq2	Eq3	D	P		REq3	REq2
SEWGS reactor 3	REq3	REq2	REq1	RP	F				R		Eq1	Eq2	Eq3	D	P	
SEWGS reactor 4	P		REq3	REq2	REq1	RP	F				R		Eq1	Eq2	Eq3	D
SEWGS reactor 5	Eq3	D	P		REq3	REq2	REq1	RP	F				R		Eq1	Eq2
SEWGS reactor 6	Eq1	Eq2	Eq3	D	P		REq3	REq2	REq1	RP	F				R	
SEWGS reactor 7	R		Eq1	Eq2	Eq3	D	P		REq3	REq2	REq1	RP	F			
SEWGS reactor 8	F		R		Eq1	Eq2	Eq3	D	P		REq3	REq2	REq1	RP	F	

Figure 7: SEWGS cycle operation [45, 29]

In this cycle, the following regeneration sequence is carried out after the feed step is completed (step F in Figure 7): The regenerat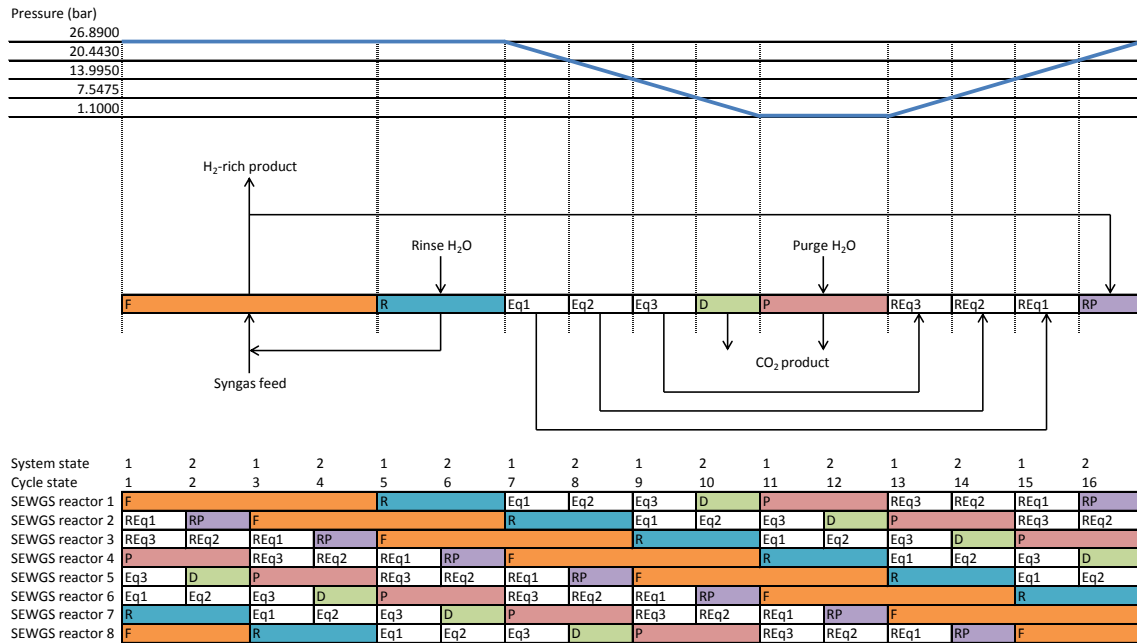ion sequence starts with a rinse step (step R), where some of the residual H$_2$ is removed by passing high-pressure steam H$_2$O countercurrently through the reactor, and this gas mixture is mixed into the feed to another reactor, to avoid the loss of H$_2$ [45]. According to Wright et al. [45], the amount of steam used here should be minimized, as this steam is taken from the power island, thus reducing the power produced in the steam turbine, and lowering the overall efficiency of the plant.

The desorption of CO$_2$ is carried out by lowering the pressure in the reactor down to atmospheric pressure in a series of steps called equalizations (steps Eq1, Eq2, Eq3). The reactor is connected to another reactor whose pressure are to be increased after CO$_2$ has been removed (steps REq3, REq2, REq1). The purpose of this is to lower the energy use related to increasing the pressure in the reactor [45]. During the equalization steps, most of the remaining H$_2$ in the column will be transferred to the connected columns whose pressure are to be increased.

Then follows a final depressurization (step D) to approximately atmospheric pressure, 1.1 bar, and low-pressure steam is passed through the reactor to desorb CO$_2$ and regenerate the adsorbent (purge step P) [45, 44]. Water is then removed from the gas mixture, and the resulting CO$_2$-rich gas can then be sent to conditioning, followed by transport and storage [44].

After this, the reactor is repressurized (steps REq3, REq2, REq1) in equalizations with other reactors which are to be depressurized [45].

Finally, some of the effluent product gas from other reactors, which contains close to no CO_2, are used to bring the reactor up to pressure equal to that of the syngas. This is the final repressurization step (RP) [45].

According to Wright et al. [45], this type of cycle probably can be improved with respect to steam consumption. The steam consumption is the main reason for increased energy use in an IGCC power plant with an integrated SEWGS reactor system for syngas treatment and CO_2 capture, compared to that of an IGCC plant without CO_2 capture. The CAESAR project are investigating the feasibility of SEWGS integration in IGCC plants, and have determined that the steam consumption for the rinse and purge steps should not exceed 2 moles of steam per mole of carbon in the feed syngas, to be able to compete with other technologies for pre-combustion CO_2 capture. In their work from 2011, they determine that this is possible [45]. Their work also suggests that the syngas feed pressure should be in the range 20-30 bar to minimize steam consumption.

To summarize, there are several advantages by using a system of SEWGS reactors instead of the conventional WGS reactors:

- A system of SEWGS reactors can be used instead of two WGS reactors with a downstream reactor for CO_2 capture. This could lower the capital costs for reactor equipment.

- The SEWGS reactor can operate at higher temperatures than the low-temperature WGS reactor. This is an advantage as the effluent gas is to be sent to combustion.

- The SEWGS reactor can operate at a lower steam to carbon ratio than the WGS reactor. This is an advantage with respect to steam consumption, which lowers the power plant overall efficiency.

- The SEWGS reactor is able to overcome the thermodynamic limitations of the WGS reaction, leading to almost complete conversion of CO.

1.1. Objectives and novel contributions

The objective of this thesis is twofold. First, a model for a SEWGS reactor integrated in an IGCC plant developed in the project thesis and the subsequent modifications to this model, is to be presented. Second, a mathematical framework and operating schedule for the simulation of a system of 8 SEWGS reactors is to be developed using methods and parameters obtained from literature and the modified reactor model as a basis. This mathematical framework is to be implemented in the process modelling software gPROMS from Process Systems Enterprise Ltd. The operation and performance of the SEWGS system is to be simulated using constant feed syngas flow rates. The SEWGS cycle utilized is the setup with 8 reactors and necessary cycle steps presented in Section 1.

In later work, the SEWGS system model developed in the present work shall be used to investigate the effects of changes in time of the flow rate of feed syngas. This is a very relevant aspect to evaluate, as the SEWGS system should be integrated in a IGCC power plant, where changes in power demand and thus changes in the amount of feed syngas which needs to be treated in the SEWGS system, is something that should be expected. The chosen method of modelling the system should therefore be able to take into account these aspects. Integrated in an IGCC power plant, the SEWGS system should treat syngas and deliver a gas mixture containing mostly H_2, steam H_2O, N_2, with close to no CO_2 and CO. In addition, the SEWGS system should be able to deliver this gas mixture at a close to constant flow rate, and even more importantly, close to constant composition. The reason for these latter two requirements is that the gas mixture delivered from the SEWGS system is to be sent to the gas turbines in the power island, which as of today cannot handle larger variations in feed gas heating value than ± 5 % [7].

The SEWGS reactor model utilized is a dynamic one-dimensional homogeneous model for a packed bed sorption-enhanced water-gas shift reactor, which was developed in the project thesis. This model is able to simulate the non-isothermal, non-adiabatic and non-isobaric operation of such a reactor for both cocurrent and countercurrent flow. Similar models for SEWGS reactors have been developed or are under development [45, 44]. However, no complete description of such a model has been found in the open literature available.

A modelling framework for the operation of a system of SEWGS reactors in the cycle utilized in the present work or similar cycles has not been found in open literature. There are however, several modelling frameworks for other types of PSA systems to be found in the literature. An example of this is the work by Nikolic et al. [31], where a generic modelling framework for a PSA system is presented. The authors present a detailed description of the system of reactors how the necessary interconnections are realized. However, during the different steps of the cycle a reactor in the system undergoes, it is from a modelling perspective, necessary to change the boundary conditions for the reactor. The method of carrying out these switches in boundary conditions is not described in the work by Nikolic et al. [31], and it has not possible to obtain this from the open literature available. Therefore, a novel methodology for realizing the switches in the boundary conditions has been developed in the present work.

1.2. Selection of adsorbent and catalyst

There are several possible combinations of adsorbent and catalyst that could be utilized in a SEWGS reactor. The choice of adsorbent for the adsorption of CO_2 and catalyst for the WGS reaction is important for the performance of the reactor.

Concerning the choice of adsorbent, the literature suggests many options. Several screening studies have been performed to compare the suitability of different adsorbents for the use in SEWGS processes.

In 2005, Allam et al. [2] conducted a screening study to identify suitable adsorbents for use in SEWGS in a integrated reforming combined cycle (IRCC) power plant utilizing either air-fed or O_2-fed autothermal reforming (ATR) of natural gas. They required that the adsorbent should be able to effectively adsorb and desorb CO_2 in PSA cycles between approximately 30 and 1.5 bar within the temperature range 400 to 500 °C. The materials evaluated were commercial sodium oxides (CL750), K_2CO_3-promoted hydrotalcites (K-HTCs), lead oxide adsorbents (PbO), and double salt adsorbents (DS) [2]. They conclude that the lead oxide have low adsorption capacity at high temperatures. The sodium oxide tested showed reasonable capacity at cycle time of 120 minutes at 400 °C. Significant effort was made to develop supported double salts. The adsorption capacities of these materials were found to be significantly lower than for K-HTC. The conclusion of this screening study was that K-HTC was the best suited material with respect to their requirements. Reported adsorption capacity for the K-HTC was 1.6 mol CO_2/kg adsorbent at 400 to 450 °C with 5 minutes cycle time. By doubling the cycle time, the capacity is also approximately doubled.

In a more recent screening study from 2009 by Singh et al. [38], the objective was to identify high-temperature adsorbents suitable for pre-combustion CO_2 capture employed in IGCC plants. Materials evaluated were zeolites (NaX, calcium chabazite), commercially available hydrotalcite, layered double hydroxides/oxides (LDH/Os), and magnesium double salts [38].

The authors state that, in the case of integrating a SEWGS unit in an IGCC plant, one wants to keep the temperature of the gas exiting the SEWGS reactor which are to be sent to a gas turbine for combustion as high as possible. This limits the choice of adsorbent to the ones which can operate at high temperature [38]. However, the WGS reaction conversion of CO into CO_2 is not favoured at high temperatures, and the reaction is thermodynamically limited at lower temperatures [41]. According to Stevens Jr. et al. [41], a suitable adsorbent for the SEWGS reactor must be able to operate in the temperature range of the WGS reaction, 200-400 °C. Specific to the integration of this reactor in an IGCC plant, Singh et al. [38] states that this temperature range should ideally be 250-450 °C. This implies that a trade-off will have to be made between the need for lower temperatures for the WGS reaction and the need for higher temperatures of the effluent gas exiting the reactor.

In addition to this temperature requirement, Singh et al. [38] proposes among others the following requirements for an adsorbent which are to be used in a SEWGS reactor within

a IGCC plant: high selectivity for CO_2, high adsorption capacity, sufficiently good adsorption and desorption kinetics, the regeneration of the adsorbent should be possible to perform in appropriate temperature and pressure levels, the adsorbent should be able to be used for a sufficient amount of adsorption/regeneration cycles without the need to be replaced, adequate mechanical strength for durability and ability to be formed into pellets, should be able to tolerate impurities in the gas, cause a low pressure drop and be able to be formed into pellets [38].

Singh et al. [38] proposes the following three candidates as adsorbents to be used in integration with an IGCC plant [38]

- Zeolite 13X

- K-promoted hydrotalcites

- Double salt adsorbents

Zeolite 13X can be used for adsorption in temperatures up to 200 °C. While this is not ideal, it is possible to use this adsorbent in an SEWGS reactor in an IGCC plant [38]. At temperatures above 200 °C, the adsorption capacity of zeolites are very low [39].

Hydrotalcites can be used effectively at a temperature of 350 °C in the presence of water [38]. This is appropriate as the WGS reaction requires water vapour to be present. Singh et al. [38] points out that the presence of H_2S might pose a problem, so this suggests that the removal of H_2S before a SEWGS reactor using this type of adsorbent is a proper choice. Wright et al. [45] also points out that H_2S in syngas produced from coal could lower the adsorbent stability and long-term capacity for CO_2.

According to Singh et al. [38], double salt adsorbents are very promising. However, the effects of water present are not yet fully understood [38]. Also, an appropriate method for producing pellets which can be used in a packed bed reactor has not been found yet [34]. Due to the uncertainty in the possible detrimental effect of water present and the problems with producing pellets, it is chosen in this work to not consider double salts further as a adsorbent candidate. This is because one of the objectives of this thesis is to model the combination of the WGS reaction and the adsorption reaction in one single reactor vessel, the SEWGS reactor, where water present is a prerequisite and the adsorbent should able to be formed to pellets.

In the work of Stevens Jr. et al. [41] from 2010, a novel adsorbent for use in SEWGS reactors in IGCC plants is presented. This adsorbent, NaOH-promoted CaO, is capable of CO_2 capture at temperatures between 300 and 600 °C and pressures between 1 and 11.2 atm. These operating conditions are suitable for integration with the WGS reaction in a SEWGS reactor. CaO adsorbents are a common choice for CO_2 capture, but require high temperatures to be regenerated through TSA. By promoting the CaO with NaOH, the

regeneration temperature is significantly lowered, to 700 °C [39]. In addition, the adsorption capacity is increased. It should be noted that conventional calcium oxide adsorbents have very high CO_2 capacity compared to K-HTCs [34, 8]. This type of calcium oxide is therefore a promising adsorbent candidate for the use in SEWGS reactors.

According to a comprehensive review of adsorbents for CO_2 capture by Choi et al. [8] from 2009, "it is well-established that calcium oxide-based adsorbents suffer from a rapid degradation of CO_2 capture capability during the repetition of carbonation/calcination cycles". After several cycles, the adsorbent capacity can stabilize at as low as 25 % of the initial capacity [8]. With respect to regenerability and durability, K-HTCs perform better than conventional calcium oxides CaO. The adsorption capacity of K-HTCs are reported to decrease by about 0.1 mol CO_2/kg adsorbent during the first operational cycles, thereafter stabilizing [8].

The NaOH-promoted CaO adsorbent presented by Stevens Jr. et al. [41] is under development, and according to the authors the technical challenges related to their adsorbent are related to adsorbent reactivity and durability, and lowering the degradation of the adsorbent [41]. The high temperatures associated with regeneration of CaO-based adsorbents could pose a problem with respect to the reactor vessel, where heat-resistant alloys could be required [34].

Hydrotalcites (HTC) have been studied intensively in the literature. HTC is a chemical compound which when heated, decomposes into mixed metal oxides. It is common to impregnate the HTC with K_2CO_3, resulting in what is called potassium-promoted HTC, or K-HTC. This significantly enhances the adsorption capacity [2]. Compared to other possible adsorbents HTC have poor adsorption capacity of CO_2, good stability and poor adsorption kinetics [34]. Although the capacity and kinetics of K-HTC are poor, they have been found to be suitable for adsorption of CO_2 at high temperatures such as 400 °C, and especially suitable for the use in SEWGS reactors [9, 23, 2]. According, to Choi et al. [8], K-HTC adsorbents can be used in temperatures up around 800 K. According to Reijers et al. [34], the presence of water is contributing to the adsorption process for K-HTCs [34, 8]. This is positive for the use in a SEWGS reactor, as the presence of water is required for the WGS reaction.

However, Singh et al. [38] states that reduction in adsorption capacity over several cycles is a problem. Also, according to the authors, there has been significant debate about whether or not the adsorption kinetics of K-HTC are as good as required [38, 25].

Irrespective of this, there is significant work being done on investigating the suitability and performance of SEWGS reactors using K-HTC as an adsorbent in IGCC plants. The CAESAR project is putting a lot of effort into this. A experimental and modelling study from 2011 by Wright et al. [45] has been carried out utilizing an improved type of K-HTC,

which concludes that the use of this type of K-HTC is promising in a SEWGS reactor in a IGCC plant [45, 43, 5].

The adsorbent capacity of this material is reported to be 27 % higher than a reference sorbent [45]. The reference sorbent is a K_2CO_3-promoted hydrotalcite-based material, designated as PURALOX MG70 [42]. Also, the mechanical strength of this material is significantly higher than for the reference material [45].

The CO_2 capacity for the adsorbent chosen for a SEWGS reactor in an IGCC plant is something that should be considered thoroughly. One of the problems when removing CO_2 from syngas derived from coal compared to that from natural gas, is that the ratio of CO_2 to H_2 in the syngas will be approximately doubled. This implies that about twice as much adsorbent is needed to remove the CO_2 per amount of H_2 delivered, leading to significantly higher capital costs for reactors [45]. According to Wright et al. [45], this increase in adsorbent required is usually done by doubling the number of reactors compared to treating syngas made from natural gas. The authors also claim that, instead of increasing the amount of adsorbent, it is possible to reduce the cycle time.

The screening studies show a tendency for choosing K-HTC as the most suited adsorbent for SEWGS in IGCC plants. The calcium oxide-based adsorbents have very high adsorption capacity compared to K-HTCs, and are very promising. However, problems with the durability of these adsorbents are still under research. As the objective of this work is to develop a model of a SEWGS reactor designed to be integrated in an IGCC power plant based on available models and relations from literature, K-HTC is chosen as the adsorbent used in the SEWGS reactor.

In conventional IGCC setups the syngas from the gasifier usually contains high levels of H_2S. The WGS reaction could then be carried out in reactors designed to handle syngas with high H_2S concentration, called sour shift. The H_2S could then be removed from the shifted syngas in an absorber column. Another type of design is to first remove the H_2S from the syngas from the gasifier, then carry out the WGS reaction in reactors designed to handle syngas with very low H_2S concentration, called sweet shift. These two setups are illustrated in Figure 8. Concerning the WGS reactors, the main difference between these two setups is the type of catalysts used in the reactors [6].

Pre-combustion – fuel dependence for configuration
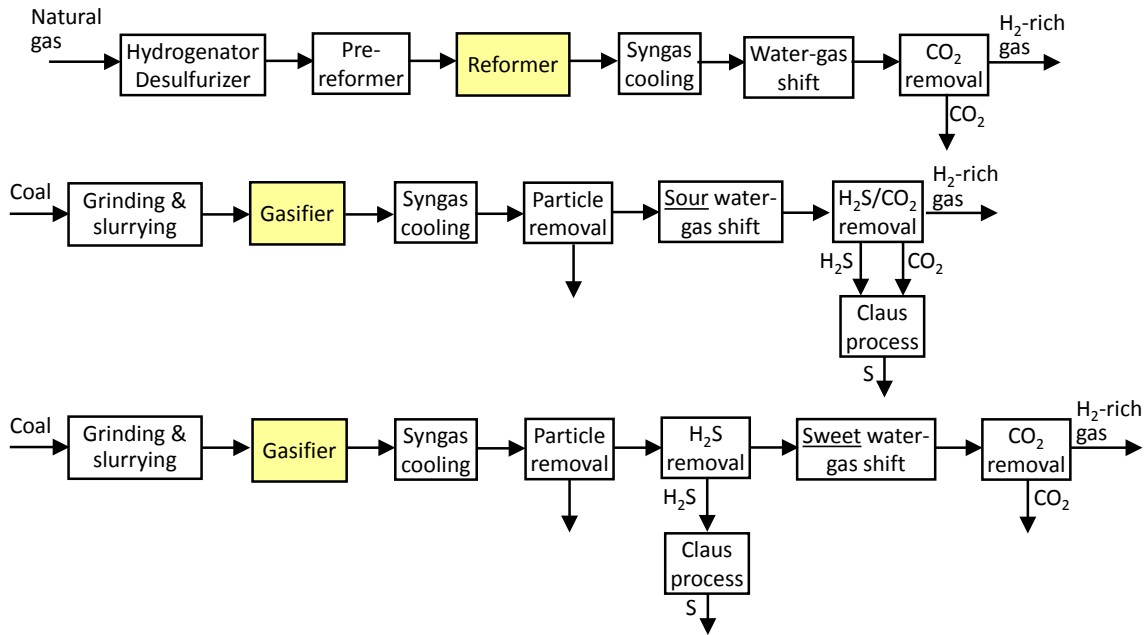
Figure 8: H_2S removal configurations [6]

The use of K-HTC requires that H_2S concentrations in the feed syngas are very low. With low concentration of H_2S, it is possible to use a conventional sweet-shift high temperature shift catalyst, based on the active component Fe_3O_4 with Cr_2O_3 as a stabilizer [6]. This will later be referred to as the FeCr-based catalyst. According to Bolland [6], this type of catalyst can operate in the temperature range 350-500 °C. This is in accordance with the expected temperature of the gas entering the SEWGS reactor, see the discussion in Section 1.3 and stream 4 in table 2.

The setup of K-HTC and a commercial high-temperature FeCr-based shift catalyst for SEWGS reactors designed to be integrated in natural gas IRCC plants have been extensively applied in literature. In a modelling, experimental and techno-economic integration study by Allam et al. [2], a study of SEWGS integration in IRCC plants were conducted, using this adsorbent and catalyst setup. The same applies to an experimental study by Van Selow et al. [42]. However, few studies have been conducted for this type of SEWGS reactor setup integrated in coal-fed IGCC plants. The only ongoing modelling and experimental projects found is the works by Wright et al. [45] and Wright et al. [44], within the CAESAR project. This is the motivation for the present work.

1.3. Defining the SEWGS system and its integration in the IGCC power plant

The SEWGS system should be integrated in an IGCC power plant. The power plant layout is based on the assumptions and test case IGCC plant setup with CO_2 capture employed in the DECARBit report by Franco et al. [16], with several modifications. The DECARBit test case IGCC plant with CO_2 capture delivers a net electric power output of 352.74 MW at a net electric efficiency of 36.66 %. The DECARBit test case IGCC plant without CO_2 capture delivers in comparison a net electric power output of 391.45 MW at a net electric efficiency of 46.88 % [16].

The feedstock of the power plant is assumed to be bituminous Douglas Premium coal, with the composition given in table 1. The DECARBit test case utilizes a Shell oxygen-fed entrained flow gasifier [16].

Table 1: Coal composition mol-% [16]

Carbon	Nitrogen	Hydrogen	Total sulphur	Ash	Chlorine	Moisture	Oxygen
66.520	1.560	3.780	0.520	14.150	0.009	8.000	5.460

The DECARBit IGCC plant with CO_2 capture employs two sour shift WGS reactors to shift the syngas received from the gasifier. The sour syngas is then cleaned of H_2S [16]. In the present work, this setup is replaced by first H_2S cleaning, and then the SEWGS process. Please refer to Figure 5. The syngas stream 1 in Figure 5 is assumed to have the same composition and flow rate as the corresponding stream in the DECARBit test case with capture [16]. Please refer to Table 2.

H_2S is then removed from stream 1, resulting in stream ref2 in Table 2. New mole fractions and flow rates are calculated. This stream is assumed to be at same temperature and pressure as stream 1, which is a oversimplification with respect to the operating conditions of the H_2S removal unit.

According to the DECARBit test case, the syngas should then be heated to 573 K and mixed with stream ref3 high-pressure steam H_2O, resulting in stream ref4 [16]. This implies that the pressure of stream ref4 will be between 41 and 51 bar, and the temperature between 573 and 668 K. However, in the present work, it is desired that the temperature and pressure of the syngas after being mixed with steam is 673 K and 26.89 bar according to the SEWGS inlet conditions suggested by Allam et al. [2]. This feed pressure is in the optimal range suggested by Wright et al. [45]. The pressure drop and temperature adjustment can for example be achieved by a throttle valve and heat transfer to create low-pressure steam.

In the present work, the composition and flow rate of syngas stream 2 and steam stream 3 is assumed to be equal to the corresponding reference streams ref2 and ref3. The temperature and pressure in streams 2 and 3 are assumed to be 673 K and 26.89 bar.

The steam flow rate of stream ref3 mixed into stream ref2 resulting in stream ref4 is based on the DECARBit requirements of the high-temperature WGS reactor. The situation in the present work is different, as the stream of syngas mixed with steam is subsequently mixed with rinse gas coming from one reactor, before being sent to a reactor in the feed stage. However, since the rinse step is not continued until all of the gas which is in the column at the end of the feed step is rinsed out, the rinse steam will not break through to the inlet of the reactor. The gas leaving the reactor from the inlet to be mixed in with the feed gas to two other reactors therefore only contains what was being fed the column during the feed stage. This implies that the gas will have the same steam-to-carbon ratio as the feed syngas in stream 4. The flow rate of steam in stream 3 is assumed to be the same as in stream ref3. The two streams 2 and 3 are mixed, resulting in stream 4, which is assumed to be at 673 K and 26.89 bar. The steam-to-carbon ratio in stream 4 is then 1.79. Stream 4 is then what is sent to the SEWGS system for treatment.

As discussed in Section 1, it should be possible to reduce the steam-to-carbon ratio in a stream sent to a SEWGS system compared to a case where the stream is to be sent to a ordinary WGS reactor. There was, however, not sufficient time to investigate this possibility. This is something that should be taken further in later work.

In several SEWGS integration designs, a high-temperature WGS reactor is placed upstream of the SEWGS reactor. This has the function of carrying out the bulk of the conversion of CO into CO_2 before the SEWGS reactor. By doing this, the temperature increase in the SEWGS reactor due to the heat developed by the forward WGS reaction can be lowered. Therefore it should be expected that by not having a WGS reactor before the SEWGS reactor, the temperature increase in the SEWGS reactor will be higher than in other SEWGS designs [45, 17]. However, by doing this, investment costs for the WGS reactor will be avoided.

Table 2: Streams, referred to Figure 5

Stream	Molar flow	T	p	Composition mol-%							
-	kmol/s	K	bar	H_2	CO	CO_2	N_2	O_2	Ar	H_2S	H_2O
1	4.22	443	41	22.02	49.23	3.45	5.77	-	1.20	0.13	18.13
2	4.21	673	26.89	22.06	49.33	3.46	5.78	-	1.20	-	18.17
3	3.21	673	26.89	-	-	-	-	-	-	-	100.0
4	**7.42**	**673**	**26.89**	**12.52**	**27.99**	**1.96**	**3.28**	**-**	**0.68**	**-**	**53.57**
ref1	7.42	577.2	37.6	39.27	1.22	28.72	3.41	-	0.55	0.07	26.72
ref2	4.21	443	41	22.06	49.33	3.46	5.78	-	1.20	-	18.17
ref3	3.21	668	51	-	-	-	-	-	-	-	100.0
ref4	7.42	-	-	12.52	27.99	1.96	3.28	-	0.68	-	53.57

The SEWGS reactor design and dimensions are taken from the SEWGS modelling work

by Wright et al. [44], which are developed to handle the syngas generated by a natural gas-fed ATR in a 330 MW IRCC power plant. The authors conclude that 4 SEWGS trains, with each train consisting of 8 reactors working in a SEWGS cycle, are sufficient to handle the syngas feed. The purge step is assumed to take place using steam at 1.1 bar Wright et al. [44]. A summary of the syngas flow rate composition in comparison to those used in the present work is found in Table 3. With reference to the discussion in Section 1.2, it can be seen in Table 3 that the amount of CO_2 and CO to be treated in the IGCC syngas feed in the present case is approximately twice of that in a IRCC syngas feed, when correcting for the different power outputs of the two power plants. Wright et al. [45] reasons that this requires that the amount of adsorbent should be doubled, either by doubling the size of the reactors, or by doubling the number of SEWGS trains. Another possibility is utilize the same amount of adsorbent, and reducing the cycle time. In the present work, it is chosen to increase the number of SEWGS trains. As suggested by the discussion by Wright et al. [45], the number of SEWGS trains necessary in the present case is calculated as follows:

$$\text{Number of trains} = \frac{\text{Flow rate of } CO_2 \text{ and CO to treat, present case}}{\text{Flow rate of } CO_2 \text{ and CO to treat, Wright}}$$

$$\cdot \frac{\text{Power output, present case}}{\text{Power output, Wright}} \cdot \text{Number of trains, Wright}$$

(7)

$$= \frac{2.222 \text{ kmol/s}}{1.001 \text{ kmol/s}} \cdot \frac{400 \text{ MW}}{330 \text{ MW}} \cdot 4 \text{ trains}$$

$$\approx 10.76 \text{ trains}$$

This calculation should give an indication of the number of SEWGS trains required in the IGCC plant in the present case. The calculation suggests that at least 11 trains are required, but the simulation results have shown that 10 trains are sufficient.

The flow rate of stream 4 in Table 2 is assumed splitted and distributed equally to the 10 SEWGS trains, resulting in a flow rate of 0.742 kmol/s of syngas to each train. As two reactors in each train are operating in the feed step at each point in time, this flow is splitted into 2, giving a flow rate of 0.371 kmol/s of syngas to each reactor in the feed step. Using the ideal gas law, this gives an inlet velocity of

$$u = \frac{371 \text{ mol/s} \cdot 8.314 \text{ J/(mol} \cdot \text{K)} \cdot 673 \text{ K}}{2689000 \text{ Pa} \cdot \pi \cdot (3.658 \text{ m/2})^2} \approx 0.0735 \text{ m/s} \quad (8)$$

This velocity is approximately 0.44 times the corresponding inlet velocity found by doing the same calculation for the setup in the work by Wright et al. [44]. This feed gas velocity is comparable the ones used in other modelling studies, for example 0.08 m/s used in

Table 3: Comparison of present case to the work by Wright et al. [44]

Present case 400 MW IGCC			Wright et al. [44] 330 MW IRCC		
Syngas flow rate	kmol/s	7.42	Syngas flow rate	kmol/s	7.00
Temperature	K	673	Temperature	K	673
Pressure	bar	26.89	Pressure	bar	28.00
Mol-% H_2	-	12.52	Mol-% H_2	-	32.2
Mol-% CO	-	27.99	Mol-% CO	-	2.6
Mol-% CO_2	-	1.96	Mol-% CO_2	-	11.7
Mol-% H_2O	-	53.57	Mol-% H_2O	-	15.2
Mol-% inert Ar and N_2	-	3.96	Mol-% inert	-	38.2
Flow rate of CO_2 and CO	kmol/s	2.222	Flow rate of CO_2 and CO	kmol/s	1.001
SEWGS trains	-	10	SEWGS trains	-	4
Reactors per train	-	8	Reactors per train	-	8
Reactors on feed per train	-	2	Reactors on feed per train	-	2
Reactor length	m	7.377	Reactor length	m	7.377
Reactor diameter	m	3.658	Reactor diameter	m	3.658
Adsorbent per reactor	kg	44465	Adsorbent per reactor	kg	44465
Catalyst per reactor	kg	12927	Catalyst per reactor	kg	12927

the modelling of sorption-enhanced steam-methane reforming by Xiu et al. [46], with a column length of 4 and 6 m, column internal diameter of 0.025 m, and particle diameter 1 mm.

As in the work by Wright et al. [44], the adsorbent is a K_2CO_3-promoted hydrotalcite-based material and the catalyst for the water-gas shift reaction is FeCr-based high-temperature shift catalyst material. The work by Wright et al. [44] does not explain which adsorbent and catalyst particle size that were utilized. Therefore, this data had to be found from the SEWGS experimental work by Van Selow et al. [42], where the adsorbent and catalyst obtained from industrial manufacturers are in pellet form with a diameter of 4.8 mm.

Late during the work process, it was discovered that the methodology suggested by Wright et al. [45] might not be the best choice with respect to the capital costs of the SEWGS system. Their suggestion of increasing the number of SEWGS trains to accommodate the increased content of CO_2 and CO in the syngas made from coal compared to natural gas, implies that the capital costs will increase accordingly. It might be possible that the approximately same number of trains utilized in the natural gas case in the work by Wright et al. [44] might be used for the coal case in the present work. The increased amount of CO_2 and CO in the syngas implies that a reactor in the feed stage will reach its CO_2 adsorption capacity faster than in the natural gas case. This means that the feed step of the SEWGS cycle will have to be stopped after a shorter period of time, to avoid

excessive breakthrough of CO_2 into the H_2 product. To accommodate this, it is possible to reduce the total cycle time of the SEWGS cycle, thereby running each step in the cycle for a shorter period of time. However, the increased mole fraction of CO_2 and CO in the syngas implies that also the driving force for adsorption will be higher. Attempts to simulate a system such as this were made, but there was not sufficient time to configure the model such that convergence in the simulations was reached. This should be further investigated in later work.

1.4. Risk assessment

According to the assignment text of this thesis, a risk assessment should be carried out. The work with this thesis, consists of simulations using a computer, and has been carried out in an office environment. No laboratory work or potentially hazardous work was undertaken. Having consulted the supervisor of this thesis, it was decided that further risk assessment was not necessary.

2. Mathematical modelling: SEWGS reactor

A dynamic one-dimensional homogeneous model for a packed bed sorption-enhanced water-gas shift reactor has been developed. The reactor is a cylindrical column of length L and internal diameter d_t, and consists of a inlet and a outlet, with the temperature of the wall of the reactor being kept at a constant temperature T_{wall} by a cooling jacket. As in the modelling work of a sorption-enhanced steam-methane reforming (SE-SMR) reactor by Ding and Alpay [13], the reactor is assumed to be packed with adsorbent and catalyst particles, which in total gives a void fraction ε_t. Please refer to Figure 9.
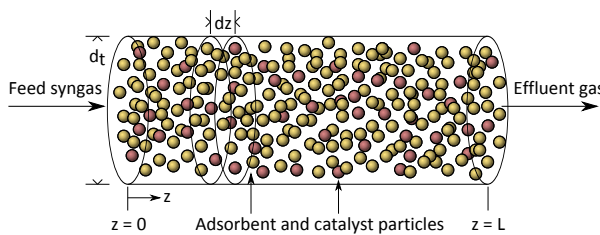

Figure 9: SEWGS reactor

The mass, energy and momentum balances are based on the work by Ding and Alpay [13], with some adaptations. Their one-dimensional homogeneous dynamic model was developed to describe the non-isothermal, non-adiabatic and non-isobaric operation of a packed bed reactor where steam-methane reforming reactions are taking place - and adsorption of CO_2 onto a solid K-HTC adsorbent. One of the reactions taking place during steam-methane reforming is the WGS reaction [13]. Therefore, the difference between the model by Ding and Alpay [13] and the model which are to be developed in this work, is that only the WGS reaction is assumed to take place. This implies that the same mass, energy and momentum balances may be applied. The only difference is that another type of catalyst is employed, one for catalysing the WGS reaction instead of the steam-methane reforming reactions. This implies that an expression for the reaction kinetics for the WGS reaction over the selected catalyst must be found.

The additional equations required for describing effects such as axial dispersion, thermal conductivity and so on, are also based on the expressions used by Ding and Alpay [13] where these are found to be applicable.

The model assumptions are based on those by Ding and Alpay [13], with some modifications

- One-dimensional calculation of all variables along the axial z-direction of the reactor column

- No radial concentration gradients

- No radial temperature gradients

- Ideal gas behaviour

- Axially dispersed plug flow

- Only CO_2 can be adsorbed

- Linear driving force (LDF) model for the mass transfer of CO_2 between the gas phase and the adsorbent

- Modified Langmuir isotherm for the equilibrium adsorption capacity of CO_2 as proposed by Lee et al. [25]

- A model of the water-gas shift reaction kinetics as proposed by Hla et al. [21]

- The adsorbent and catalyst particles of the same spherical, uniform particle size

- Temperature in gas-phase and in adsorbent and catalyst particles are equal

The following N components have been considered: $i = CO_2$, H_2, CO, H_2O and N_2. Nitrogen N_2 and argon Ar are assumed to be inert, and the mole fractions of N_2 and Ar have been added together from the data in stream 4 in Table 2. The model should therefore consider $N = 5$ components.

The mathematical model should be able to calculate the decision variables for

- each point along the axial direction in the reactor between the inlet at $z = 0$ and the outlet at $z = L$

- each time step from $t = 0$ to the end of the period of analysis

The following 10 variables are to be determined: component concentrations $\bar{c}_i$, total concentration $\bar{c}$, temperature T, total pressure p, velocity u and amount of CO_2 adsorbed q_{CO_2}. As the variables are functions of the axial position z in the reactor, this requires in total 10 equations for each axial position z in the reactor. Accordingly, 10 governing equations are required to determine the solution. Additional equations are required to determine auxiliary variables which are used by the governing equations. These can be found in Section 2.8.

There has been significant problems with determining the correct set of governing equations which should be utilized for modelling the SEWGS reactor. It was not possible to implement the one-dimensional homogeneous dynamic model by Ding and Alpay [13] directly, as there was several unexplained aspects in the model description. The model by Ding and Alpay [13] utilizes one mass balance for each of the components considered, and does not include a total mass balance. The authors do not state how they have related the component concentrations to the total concentration. The vacuum pressure-swing adsorption (VPSA) modelling work by Liu et al. [28] utilizes one mass balance for each of the components considered, and does not include a total mass balance. The authors relate the total pressure to the total concentration using the ideal gas law, and includes

a relationships defining the total concentration to be equal to the sum of the component concentrations. The SE-SMR modelling work by Reijers et al. [35] utilizes one mass balance for each of the components considered, and includes a total mass balance. Neither of these works provided enough information to be able to describe a coherent model with zero degrees of freedom which was able to reach convergence in gPROMS utilizing the configuration in the present work. Therefore, several assumptions and modifications to these models had to be made to be able to describe a model which could be utilized in the present work. This is not ideal, and it was discovered very late during the work process with this thesis, that the reason for the problems with convergence was partly due to the choice of governing equations, and partly the implementation of the model in gPROMS. The model utilized to run the simulations in the present work will now be presented. Please refer to Section 5.2 for a summary of the necessary modifications to the reactor model, which should be taken into account in later work with this model.

To be able to reach convergence in the simulations, it was necessary to define the mass balance for all N components except one and include a total mass balance (equation of continuity).

The model should accommodate both cocurrent and countercurrent flow. Cocurrent flow is defined as flow from $z = 0$ in the direction of $z = L$, and countercurrent flow vice versa. As a convention, $z = 0^-$ is defined as the *inlet*, and $z = L^+$ as the *outlet* of the reactor.

The governing equations of the model will now be presented. The default type of flow direction is defined to be cocurrent flow. Therefore, the boundary conditions for cocurrent flow will be introduced together with their corresponding governing equation. The boundary conditions for the other types of flow will be presented later in Section 2.10.

2.1. Mass balance

The mass balance for $i = CO_2$ in the reactor in the axial domain $z \in (0, L)$ can be formulated as follows, adapted from [13, 36]

$$\varepsilon_t \frac{\partial \bar{c}_{CO_2}}{\partial t} = -\frac{\partial (u\bar{c}_{CO_2})}{\partial z} + \frac{\partial}{\partial z}\left(\bar{c}D_{ax}\frac{\partial y_{CO_2}}{\partial z}\right) + \rho_{b,cat}\eta_{CO_2}r - \rho_{b,ads}\frac{\partial q_{CO_2}}{\partial t} \qquad (9)$$

The mass balance for components $i = H_2$, CO, H_2O in the reactor in the axial domain $z \in (0, L)$ can be formulated similarly, not including the adsorption term

$$\varepsilon_t \frac{\partial \bar{c}_i}{\partial t} = -\frac{\partial (u\bar{c}_i)}{\partial z} + \frac{\partial}{\partial z}\left(\bar{c}D_{ax}\frac{\partial y_i}{\partial z}\right) + \rho_{b,cat}\eta_i r \qquad (10)$$

Boundary condition for cocurrent flow at $z = 0$: [13, 3]

$$\frac{\partial \bar{c}_i(z = 0)}{\partial z} = -\frac{u(z = 0)(\bar{c}_{i,inlet} - \bar{c}_i(z = 0))}{D_{ax}(z = 0)} \qquad (11)$$

Boundary condition for cocurrent flow at $z = L$: [13, 3]

$$\frac{\partial \bar{c}_i(z = L)}{\partial z} = 0 \tag{12}$$

The mass balance and boundary conditions are defined for $N - 1$ components $i = CO_2$, H_2, CO, H_2O. Together with the total mass balance, this determines the values of $\bar{c}_i$ for the whole axial domain $z \in [0, L]$. In total 4 equations for each point z.

2.2. Total mass balance

The total mass balance in the axial domain $z \in (0, L)$ can be formulated as follows [35]

$$\varepsilon_t \frac{\partial \bar{c}}{\partial t} = -\frac{\partial(u\bar{c})}{\partial z} + \rho_{b,cat} \sum_i (\eta_i)\, r - \rho_{b,ads} \frac{\partial q_{CO_2}}{\partial t} \tag{13}$$

Boundary condition for cocurrent flow at $z = 0$: [13]

$$u(z = 0) = u_{inlet} \tag{14}$$

Boundary condition for cocurrent flow at $z = L$: [13]

$$p(z = L) = p_{outlet} \tag{15}$$

The total mass balance and boundary conditions determine the values of u for the whole axial domain $z \in [0, L]$. In total 1 equation for each point z.

2.3. Energy balance

The energy balance in the axial domain $z \in (0, L)$ can be formulated as follows, adapted from [12, 13]

$$\left(\bar{c}\bar{C}_{p,gas}\varepsilon_t + \rho_{b,cat}C_{p,cat} + \rho_{b,ads}C_{p,ads} \right) \frac{\partial T}{\partial t} = \frac{\partial}{\partial z}\left(k_z \frac{\partial T}{\partial z} \right) - \bar{c}\bar{C}_{p,gas} u \frac{\partial T}{\partial z}$$

$$-\rho_{b,cat} \sum_i \left(\bar{h}_i \eta_i \right) r + \rho_{b,ads} \Delta \bar{h}_{ads,CO_2} \frac{\partial q_{CO_2}}{\partial t} + \frac{4U}{d_t}(T_{wall} - T) \tag{16}$$

Please note that the term $\varepsilon_t \frac{\partial p}{\partial t}$ which is used in [12, 13] has been omitted. The reason for this simplification is that it is assumed that pressure change is instantaneous. Please refer to Section 2.4.

Boundary condition for cocurrent flow at $z = 0$: [13, 3]

$$\frac{\partial T(z = 0)}{\partial z} = -\frac{\bar{c}(z = 0)\bar{C}_{p,gas}(z = 0)u(z = 0)(T_{inlet} - T(z = 0))}{k_z(z = 0)} \tag{17}$$

Boundary condition for cocurrent flow at $z = L$: [13, 3]

$$\frac{\partial T(z = L)}{\partial z} = 0 \qquad (18)$$

The energy balance and boundary conditions determine the values of T for the whole axial domain $z \in [0, L]$. In total 1 equation for each point z.

2.4. Momentum balance

For the momentum balance, the Ergun equation, which describes pressure drop in a packed bed column, will be used in the whole axial domain $z \in [0, L]$. This can be formulated as [13, 12, 3, 15]

$$\frac{\partial p}{\partial z} = -150u\frac{\mu(\lambda_s(1 - \varepsilon_b))^2}{d_p^2\varepsilon_b^3} - 1.75u|u|\frac{\lambda_s(1 - \varepsilon_b)\rho_{gas}}{d_p\varepsilon_b^3} \qquad (19)$$

The relationship [18]

$$Interstitial\ gas\ velocity = \frac{Superficial\ gas\ velocity}{\varepsilon_b} \qquad (20)$$

has been used.

This form of the momentum balance assumes that pressure change is instantaneous. The last term uses $u|u|$ instead of u^2. This is accommodate countercurrent as well as cocurrent flow. The momentum balance determine the values of p for the whole axial domain $z \in [0, L]$. In total 1 equation for each point z.

2.5. Ideal gas law

The ideal gas law for the total concentration $\bar{c}$ will be used in the whole axial domain $z \in [0, L]$.

$$\bar{c} = \frac{p}{RT} \qquad (21)$$

The ideal gas law determine the values of $\bar{c}$ for the whole axial domain $z \in [0, L]$. In total 1 equation for each point z.

2.6. Relationship between component and total concentration

Defined in the whole axial domain $z \in [0, L]$.

$$\bar{c} = \sum_i (\bar{c}_i) \qquad (22)$$

This equation determine the values of the concentration of the last component $\bar{c}_{N_2}$ for the whole axial domain $z \in [0, L]$. In total 1 equation for each point z.

2.7. Linear Driving Force model

The linear driving force model for adsorbent loading has been used to account for mass transfer limitations in the adsorbent. The adsorption rate of CO_2 in the whole axial domain $z \in [0, L]$ can be formulated as follows [13, 25]

$$\frac{\partial q_{CO_2}}{\partial t} = k_{LDF}(q^*_{CO_2} - q_{CO_2}) \tag{23}$$

This equation for the adsorbent loading of CO_2 determine the values of q_{CO_2} for the whole axial domain $z \in [0, L]$. In total 1 equation for each point z.

2.8. Additional equations

The following equations are, unless otherwise noted, evaluated on the whole axial domain $z \in [0, L]$.

2.8.1. Axial dispersion coefficient

As suggested by Ding and Alpay [13], the axial dispersion coefficient for gas dispersion in a packed bed can be approximated by the following expression by Edwards and Richardson [14]

$$D_{ax} = 0.73D_m + \frac{0.5d_p u}{\varepsilon_b + \dfrac{9.7\varepsilon_b^2 D_m}{d_p u}} \tag{24}$$

which is valid for Reynolds numbers and particle diameters:

$$0.008 < Re_p < 50, 0.000377 \text{ m} < d_p < 0.0060 \text{ m} \tag{25}$$

where [19, 32]

$$Re_p = \frac{\rho_{gas} u d_p}{\mu} \tag{26}$$

Referring to Table 10, the particle diameter used in the present case, $d_p = 0.0048$ m, is inside this range. The relationship from Eq. (20) has been used here as well.

This relationship for the axial dispersion coefficient is used in several reactor modelling schemes in literature: Reijers et al. [35], in an one-dimensional homogeneous dynamic model of a reactor for sorption-enhanced steam-methane reforming. Halabi et al. [19],

in an one-dimensional heterogeneous dynamic model of a reactor for sorption-enhanced autothermal reforming of methane.

However, for reasons discussed in Section 2.11, the expression in Eq. (24) was not used in the simulations. A constant value was used instead.

2.8.2. Effective, axial thermal conductivity

As suggested by Ding and Alpay [13], the effective, axial thermal conductivity can be expressed by the relations by Yagi and Kunii [47] and Kunii and Smith [24] as

$$
k_z = \left(\varepsilon_b \left(1 + \beta_1 \frac{h_{rv} d_p}{k_g} \right) + \frac{\beta_1 (1 - \varepsilon_b)}{\dfrac{1}{\dfrac{1}{\Phi} + \dfrac{d_p h_{rs}}{k_g}} + \gamma \dfrac{k_g}{k_s}} \right) k_g + a_{k_z} Pr Re_p k_g \tag{27}
$$

$$
h_{rv} = \frac{0.1952 (T/100)^3}{1 + \dfrac{\varepsilon_b}{2(1 - \varepsilon_b)} \dfrac{1 - e}{e}} \tag{28}
$$

$$
h_{rs} = 0.1952 (T/100)^3 \frac{e}{2 - e} \tag{29}
$$

The Prandtl number is inserted into Eq. (27) [32]

$$
Pr = \frac{C_{p,gas} \mu}{k_g} = \frac{\bar{C}_{p,gas} \bar{c} \mu}{k_g \rho_{gas}} \tag{30}
$$

This relationship is used in several reactor modelling schemes in literature: Halabi et al. [19], in an one-dimensional heterogeneous dynamic model of a reactor for sorption-enhanced autothermal reforming of methane.

2.8.3. Overall bed-to-wall heat transfer coefficient

As the wall of the reactor is assumed kept at a constant temperature T_{wall}, heat produced through the WGS reaction and the adsorption will be transferred through the wall out of the reactor. An expression for the overall heat transfer coefficient is therefore required. For spherical particles, as suggested by Ding and Alpay [13], this can be expressed by the relation by Li and Finlayson [27] as

$$
U = \frac{k_g}{d_t} 2.03 Re_p^{0.8} \exp\left(-\frac{6 d_p}{d_t} \right) \tag{31}
$$

which is applicable when

$$20 \leq Re_p \leq 7600, 0.05 \leq \frac{d_p}{d_t} \leq 0.3 \tag{32}$$

This equation is not valid for very low Reynolds numbers, and therefore an additional expression is needed. In the work by Ding and Alpay [13], the following expression by De Wasch and Froment [11] is used

$$U_{Re_p->0} = \frac{6.15}{d_t} \left[\varepsilon_b \left(1 + \beta_1 \frac{h_{rv} d_p}{k_g} \right) + \frac{\beta_1 (1 - \varepsilon_b)}{\dfrac{1}{\dfrac{1}{\Phi} + \dfrac{d_p h_{rs}}{k_g}} + \gamma \dfrac{k_g}{k_s}} \right] k_g \tag{33}$$

which according to De Wasch and Froment [11], only takes into account the static contribution to the overall heat transfer coefficient.

In the work by Ding and Alpay [13], Eqs. (31) and (33) are linearly combined to give an approximation of the heat transfer coefficient over the range of Reynolds numbers from 0 to 7600:

$$U = \frac{6.15}{d_t} \left[\varepsilon_b \left(1 + \beta_1 \frac{h_{rv} d_p}{k_g} \right) + \frac{\beta_1 (1 - \varepsilon_b)}{\dfrac{1}{\dfrac{1}{\Phi} + \dfrac{d_p h_{rs}}{k_g}} + \gamma \dfrac{k_g}{k_s}} \right] k_g + \left(\frac{k_g}{d_t} 2.03 Re_p^{0.8} \exp\left(-\frac{6 d_p}{d_t} \right) \right) \tag{34}$$

The Reynolds numbers for the flow in the present work is expected to cover the ranges governed by the expressions in both Eq. (33) and (31). The relation for high Reynolds numbers given in Eq. (31) is not valid for the particle to reactor diameter ratio used in the present work $d_p/d_t \approx 0.0013$. This implies that this expression can not be used in the present work. As no other applicable relations for the overall heat transfer coefficient could be found, a constant value was utilized in the simulations. Please see Section 2.11 for the determination of this constant value. This is something that could be investigated in further work with the model.

2.8.4. Reaction rate

The reaction rate for the forward WGS reaction , i.e. conversion rate of CO, can be expressed by a model by Hla et al. [21]

$$r = 1000 \cdot 10^{2.845 \pm 0.003} \exp\left(\frac{-111000 \pm 2630}{\bar{R}T}\right)$$

$$\cdot \left(\frac{p_{CO}}{1000}\right)^{1.0 \pm 0.031} \left(\frac{p_{CO_2}}{1000}\right)^{-0.36 \pm 0.043} \left(\frac{p_{H_2}}{1000}\right)^{-0.09 \pm 0.007} \left(1 - \frac{1}{K_{WGS}} \frac{p_{CO_2} p_{H_2}}{p_{CO} p_{H_2O}}\right) \qquad (35)$$

This expression is valid at atmospheric pressure and 450 °C for a FeCr-based high-temperature shift catalyst called HTC1, with the following composition: 80-90% Fe_2O_3, 8-13% Cr_2O_3, 1-2% CuO [21]. The expression was determined in an experiment utilizing ground catalyst with particle size in the range 53-150 μm. The particle diameter 150 μm is 3.1 % of the particle diameter used in the present work, d_p = 4.8 mm. It is unknown whether or not this affects the behaviour of the catalyst. According to Hla et al. [21], this rate expression was determined using gas streams with compositions consistent with the syngas from a dry-feed Shell gasifer in an IGCC plant, and this rate expression showed a very good fit to experimental data for these CO-rich streams.

The syngas used in the experiments had the following dry-basis composition: 65 % CO, 30 % H_2, 2 % CO_2, 3 % N_2 [21]. Compared to dry-basis composition of stream 4 in Table 2, 60.28 % CO, 26.96 % H_2, 4.23 % CO_2, 8.53 % N_2, it can be seen that the use of this rate model is reasonable. According to a review of water-gas shift reaction kinetics by Smith et al. [40], this expression is used in several recent literature publications.

However, this rate expression was determined at atmospheric pressure. Smith et al. [40] suggests that since most such rate expressions are determined at atmospheric pressure, the pressure modification recommended by Rase [33] can be used. This modification takes the form of multiplying the rate expression with an activity factor, which depends on the total pressure. For total pressures p above 20 atm = 20.265 bar, this factor is 4 according to Rase [33]. The feed syngas pressure is ca. 28.69 bar, well above 20.265 bar, and the total pressure in the column p, is not likely to fall below this range. Another suggested pressure scale-up factor commonly used is a correlation by Singh and Saraf [37], which is valid up to 30 atm [1]:

$$F_{press} = (p/101325)^{0.5 - p/(250 \cdot 101325)} \qquad (36)$$

The value of this factor is increasing slowly from 3.52 at 20 atm up to 3.64 at 30 atm, which is in the order of magnitude suggested by the factor of Rase [33]. This behaviour of the activity factor is also in accordance with what Atwood et al. [4] concludes, that the activity factor only increases slightly as the pressure is increased further than 10 atm.

It is chosen here to use the correlation by Singh and Saraf [37], which is also used in a model for a WGS reactor in an IGCC plant in the work by Adams II and Barton [1]. Implementing this in the expression for the reaction rate and leaving out uncertainties in the values in the original expression, the expression for the forward WGS reaction at total

pressures up to 30 bar and temperature in the range of 450 °C becomes

$$r = (p/101325)^{0.5-p/(250 \cdot 101325)} \cdot 10^{5.845} \exp\left(\frac{-111000}{\bar{R}T}\right)$$

$$\cdot \left(\frac{p_{CO}}{1000}\right)^{1.0} \left(\frac{p_{CO_2}}{1000}\right)^{-0.36} \left(\frac{p_{H_2}}{1000}\right)^{-0.09} \left(1 - \frac{1}{K_{WGS}} \frac{p_{CO_2}p_{H_2}}{p_{CO}p_{H_2O}}\right) \tag{37}$$

2.8.5. Equilibrium constant

The equilibrium constant for the WGS reaction is a function of temperature. According to Adams II and Barton [1], the most commonly used relationship is [1, 40]

$$K_{WGS} = \exp\left(\frac{4577.8}{T} - 4.33\right) \tag{38}$$

2.8.6. Equilibrium adsorbent CO_2 loading - Modified Langmuir isotherm

The equilibrium adsorbent CO_2 loading is a function of the partial pressure of CO_2 and temperature. Several analytical expressions for approximation are suggested in literature, and there has been significant discussion about how the actual isotherm of K-HTC is. It appears that the confusion is due to the different types of K-HTC used in the experiments.

An isotherm developed in 2007 by Lee et al. [25] suggests that the isotherms used in earlier K-HTC adsorption schemes are not as accurate as assumed, especially at higher partial pressures of CO_2. The authors state that earlier developed isotherms, referring to the isotherm developed by Ding and Alpay [12], predict too low adsorption capacity at higher partial pressures. The capacity in their isotherm approaches 0.875 mol CO_2 adsorbed/kg adsorbent at the highest partial pressure of 3 atm.

In the SEWGS experimental study from 2009 by Van Selow et al. [42], the authors have reviewed the adsorption isotherms found in literature, among them the isotherm developed by Lee et al. [25]. The authors conclude that the adsorption isotherms reported in literature are of limited use for SEWGS modelling, since most isotherms are developed for lower partial pressures and predict too low adsorption capacities compared to their findings. The authors report a breakthrough adsorption capacity of 1.4 mol CO_2/kg adsorbent.

Compared to the value reported by Van Selow et al. [42], the adsorption isotherm by Lee et al. [25] is conservative with respect to adsorption capacity. However, until there is developed new isotherms which are consistent with respect to higher partial pressures and adsorption capacities, the isotherms reported in literature will have to be used for modelling. The modified isotherm developed in the work by Lee et al. [25] will be employed, which is reported to give good fit to experimental data in the partial pressure region of 0 - 3 atm at a temperature of 400 °C [25].

$$q^*_{CO_2}(p_{CO_2}, T) = \frac{mK_C p_{CO_2}\left[1 + (a+1)K_R p^a_{CO_2}\right]}{1 + K_C p_{CO_2} + K_C K_R p^{a+1}_{CO_2}} \tag{39}$$

where

$$K_C = K_C^0 \exp\left(q_C/\bar{R}T\right) \tag{40}$$

$$K_R = K_R^0 \exp\left(\Delta H_R/\bar{R}T\right) \tag{41}$$

This isotherm was developed from data found in experiments using particles with a diameter of approximately 0.30 cm. This particle diameter is 62.5 % of the diameter chosen for the adsorbent particles in the present work, d_p = 0.48 cm. This could affect the accuracy of the model. A shortcoming with the isotherm by Lee et al. [25] is that it does not state specifically which type of K-HTC that were used in the experiments. The only information given is that the K-HTC sample was obtained from Air Products and Chemicals, Inc.

It should also be noted that since the CO mole fraction in the syngas feed is so high, the partial pressure of CO_2 will be very high in some regions of the reactor, quite probably over 3 atm. However, this isotherm will have to be used. Referring to Figure 2 in [25], extrapolating to higher partial pressures will not increase the adsorption capacity significantly. It will therefore not pose a computational problem to use this isotherm, since the equilibrium adsorbent loading determined by Eq. 39 will not increase significantly when the partial pressure is higher than 3 atm. According to Lee et al. [25], as

$$\lim_{p_{CO_2} \to \infty} q^*_{CO_2}(p_{CO_2}, T) = m(a+1) = 0.875 \text{ mol } CO_2 \text{ adsorbed/kg adsorbent} \tag{42}$$

2.8.7. Isoteric heat of adsorption of CO_2

As CO_2 is adsorbed, heat will be developed. In several modelling schemes for K-HTC adsorption, constant values for the isoteric heat of adsorption of CO_2 are used. In the SE-SMR modelling work of Reijers et al. [35], a constant value $\Delta\bar{h}_{ads,CO_2}$ = 17000 J/mol CO_2 adsorbed is used. This value is also used in the SE-SMR modelling work of Ding and Alpay [13]. However, according to Lee et al. [25], the heat of adsorption is approximately constant = q_C = 21003.68 J/mol when the loading of the adsorbent is in the lower region, and then sharply shifts to another approximately constant value = $\Delta H_R/a$ = 16853.15 J/mol in the higher loading region. The authors state that the isoteric heat of adsorption can be described by [25]

$$\Delta\bar{h}_{ads,CO_2} = q_C + \frac{a\left(\dfrac{K_R p_{CO_2}^a(1 + a(1 + K_C p_{CO_2}))}{1 + (a + 1)K_R p_{CO_2}^a}\right)(\Delta H_R/a - q_C)}{1 + a\left(\dfrac{K_R p_{CO_2}^a(1 + a(1 + K_C p_{CO_2}))}{1 + (a + 1)K_R p_{CO_2}^a}\right)} \tag{43}$$

where $\Delta\bar{h}_{ads,CO_2} > 0$ J/mol CO_2 adsorbed. The authors report that this correlation qualitatively fits data from literature.

2.8.8. Linear Driving Force model mass-transfer coefficient

According to Ding and Alpay [12], this variable may be a function of pressure, temperature and the adsorbent loading. They propose the following relationship

$$k_{LDF} = \frac{15D_p}{\left(\dfrac{d_p}{2}\right)^2} \frac{1}{1 + \left[\dfrac{(1 - \varepsilon_{p,ads})\rho_{p,ads}\bar{R}T}{\varepsilon_{p,ads}}(\delta q_{CO_2}^*/\delta p_{CO_2})_T\right]} \tag{44}$$

To be able to implement Eq. (44) in gPROMS, it is required to determine explicitly the partial derivative $\delta q_{CO_2}^*/\delta p_{CO_2}$

$$\frac{\delta q_{CO_2}^*}{\delta p_{CO_2}} = \frac{mK_C\left(1 + 2K_R p_{CO_2}^a a + K_R p_{CO_2}^a + K_R p_{CO_2}^a a^2 + K_C K_R p_{CO_2}^{a+1} a^2\right)}{\left(1 + K_C p_{CO_2} + K_C K_R p_{CO_2}^{a+1}\right)^2} \tag{45}$$

k_{LDF}

$$= \frac{\dfrac{15D_p}{\left(\dfrac{d_p}{2}\right)^2}}{1 + \left[\dfrac{(1 - \varepsilon_{p,ads})\rho_{p,ads}\bar{R}T}{\varepsilon_{p,ads}} \dfrac{mK_C\left(1 + 2K_R p_{CO_2}^a a + K_R p_{CO_2}^a + K_R p_{CO_2}^a a^2 + K_C K_R p_{CO_2}^{a+1} a^2\right)}{\left(1 + K_C p_{CO_2} + K_C K_R p_{CO_2}^{a+1}\right)^2}\right]}$$

$$\tag{46}$$

According to the relationship in Eq. (44), the value of k_{LDF} decreases when the partial pressure of CO_2 decreases. This implies that the rate of desorption, which is undertaken at lower total pressures, is lower than the rate of adsorption. This is accordance with experimental work from literature, see for example Allam et al. [2, p.238] and Ding and Alpay [12]. As discussed in Section 1.2, there is significant debate about the adsorption kinetics of K-HTCs. Therefore, it has been difficult to find good data for which correlations that should be used when modelling the adsorption on K-HTC.

In the experimental work on the adsorption kinetics of K-HTC by Allam et al. [2] from 2005, the authors report that during adsorption, the mass transfer coefficient k_{LDF} = 0.1 s^{-1}. The experiments were undertaken at 723 K and 24.5 bar. However, during desorption, the reported value is k_{LDF} = 0.001 s^{-1} for one specific flow rate. The authors state that this value does not describe the results using other flow rates very well.

The work by Lee et al. [25] from 2007 reports a value of the mass transfer coefficient $k_{LDF} \approx 0.05$ s^{-1} at 400 °C, and $k_{LDF} \approx 0.0833$ s^{-1} at 520 °C. The authors state that k_{LDF} was found to be independent of the adsorbent CO_2 loading and only a weak function of temperature in the range of the experimental data. This is not in accordance with the findings in the work from 2000 by Ding and Alpay [12].

According to a work carried out in 2008 by Lee et al. [26], it is possible to utilize the same constant value for k_{LDF} for desorption as for adsorption on K-HTC, citing a value of $k_{LDF} \approx 0.05$ s^{-1} at 400 °C. This will be employed in the present work, leaving out the need for the expression in Eq. (44). It should be noted that the temperature in the reactor will increase above 400 °C due to the heat developed by the heat of the exothermic WGS reaction and the adsorption of CO_2. However, since no consistent expression for k_{LDF} as a function of temperature could be found, a constant value will have to be utilized as for now.

2.8.9. Enthalpy of component i at temperature T

The enthalpy of an ideal gas is only a function of temperature [30]

$$\bar{h}_i = \bar{h}_i(T) = \bar{h}_{f,i}^{\circ} + \int_{T_{ref}}^{T} \bar{C}_{p,i}(T)\, dT = \bar{h}_{f,i}^{\circ} + (\bar{h}_i(T) - \bar{h}_i(T_{ref})) \tag{47}$$

where the standard reference state is T_{ref} = 25 °C and p_{ref} = 1 atm. $\bar{h}_i$ is evaluated from the Multiflash physical property package in gPROMS using the functions IdealGasEnthalpy-OfFormationAt25C(i) + VapourEnthalpy(T, p, array of mole fractions of i components, where only y_i = 1).

2.8.10. Specific molar heat capacity of gas-phase at constant pressure

$\bar{C}_{p,gas}$ is evaluated from Multiflash using the function VapourHeatCapacity(T,p,y).

2.8.11. Partial pressures

$$p_i = \bar{c}_i \bar{R} T \tag{48}$$

2.8.12. Mole fractions

$$y_i = \frac{\bar{c}_i}{\bar{c}} \tag{49}$$

2.8.13. Mass density of gas-phase

$$\rho_{gas} = \sum_i \bar{c}_i M_i \tag{50}$$

2.9. Model summary and degrees of freedom

It is necessary to distinguish between *model variables* and *stream variables*. The physical behaviour of the SEWGS reactor, represented by the model variables, is a result of the thermodynamic state and flow rates at the inlet and the outlet of the reactor, represented by the stream variables. The relationships between the model and stream variables are defined through the boundary conditions of the model.

To be able to reach convergence in gPROMS, it was necessary to assume that the mole fractions y_i, the component concentrations $\bar{c}_i$, the total concentration $\bar{c}$, the partial pressures p_i could take negative values. This is not physically consistent, as the lower bound of these variables should be set to zero. The reason for this assumption is that expressions such as Eq. (37) will go towards infinity as these variables goes towards zero. However, using the appropriate solver settings, the values of these variables in the simulation results will not be negative.

The following 40 model variables are defined over the whole domain $z \in [0, L]$: $\bar{c}_i$, $\bar{c}$, T, p, u, q_{CO_2}, D_{ax}, Re_p, k_z, h_{rv}, h_{rs}, U, r, K_{WGS}, $q^*_{CO_2}$, K_C, K_R, $\Delta\bar{h}_{ads,CO_2}$, k_{LDF}, $\bar{h}_i$, $\bar{C}_{p,gas}$, p_i, y_i, ρ_{gas}. An overview of the corresponding 40 equations which were implemented in gPROMS are given in Table 4.

Table 4: Model variables and equations. MF = Multiflash

Variable:	$\bar{c}_i$	$\bar{c}$	T	p	u	q_{CO_2}
Eq.:	(9)(10)(11)(12)(22)	(21)	(16)(17)(18)	(19)	(13)(14)(15)	(23)
Variable:	D_{ax}	Re_p	k_z	h_{rv}	h_{rs}	U
Eq.:	const.	(26)	(27)	(28)	(29)	const.
Variable:	r	K_{WGS}	$q^*_{CO_2}$	K_C	K_R	$\Delta\bar{h}_{ads,CO_2}$
Eq.:	(37)	(38)	(39)	(40)	(41)	(43)
Variable:	k_{LDF}	$\bar{h}_i$	$\bar{C}_{p,gas}$	p_i	y_i	ρ_{gas}
Eq.:	const.	MF	MF	(48)	(49)	(50)

The following 8 stream variables are defined for the inlet: Mole fractions $y_{i,inlet}$, temperature T_{inlet}, pressure p_{inlet} and molar flow rate $\dot{n}_{inlet}$. Correspondingly, 8 stream variables for the outlet: Mole fractions $y_{i,outlet}$, temperature T_{outlet}, pressure p_{outlet} and molar flow rate $\dot{n}_{outlet}$.

Currently, the system consists of 40 model variables and 16 stream variables, with corresponding 40 model equations. The system now has 40 + 16 - 40 = 16 degrees of freedom. Sixteen additional equations are required to determine the system. With the situation of cocurrent flow as an example, it is desirable to assume that the inlet mole fractions $y_{i,inlet}$, inlet temperature T_{inlet}, inlet molar flow rate $\dot{n}_{inlet}$ and outlet pressure p_{outlet} are known. This removes 8 degrees of freedom from the system. The 8 remaining stream variables; p_{inlet}, $y_{i,outlet}$, T_{outlet} and $\dot{n}_{outlet}$ are then assumed unknown and needs to be determined from the reactor behaviour, through the model variables. This implies the need of 8 stream equations.

However, the stream variables consists of mole fractions and molar flow rates, while the model variables consists of molar concentrations and velocities. It is therefore necessary to introduce the following relationships, using the ideal gas law:

$$\bar{c}_{i,inlet} = \frac{y_{i,inlet} p_{inlet}}{\bar{R} T_{inlet}} \tag{51}$$

$$\bar{c}_{i,outlet} = \frac{y_{i,outlet} p_{outlet}}{\bar{R} T_{outlet}} \tag{52}$$

$$u_{inlet} = \frac{\dot{n}_{inlet} \bar{R} T_{inlet}}{p_{inlet} \pi (d_t/2)^2} \tag{53}$$

$$u_{outlet} = \frac{\dot{n}_{outlet} \bar{R} T_{outlet}}{p_{outlet} \pi (d_t/2)^2} \tag{54}$$

These equations relating $\bar{c}_{i,inlet}$, $\bar{c}_{i,outlet}$, u_{inlet} and u_{outlet} to the stream variables were not implemented directly in gPROMS, but were substituted into the boundary conditions and stream equations when required. The boundary conditions and the stream equations required to solve the system for cocurrent flow are presented in Table 5.

In summary, the system to be solved consists of 40 model equations, 8 stream equations, 40 model variables and 16 stream variables, where 8 of the stream variables are assumed known.

The governing and auxiliary equations together constitute a system of coupled partial differential algebraic equations (PDAE). This system of equations was implemented in the gPROMS process modelling software developed by Process Systems Enterprise Ltd. This software is able to solve such systems of equations numerically by discretizing spatial variables into finite elements and integrating in the time domain. The reactor z-axis was

discretized into a certain number of elements using the centered finite difference method (CFDM) of second order. Please refer to Section 4 for details about the simulations.

2.10. Boundary conditions

The boundary conditions for cocurrent feed flow presented in Table 5 are from the SE-SMR modelling work by Ding and Alpay [13]. These are based on the boundary conditions proposed by Danckwerts [10]. However, Ding and Alpay [13] do not provide boundary conditions for the other steps in the reactor cycle. These were found in the PSA modelling work by Ribeiro et al. [36], and are based on the Danckwerts boundary conditions.

All boundary conditions for the $N-1$ component concentrations $\bar{c}_i$ are defined for $i = CO_2$, H_2, CO, H_2O. The expressions implemented in gPROMS substitutes the variables $\bar{c}_{i,inlet}$, $\bar{c}_{i,outlet}$, u_{inlet} and u_{outlet} with the expressions found in Eqs. (51), (52), (53) and (54).

2.10.1. Cocurrent feed step (F)

Table 5: Boundary conditions for the cocurrent feed step (F)

	$z = 0$	$z = L$
BC	$\dfrac{\partial \bar{c}_i(z=0)}{\partial z} = -\dfrac{u(z=0)(\bar{c}_{i,inlet} - \bar{c}_i(z=0))}{D_{ax}(z=0)}$	$\dfrac{\partial \bar{c}_i(z=L)}{\partial z} = 0$
	$\dfrac{\partial T(z=0)}{\partial z} = -\dfrac{\bar{c}(z=0)C_{p,gas}(z=0)u(z=0)(T_{inlet} - T(z=0))}{k_z(z=0)}$	$\dfrac{\partial T(z=L)}{\partial z} = 0$
	$u(z=0) = u_{inlet}$	$p(z=L) = p_{outlet}$
Stream vars	$p(z=0) = p_{inlet}$	$\bar{c}_i(z=L) = \bar{c}_{i,outlet}$
		$T(z=L) = T_{outlet}$
		$u(z=L) = u_{outlet}$

These boundary conditions assume that the 8 variables $\bar{c}_{i,inlet}$, T_{inlet}, u_{inlet}, p_{outlet} are known. The 8 variables p_{inlet}, $\bar{c}_{i,outlet}$, T_{outlet}, u_{outlet} are assumed unknown.

2.10.2. Countercurrent rinse step (R) and purge step (P)

Table 6: Boundary conditions for the countercurrent rinse step (R) and purge step (P)

	$z = 0$	$z = L$
BC	$\dfrac{\partial \bar{c}_i(z=0)}{\partial z} = 0$	$\dfrac{\partial \bar{c}_i(z=L)}{\partial z} = -\dfrac{u(z=L)(\bar{c}_{i,outlet} - \bar{c}_i(z=L))}{D_{ax}(z=L)}$
	$\dfrac{\partial T(z=0)}{\partial z} = 0$	$\dfrac{\partial T(z=L)}{\partial z} = -\dfrac{\bar{c}(z=L)\bar{C}_{p,gas}(z=L)u(z=L)(T_{outlet} - T(z=L))}{k_z(z=L)}$
	$p(z=0) = p_{inlet}$	$u(z=L) = u_{outlet}$
Stream vars	$\bar{c}_i(z=0) = \bar{c}_{i,inlet}$	$p(z=L) = p_{outlet}$
	$T(z=0) = T_{inlet}$	
	$u(z=0) = u_{inlet}$	

These boundary conditions assume that the 8 variables p_{inlet}, $\bar{c}_{i,outlet}$, T_{outlet}, u_{outlet} are known. The 8 variables $\bar{c}_{i,inlet}$, T_{inlet}, u_{inlet}, p_{outlet} are assumed unknown.

2.10.3. Countercurrent equalization steps (Eq1), (Eq2), (Eq3) and countercurrent depressurization step (D)

Table 7: Boundary conditions for the countercurrent equalization steps (Eq1), (Eq2), (Eq3) and countercurrent depressurization step (D)

	$z = 0$	$z = L$
BC	$\dfrac{\partial \bar{c}_i(z=0)}{\partial z} = 0$	$\dfrac{\partial \bar{c}_i(z=L)}{\partial z} = 0$
	$\dfrac{\partial T(z=0)}{\partial z} = 0$	$\dfrac{\partial T(z=L)}{\partial z} = 0$
	$p(z=0) = p_{inlet}$	$u(z=L) = u_{outlet} = 0$
Stream vars	$\bar{c}_i(z=0) = \bar{c}_{i,inlet}$	$p(z=L) = p_{outlet}$
	$T(z=0) = T_{inlet}$	
	$u(z=0) = u_{inlet}$	

These boundary conditions assume that the 8 variables p_{inlet}, u_{outlet}, $\bar{c}_{i,outlet}$, T_{outlet} are known. The 8 variables $\bar{c}_{i,inlet}$, T_{inlet}, u_{inlet}, p_{outlet} are assumed unknown.

2.10.4. Cocurrent re-equalization steps (REq3), (REq2), (REq1)

Table 8: Boundary conditions for the cocurrent re-equalization steps (REq3), (REq2), (REq1)

	$z = 0$	$z = L$
BC	$\dfrac{\partial \bar{c}_i(z=0)}{\partial z} = -\dfrac{u(z=0)(\bar{c}_{i,inlet} - \bar{c}_i(z=0))}{D_{ax}(z=0)}$	$\dfrac{\partial \bar{c}_i(z=L)}{\partial z} = 0$
	$\dfrac{\partial T(z=0)}{\partial z} = -\dfrac{\bar{c}(z=0)C_{p,gas}(z=0)u(z=0)(T_{inlet} - T(z=0))}{k_z(z=0)}$	$\dfrac{\partial T(z=L)}{\partial z} = 0$
	$u(z=0) = u_{inlet}$	$u(z=L) = u_{outlet} = 0$
Stream vars	$p(z=0) = p_{inlet}$	$\bar{c}_i(z=L) = \bar{c}_{i,outlet}$
		$T(z=L) = T_{outlet}$
		$p(z=L) = p_{outlet}$

These boundary conditions assume that the 8 variables $\bar{c}_{i,inlet}$, T_{inlet}, u_{inlet}, u_{outlet} are known. The 8 variables p_{inlet}, $\bar{c}_{i,outlet}$, T_{outlet}, p_{outlet} are assumed unknown.

2.10.5. Countercurrent pressurization step (RP)

Table 9: Boundary conditions for the countercurrent pressurization step (RP)

	$z = 0$	$z = L$
BC	$\dfrac{\partial \bar{c}_i(z=0)}{\partial z} = 0$	$\dfrac{\partial \bar{c}_i(z=L)}{\partial z} = -\dfrac{u(z=L)(\bar{c}_{i,outlet} - \bar{c}_i(z=L))}{D_{ax}(z=L)}$
	$\dfrac{\partial T(z=0)}{\partial z} = 0$	$\dfrac{\partial T(z=L)}{\partial z} = -\dfrac{\bar{c}(z=L)C_{p,gas}(z=L)u(z=L)(T_{outlet} - T(z=L))}{k_z(z=L)}$
	$u(z=0) = u_{inlet} = 0$	$p(z=L) = p_{outlet}$
Stream vars	$\bar{c}_i(z=0) = \bar{c}_{i,inlet}$	$u(z=L) = u_{outlet}$
	$T(z=0) = T_{inlet}$	
	$p(z=0) = p_{inlet}$	

These boundary conditions assume that the 8 variables u_{inlet}, $\bar{c}_{i,outlet}$, T_{outlet}, p_{outlet} are known. The 8 variables $\bar{c}_{i,inlet}$, T_{inlet}, p_{inlet}, u_{outlet} are assumed unknown.

2.11. Determination of parameters

It has been very challenging to find consistent parameters for the different expressions used in the model which with certainty can be said to describe the dynamic behaviour of the SEWGS reactor. As the objective is to model a SEWGS reactor which could be used industrially in an IGCC plant, several crude assumptions have been made when collecting

the parameters for both adsorption and WGS reactions. These assumptions will now be elaborated. For a full overview of parameters used in the model, please refer to Table 10.

It is assumed that the adsorbent particles and the catalyst particles are spherical and of the same diameter d_p. The particle diameter have been chosen to be 4.8 mm, taken from the SEWGS experimental work by Van Selow et al. [42], which utilizes the same adsorbent and catalyst. The reactor length and diameter used in their work were respectively 2 m and 38 mm.

The internal space of a packed bed reactor can be said to consist of the voids, which contains the gas in the reactor, and the solid parts of the adsorbent and catalyst particles. Since the particles themselves are porous, some of the total void volume in the reactor is inside the outer perimeter of the spherical particles. The void fractions ε_t, ε_b and ε_p describes the ratios between three different types of void volumes and either the total unfilled volume of the reactor column or the particle total volume. They are related to each other by the following relationship [3, 32]

$$\varepsilon_t = \varepsilon_b + \varepsilon_p(1 - \varepsilon_b) \tag{55}$$

The total void fraction ε_t includes both intra-particle voids and inter-particle voids. The inter-particle void fraction ε_b is the void volume between particles in the bed per volume of unfilled reactor, while the intra-particle void fraction ε_p is the void volume inside the particles in the bed per volume of particles. The total void fraction is then total void volume between particles and inside particles per volume of unfilled reactor. Please refer to Figure 10.
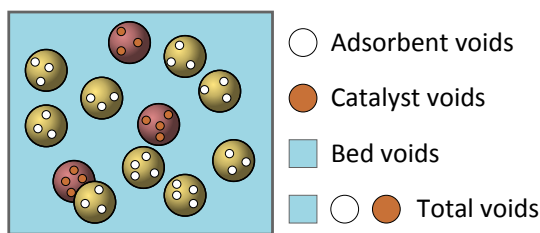

Figure 10: Relationships between the void fractions

However, since the particle void fractions of the adsorbent $\varepsilon_{p,ads}$ and catalyst $\varepsilon_{p,cat}$ particles are different, a modification is necessary. In the works on SEWGS modelling by Van Selow et al. [42], Allam et al. [2] and Hufton et al. [23], the volume of catalyst is much lower than the volume of adsorbent (1:5 volumetric ratio). In the present work, the mass of adsorbent and catalyst per reactor were found from the work by Wright et al. [44], please refer to Table 3. As no information could be found in the work by Wright et al. [44] on which volumetric ratio this corresponds to, it is assumed that these masses of catalyst and adsorbent gives a volumetric ratio of 1:5. By using this assumption about the volumetric ratio, the following expression is obtained

$$\varepsilon_t = \varepsilon_b + \varepsilon_{p,ads}(1 - \varepsilon_b) \cdot \frac{5}{6} + \varepsilon_{p,cat}(1 - \varepsilon_b) \cdot \frac{1}{6} \tag{56}$$

It has been difficult to find a consistent set of void fractions suitable for SEWGS reactor design, so the parameters had to be found from different sources, which is not ideal. The value of the total void fraction ε_t required in the SEWGS reactor is from the work by Allam et al. [2]. The adsorbent particle void fraction is from the experimental work on K-HTC adsorption kinetics by Ding and Alpay [12]. The catalyst particle void fraction is from an experimental work by Hoogschagen [22] on a WGS catalyst with similar composition ($Fe_2O_3 + 7\% \ Cr_2O_3$) as the catalyst used in to determine the reaction rate expression from Section 2.8.4. With these assumptions, the bed void fraction ε_b can then be derived using Eq. (56)

$$\varepsilon_b \approx 0.6286 \tag{57}$$

The bulk densities of adsorbent and catalyst in the reactor are determined using the mass of adsorbent and catalyst and the reactor dimensions from Table 3.

$$\rho_{b,ads} = \frac{Mass \ of \ adsorbent}{Total \ reactor \ volume} = \frac{44465 \ \text{kg}}{\pi \left(\dfrac{3.658 \ \text{m}}{2} \right)^2 \cdot 7.377 \ \text{m}} \tag{58}$$

$$\approx 573.5367 \ \text{kg adsorbent/m}^3 \ \text{reactor}$$

$$\rho_{b,cat} = \frac{Mass \ of \ catalyst}{Total \ reactor \ volume} = \frac{12927 \ \text{kg}}{\pi \left(\dfrac{3.658 \ \text{m}}{2} \right)^2 \cdot 7.377 \ \text{m}} \tag{59}$$

$$\approx 166.7404 \ \text{kg catalyst/m}^3 \ \text{reactor}$$

As discussed in Section 2.8.8, the expression for k_{LDF} in Eq. (46) is not utilized in the present model. A constant value $k_{LDF} \approx 0.05 \ \text{s}^{-1}$ is used instead. However, during the work process, some of the data necessary to utilize this expression was collected from literature. The adsorbent particle density $\rho_{p,ads}$ to be used in Eq. (46) was found from Xiu et al. [46], which employs the same adsorbent and same equation for k_{LDF} as Ding and Alpay [12]. This could be used in further work with the model, if it is chosen to utilize the expression in Eq. (46).

The specific heat capacity of the K-HTC adsorbent $C_{p,ads}$ is found from Ding and Alpay [12]. As no data for the specific heat capacity of the catalyst $C_{p,cat}$ could be found, it is assumed that this is equal to that of the adsorbent. This is a crude simplification.

There was not sufficient time to determine the molecular diffusion coefficient D_m which is to be used in Eq. (24). Therefore, a constant value of $D_{ax} = 5.0 \times 10^{-4}$ m^2/s, from the SE-SMR modelling work by Xiu et al. [46], was used. This is an obvious shortcoming to the model, as the axial dispersion coefficient is a function of velocity, temperature and composition. However, the velocity and temperature used by Xiu et al. [46] is 0.08 m/s and 723 K, which is in the same range as in the present work. The composition in an SE-SMR reactor is similar, the difference being the presence of methane CH$_4$.

As discussed in Section 2.8.3, the expressions for the overall heat transfer coefficient U could not be used. During preliminary work with single-reactor simulations using low feed flow rates giving Reynolds numbers below 20, the expression in Eq. (33) was valid. From these simulations, an average value of $U \approx 22.366$ W/(m$^2 \cdot$ K) was determined. This constant value was utilized in the subsequent simulations. This could have significant influence on the results, especially with respect to the high temperatures developed in the reactor due to the exothermic forward WGS reaction. The necessity of implementing a correlation or utilizing another constant for the value of U is something that should be investigated in further work with the model.

The parameters β_1, γ, Φ, e, k_g, k_s, a_{k_z} are used in the correlations for the thermal conductivity in Eq. (27) and the overall heat transfer coefficient in Eq. (33). The values for these parameters are found in the SE-SMR work by Ding and Alpay [13], which use a nickel-based steam-methane reforming catalyst. As these parameters are based on the physical properties of the particles in the reactor, to use these directly in the present work might not give correct results. The task of determining appropriate values for these parameters which are consistent with the materials used in the present work is something that should be worked further with.

According to [12], λ_s is the shape factor of the particles. Ding and Alpay [13] uses spherical particles, with $\lambda_s = 1.0$. This value will be used here as well.

It is assumed that the catalyst efficiencies (including stoichiometric coefficients) η_i for the reacting species CO$_2$ and H$_2$ are equal to 1, while for CO and H$_2$O equal to -1, as no other data could be found. This could influence the accuracy of the results.

A constant value for the gas-phase dynamic viscosity μ is used, from the work by Ding and Alpay [13]. This is a simplification, as the calculation of an average dynamic viscosity could easily have been carried out. It is possible to calculate μ using the Multiflash physical property package in gPROMS, and implement μ as a variable in gPROMS, instead of using a constant value. This is something that should be considered in further work with the model.

Parameters related to the expression for the equilibrium adsorbent capacity in Eqs. (39), (40) and (41), K_C^0, q_C, K_R^0, ΔH_R, m and a at temperature 400 °C are from the work by Lee

et al. [25].

The reactor wall is assumed to be kept at a constant temperature $T_{wall} = 673$ K.

Table 10: Reactor model parameters

Parameter	Value	Unit	Reference
a	2.5	-	[25]
a_{k_z}	0.5	-	[12]
$C_{p,ads}$	850	J/(kg adsorbent $\cdot$ K)	[12]
$C_{p,cat}$	850	J/(kg catalyst $\cdot$ K)	Section 2.11
D_{ax}	5.0×10^{-4}	m^2/s	Section 2.11
d_p	0.0048	m	[42]
d_t	3.658	m	[44]
e	0.35	-	[13]
ΔH_R	42132.88	J/mol	10.07 kcal/mol from [25]
K_C^0	8.6632×10^{-6}	Pa^{-1}	0.8778 atm^{-1} from [25]
k_g	0.09	J/(m $\cdot$ K)	[13]
k_{LDF}	0.05	s^{-1}	[26, 25]
K_R^0	$4.10027766 \times 10^{-16}$	Pa$^{-2.5}$	1.34×10^{-3} atm$^{-2.5}$ from [25]
k_s	0.3	J/(m $\cdot$ K)	[13]
L	7.377	m	[44]
m	0.25	mol/kg	[25]
q_C	21003.68	J/mol	5.02 kcal/mol from [25]
$\bar{R}$	8.314	J/(mol $\cdot$ K)	-
T_{wall}	673	K	Section 2.11
U	22.366	W/(m^2 $\cdot$ K)	Section 2.11
β_1	0.95	-	[13]
ε_b	0.6286	m^3 gas in bed/m^3 reactor	Eq. (57)
$\varepsilon_{p,ads}$	0.24	m^3 gas in particle/m^3 particle	[12]
$\varepsilon_{p,cat}$	0.6	m^3 gas in particle/m^3 particle	[22]
ε_t	0.74	m^3 gas/m^3 reactor	[2]
η_{CO_2}	1	-	Section 2.11
η_{H_2}	1	-	Section 2.11
η_{CO}	-1	-	Section 2.11
η_{H_2O}	-1	-	Section 2.11
η_{N_2}	0	-	Section 2.11
Φ	0.2	-	[13]
γ	0.667	-	[13]

λ_s	1.0	-	[13]
μ	2.87×10^{-5}	$Pa \cdot s$	[13]
$\rho_{b,ads}$	573.5367	kg adsorbent/m^3 reactor	Eq. (58)
$\rho_{b,cat}$	166.7404	kg catalyst/m^3 reactor	Eq. (59)
$\rho_{p,ads}$	1300	kg ads/m^3 ads particle	[46, 12]

3. Mathematical modelling: SEWGS system

3.1. Methodology for simulation of a multi-column PSA system

As discussed in Section 1.3, the syngas flow which is to be treated is splitted into 10 parts, equally divided and delivered to the 10 SEWGS trains. From a modelling perspective, it is reasonable to assume that the behaviour of every one of the 10 SEWGS trains, where each train consists of 8 reactors, is the same. This allows for modelling the behaviour of one SEWGS train, and multiplying the resulting flow rates by 10 to obtain the total system performance.

According to the objectives discussed in Section 1.3, the model should be able to account for changes in the syngas flow rate, that is, stream 4 in Table 2. Stream 4 is the mix of the syngas from the gasifier, stream 2, and the desired amount of steam added, stream 3. To give the possibility of changing the amount of steam that is added in stream 3, it is assumed that one SEWGS train receives two separate streams, one feed syngas stream and one stream containing steam. The syngas stream consists of one tenth of the syngas stream 2. The steam stream consists of one tenth of stream 3.

As the objective of the present work is to develop a model of the SEWGS system based on data and information available in the literature, the cycle steps and reactor configuration proposed by Wright et al. [45] will be utilized. The cycle consists of 11 separate steps which one reactor must undergo. With reference to Figure 7, it can be observed that in all steps except the depressurization (D) and purge (P) steps, there is interaction between the reactor and the other reactors in the system.

Liu et al. [28] carried out a simulation of a multi-column vacuum pressure-swing adsorption (VPSA) system. According to the authors, there are several approaches for such type of simulation. They suggest that the simplest approach is to simulate the behaviour of a single reactor, assuming fixed gas compositions for the streams which in reality is coming from other reactors. This functions as a simplification of the interactions between the reactors in the system. The resulting flow rates from the single reactor simulation could then be multiplied by the real number of reactors in the system to determine the behaviour of the complete system.

In the cycle utilized in the present work such assumptions would have to be made for the following steps:

- The feed step, where rinse gas from another reactor is mixed into the feed gas.

- The equalization and re-equalization steps, where gas is exchanged between two reactors.

- The repressurization step, where the reactor is repressurized using product gas from a reactor in the feed step.

The fixed gas compositions could be determined by simulating the operation of the single reactor throughout a complete cycle, then using results from the simulation to calculate approximate gas compositions and flow rates for the streams coming from other reactors.

This approach is quite simple in means of computational efforts. However, the reliability of the results is questionable, especially for the type of cycle and reactor interactions inherent in the cycle configuration used in the present work. If this approach was to be used, the aspect causing most concern is the interaction between the reactor being in the rinse step and those in the feed step. The amount of gas coming from the reactor being rinsed is the determining factor for how much new feed syngas that can be sent into the system without reaching breakthrough of CO_2 into the H_2 product.

Liu et al. [28] presents a more realistic approach; The modelling of the complete multi-column PSA system, with all the required connecting streams and valves. This approach is computationally much more requiring and difficult to solve. However, with the appropriate simplifications and solution strategy, the simulation results will be more accurate and reliable than for a single-reactor simulation. This approach takes into account all relevant interactions between the reactors in the system, and enables the possibility to investigate the stability of the PSA system over several cycles, and also the effect of changes in time in the feed conditions and compositions.

This latter approach is chosen for the present work, as the objective for later work is to use the model for the SEWGS system in an IGCC power plant model, where the dynamic behaviour and reliability of the total system is of significant interest.

The modelling of the SEWGS system of reactors consists of two parts. First, the mathematical model for the behaviour of the system must be developed, accounting for all the different flow patterns between the reactors for all points in time throughout the SEWGS cycle. When this has been established, the second part must be considered: the implementation of a operating schedule for the system as time passes, that is, running the system of reactors according to the SEWGS cycle in Figure 7. This operating schedule consists of aspects such as regulating the flow rates of feed syngas, steam for the feed, rinse and purge, and perhaps most importantly, the switching of the connections between the reactors and the change in boundary conditions of the reactors affected. This second part is mathematically quite complicated, and needs to be carried out carefully and thoroughly to ensure that the model is able to describe the actual physical behaviour of the system with appropriate accuracy, and that the simulation in the modelling software gPROMS is able to reach convergence.

Now, the first part will be presented: establishing a mathematical model for the SEWGS

system. Following this, the implementation of the model in gPROMS, and the closely related task of establishing an operating schedule, will be presented in Section 3.15.

3.2. *Identification of the different states of the SEWGS system*

One of the objectives of this thesis is to develop a modelling framework for the parallel operation of 8 individual SEWGS reactors, a SEWGS train, in accordance with the operating schedule presented in Figure 7. By inspecting the operating schedule, it can be seen that there is 16 different states that a system of 8 reactors can be in. These 16 different states will be referred to as *cycle state* 1 through 16. However, among these 16 cycle states, there are only 2 fundamentally different states that the system switches between, referred to as *system states*. Using cycle state 1 as an example of system state 1 and cycle state 2 as an example of system state 2, these two system states will now be elaborated on. Figure 11 defines the system border for the SEWGS train, with the relevant streams going in and out of the train.
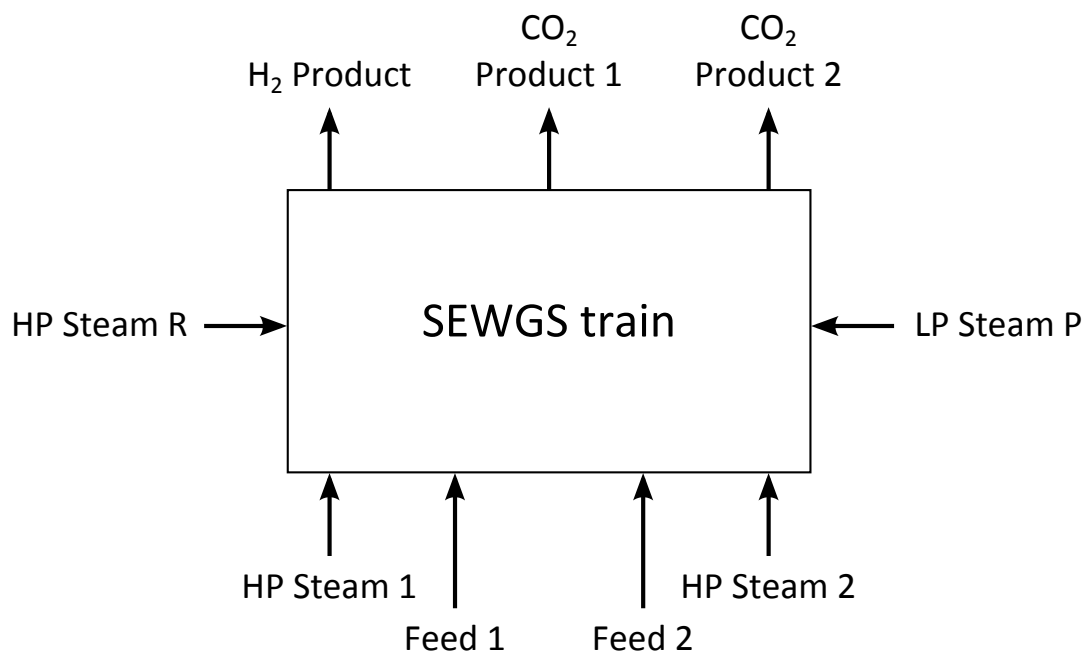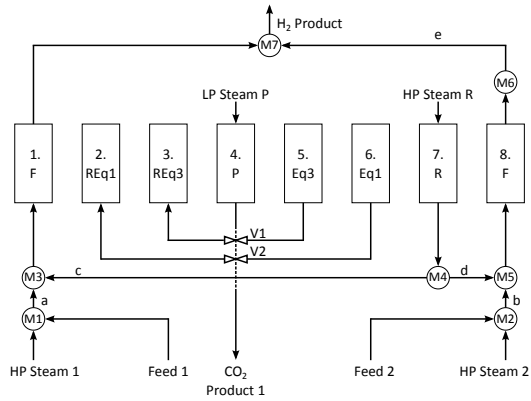

Figure 11: SEWGS train flow sheet

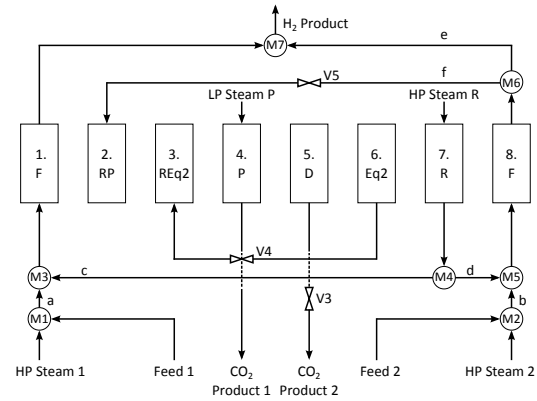**Figure 12:** System state 1 example.   External streams referred to Figure 11.

Figure 13: System state 2 example.   External streams referred to Figure 11.

The first state, referred to as system state 1, can be illustrated by the flow sheet in Figure 12, which shows the flows and interconnections between the system of reactors. System state 1 can be said to consist of:

- One reactor being in the first fourth of its feed step (F).

  The gas sent to the inlet of this reactor consists of feed syngas, appropriate amounts of steam and half of the gas exiting the inlet of the reactor being in the rinse step.

- One reactor being in the third fourth of its feed step (F).

  The gas sent to the inlet of this reactor consists of feed syngas, appropriate amounts of steam and half of the gas exiting the inlet of the reactor being in the rinse step.

- One reactor being in the first equalization step (Eq1).

  The inlet is connected through a valve with the inlet of the reactor in step REq1. Keeping the outlet closed, the gas will move countercurrently out of the reactor until the pressures in the two reactors are equalized. At the beginning of this step, the reactor pressure is approximately 26.89 bar, and ends up at a lower pressure of 20.443 bar.

- One reactor being in the third equalization step (Eq3).

  The inlet is connected through a valve with the inlet of the reactor in step REq3. Keeping the outlet closed, the gas will move countercurrently out of the reactor until the pressures in the two reactors are equalized. At the beginning of this step, the reactor pressure is approximately 13.995 bar, and ends up at a lower pressure of 7.5475 bar.

- One reactor being in the first re-equalization step (REq1).

  The inlet is connected through a valve with the inlet of the reactor in step Eq1.

Keeping the outlet closed, the reactor will receive gas cocurrently until the pressures in the two reactors are equalized. At the beginning of this step, the reactor pressure is approximately 13.995 bar, and ends up at a higher pressure of 20.443 bar.

- One reactor being in the third re-equalization step (REq3).

The inlet is connected through a valve with the inlet of the reactor in step Eq3. Keeping the outlet closed, the reactor will receive gas cocurrently until the pressures in the two reactors are equalized. At the beginning of this step, the reactor pressure is approximately 1.1 bar, and ends up at a higher pressure of 7.5475 bar.

- One reactor being in the first half of the rinse step (R).

The reactor is countercurrently being fed steam at a pressure of approximately 26.89 bar at the outlet. This will rinse out some of the hydrogen, CO_2 and other gases of the reactor. The gases leaving the reactor through the inlet is assumed to be splitted in two, one half being sent to each of the two reactors being in the feed step. The rinse step is not continued until all of the gases in the reactor at the end of the feed step is removed, only parts of it. The reason for this is that the residual gas, which contains significant amounts of valuable H_2, is transferred out of the reactor during the equalization steps with other reactors undergoing re-equalization. In this way, only small amounts of H_2 is lost in the CO_2 product streams leaving the system during the depressurization and purge steps [45].

- One reactor being in the first half of the purge step (P).

The reactor is being countercurrently purged of CO_2 by feeding steam at a pressure of approximately 1.1 bar. The low pressure allows the CO_2 previously adsorbed to be desorbed into the gas phase. The desorbed CO_2 is blown out of the reactor by the steam passing through the reactor. The gas leaving the reactor at the inlet mainly consists of CO_2 and steam. The steam is removed downstream by flashing, and the remaining high purity CO_2 can be sent to CO_2 handling and storage.

The second state, referred to as system state 2, can be illustrated by the flow sheet in Figure 13, which shows the flows and interconnections between the system of reactors. System state 2 can be said to consist of:

- One reactor being in the second fourth of its feed step (F).

The gas sent to the inlet of this reactor consists of feed syngas, appropriate amounts of steam and half of the gas exiting the inlet of the reactor being in the rinse step.

- One reactor being in the last fourth of its feed step (F).

The gas sent to the inlet of this reactor consists of feed syngas, appropriate amounts

of steam and half of the gas exiting the inlet of the reactor being in the rinse step. Some of the gas product at the outlet of this reactor is sent to the reactor undergoing repressurization. The rest is sent to the H_2 product stream. It is assumed that the pressure at the outlet of this reactor is 26.89 bar, irrespective of how much of the stream which is taken out for repressurization. If the flow rate taken out is large, then this could be an incorrect assumption.

- One reactor being in the second equalization step (Eq2).

  The inlet is connected through a valve with the inlet of the reactor in step REq2. Keeping the outlet closed, the gas will move countercurrently out of the reactor until the pressures in the two reactors are equalized. At the beginning of this step, the reactor pressure is approximately 20.443 bar, and ends up at a lower pressure of 13.995 bar.

- One reactor being in the second re-equalization step (REq2).

  The inlet is connected through a valve with the inlet of the reactor in step Eq2. Keeping the outlet closed, the reactor will receive gas cocurrently until the pressures in the two reactors are equalized. At the beginning of this step, the reactor pressure is approximately 7.5475 bar, and ends up at a higher pressure of 13.995 bar.

- One reactor being in the repressurization step (RP).

  Some of the outlet gas from the reactor being in the last fourth of its feed step, containing mainly hydrogen, is being sent countercurrently to this reactor until the pressure is increased to 26.89 bar.

- One reactor being in the depressurization step (D).

  Keeping the outlet closed, the gas in the reactor is countercurrently vented out through a valve at the inlet until the reactor pressure is lowered to 1.1 bar.

- One reactor being in the second half of the rinse step (R).

  The reactor is countercurrently being fed steam at a pressure of approximately 26.89 bar at the outlet. This will rinse out the hydrogen, CO_2 and other gases of the reactor, leaving mostly steam. The gases leaving the reactor through the inlet is assumed to be splitted in two, one half being sent to each of the two reactors being in the feed step. The rinse step is not continued until all of the gases in the reactor at the end of the feed step is removed, only parts of it. The reason for this is that the residual gas, which contains significant amounts of valuable H_2, is transferred out of the reactor during the equalization steps with other reactors undergoing re-equalization. In this way, only small amounts of H_2 is lost in the CO_2 product streams leaving the system during the depressurization and purge steps [45].

- One reactor being in the second half of the purge step (P).

  The reactor is being countercurrently purged of CO_2 by feeding steam at a pressure of approximately 1.1 bar. The low pressure allows the CO_2 previously adsorbed to be desorbed into the gas phase. The desorbed CO_2 is blown out of the reactor by the steam passing through the reactor. The gas leaving the reactor at the inlet mainly consists of CO_2 and steam. The steam is removed downstream by flashing, and the remaining high purity CO_2 can be sent to CO_2 handling and storage.

With reference to the SEWGS cycle shown in Figure 7, it can be seen that throughout the SEWGS cycle consisting of 16 cycle states, the system of reactors switches between system state 1 and 2. This can be visualized by Table 11.

Table 11: Cycle states with corresponding system states

Cycle state	1	2	3	4	5	6	7	8	9	10	11	12	13	14	15	16
System state	1	2	1	2	1	2	1	2	1	2	1	2	1	2	1	2

This discussion implies that the operation of the 8 reactors through the 16 cycle states can be described by two different sets of equations, one for each system state, which can be adapted into 16 sets of equations for the 16 cycle states. Using cycle states 1 and 2 as an example, the equations for system state 1 and 2 will now be presented. These two sets of equations will be adapted for the use in cycle states 3 through 16, without being presented explicitly in this text.

Now, it can be observed from the previous discussion that the SEWGS system of reactors undergoes a significant change when going from one cycle state to the next one. Taking the gas from the outlet of reactor 8 in Figures 12 and 13 as an example, some of this gas should be diverted to repressuarize reactor 2 as the system goes from cycle state 1 to 2. It is possible to model this by using a valve model, which is assumed closed in cycle state 1, and open in cycle state 2. However, a problem arises with the change in behaviour of reactor 2, which in cycle state 1 is being cocurrently re-equalized, and in cycle state 2 should be countercurrently be repressurized by reactor 8. In the real-world operation of this change, this is not a problem, as the change will be initiated by closing one valve at the inlet of reactor 2, and opening another at the outlet. However, from a modelling perspective, this change is problematic. The reason for this is that the change also requires a switch in the boundary conditions used by reactor 2, switching from those found in Table 8 to those in Table 9. These two sets of boundary conditions assume that some of the stream variables are known. However, the variables assumed to be known are not the same. This is mathematically problematic, as the system of equations must be recalculated after the change in boundary conditions. It is therefore not straightforward to

carry out this change in the reactor behaviour using valves.

The method of modelling the system using valves to control the flows is utilized in the work by Liu et al. [28], which also have implemented the system model using gPROMS. The authors do not report how they have solved the mathematical problem when boundary conditions are switched. In the work by Nikolic et al. [31], a generic model for a multi-column PSA system implemented in gPROMS is presented. The authors state that also they have used the same modelling method, utilizing valves for the interconnections between the reactor columns, which are opened and closed according to where the flows in the system should be directed. They do not however, explain how the switch in boundary conditions is handled computationally.

As a result of this lack of available information on the appropriate solution and implementation strategy in the modelling software gPROMS, a methodology has been developed in the present work. In the previous discussion, the fundamental differences in flow directions, connections between reactors, have been elaborated using the term system states. Now, the governing equations and assumptions necessary to describe the system behaviour in each of the two system states will be presented. These two sets of equations can be generalized to describe the system in each of the 16 cycle steps. Following this, the methodology for the implementation of these 16 sets of equations into gPROMS will be presented.

In the modelling of the SEWGS system of reactors carried out in this work, the main interest is the behaviour of the reactors. Therefore, it has been, in most cases, assumed that stream variables are transferred unchanged between physical components where interconnections are necessary. An example of this is the connection between the inlet of one reactor and a valve. In a real situation, pipes and valves, with corresponding losses and dynamics, will somewhat affect the behaviour of the system. In the modelling of the present work, the effect of pipes are not modelled. In the situation of connecting two points in the system at different pressures, a simple valve model has been utilized. This model determines the flow rate based on the pressure difference and a pre-defined valve characteristic. In the situation where streams should be mixed, mass and heat balances have been applied.

As the switching from one cycle state to the next one is to take place, several assumptions and simplifications have been necessary. At the end of one cycle state, some of the flow rates of the streams going into the SEWGS train system have been ramped down to zero. The system of equations have then been changed to those describing the system in the next cycle state. Then, the flow rates of the streams going into the system have been ramped up to their designated values, and the valves controlling the internal flows of the system have been opened by ramping up the valve opening to their desired position. The detailed

description of this switch is described in Section 3.15.

With system state 1 as illustrated in Figure 12 as an example, it can be seen that mathematically, the system consists of four independent subsystems. The most complicated one consists of reactors 1, 7 and 8. This subsystem will be presented first.

3.3. System state 1 - Subsystem 1

This subsystem consists of reactors 1, 7 and 8, together with the connected streams, splitters and mixers. The boundary conditions for reactor 1 and 8 is those for the cocurrent feed step found in Table 5, for reactor 7 the boundary conditions are those for the countercurrent rinse step found in Table 6.

3.3.1. Mixer M1

The stream Feed 1 in Figure 12 is assumed to have the same composition and temperature as stream 2 in Table 2. With reference to the discussion in Section 1.3, the flow rate of stream Feed 1 is then $1/(10 \cdot 2)$ of the flow rate of stream 2. Please refer to Table 13.

The stream HP Steam 1 in Figure 12 is assumed to have the same composition and temperature as stream 3 in Table 2. According to the discussion in Section 1.3, the flow rate of stream HP Steam 1 should be one tenth of the flow rate of stream 3. Please refer to Table 13. However, since the flow rate of the stream Feed 1 will be changed in later work, it is assumed the flow rate of stream HP Steam 1 should be determined as a function of the flow rate of stream Feed 1, such that the composition of stream a will be equal to that of stream 4 in Table 2.

It is assumed that the stream HP Steam 1 contains only steam, i.e. $y_{H_2O,HP\ Steam\ 1} = 1$. To determine how much steam that should be added to the syngas feed stream, a steam mole balance is used:

$$y_{H_2O,a} \cdot \dot{n}_a = y_{H_2O,Feed\ 1} \cdot \dot{n}_{Feed\ 1} + y_{H_2O,HP\ Steam\ 1} \cdot \dot{n}_{HP\ Steam\ 1} = y_{H_2O,Feed\ 1} \cdot \dot{n}_{Feed\ 1} + 1 \cdot \dot{n}_{HP\ Steam\ 1}$$

$$(60)$$

Since there is only steam in stream HP Steam 1, a mole balance on CO yields:

$$y_{CO,a} \cdot \dot{n}_a = y_{CO,Feed\ 1} \cdot \dot{n}_{Feed\ 1} \qquad (61)$$

A steam-to-CO ratio for stream a is defined:

$$S/CO = \frac{y_{H_2O,a}}{y_{CO,a}} \qquad (62)$$

Solving for $y_{H_2O,a}$ in Eq. (60) and $y_{CO,a}$ in Eq. (61) and inserting into Eq. (62) gives

$$S/CO = \frac{y_{H_2O,Feed\ 1} \cdot \dot{n}_{Feed\ 1} + \dot{n}_{HP\ Steam\ 1}}{y_{CO,Feed\ 1} \cdot \dot{n}_{Feed\ 1}} \tag{63}$$

Solving for $\dot{n}_{HP\ Steam\ 1}$

$$\dot{n}_{HP\ Steam\ 1} = S/CO \cdot y_{CO,Feed\ 1} \cdot \dot{n}_{Feed\ 1} - y_{H_2O,Feed\ 1} \cdot \dot{n}_{Feed\ 1} \tag{64}$$

This equation determines the amount of steam necessary to achieve a steam-to-CO ratio of S/CO in stream a. According to Table 2, $S/CO = 0.5357/0.2799 \approx 1.9139$. This is the value that will be used in the simulations in the present work. To account for changes in the composition of stream Feed 1, a check that the value of $\dot{n}_{HP\ Steam\ 1}$ determined by Eq. (64) is larger than zero. If not, the amount of steam added $\dot{n}_{HP\ Steam\ 1}$ is set to zero. The model of mixer M1 assumes that the temperature of the high pressure steam always is the same as the feed temperature.

Now, the equations defining the behaviour of mixer M1 can be formulated as follows:

$$\dot{n}_a = \dot{n}_{HP\ Steam\ 1} + \dot{n}_{Feed\ 1} \tag{65}$$

$$\dot{n}_a y_{i,a} = \dot{n}_{HP\ Steam\ 1} y_{i,HP\ Steam\ 1} + \dot{n}_{Feed\ 1} y_{i,Feed\ 1} \tag{66}$$

$$p_a = p_{Feed\ 1} \tag{67}$$

$$p_{HP\ Steam\ 1} = p_{Feed\ 1} \tag{68}$$

$$T_a = T_{Feed\ 1} \tag{69}$$

$$T_{HP\ Steam\ 1} = T_{Feed\ 1} \tag{70}$$

IF $S/CO \cdot y_{CO,Feed\ 1} \cdot \dot{n}_{Feed\ 1} - y_{H_2O,Feed\ 1} \cdot \dot{n}_{Feed\ 1} > 0$ THEN

$$\dot{n}_{HP\ Steam\ 1} = S/CO \cdot y_{CO,Feed\ 1} \cdot \dot{n}_{Feed\ 1} - y_{H_2O,Feed\ 1} \cdot \dot{n}_{Feed\ 1} \tag{71}$$

ELSE
$$\dot{n}_{HP\ Steam\ 1} = 0 \tag{72}$$

END IF

This model consists of 11 equations, with 12 known variables: $y_{i,HP\ Steam\ 1}$, $\dot{n}_{Feed\ 1}$, $y_{i,Feed\ 1}$, $T_{Feed\ 1}$.

3.3.2. Mixer M2

It is assumed that the temperature of the high pressure steam always is the same as the feed temperature. The flow rate of steam added $\dot{n}_{HP\ Steam\ 2}$ is determined using the same method as discussed in Section 3.3.1.

Equations defining the behaviour of mixer M2:

$$\dot{n}_b = \dot{n}_{HP\ Steam\ 2} + \dot{n}_{Feed\ 2} \tag{73}$$

$$\dot{n}_b y_{i,b} = \dot{n}_{HP\ Steam\ 2} y_{i,HP\ Steam\ 2} + \dot{n}_{Feed\ 2} y_{i,Feed\ 2} \tag{74}$$

$$p_b = p_{Feed\ 2} \tag{75}$$

$$p_{HP\ Steam\ 2} = p_{Feed\ 2} \tag{76}$$

$$T_b = T_{Feed\ 2} \tag{77}$$

$$T_{HP\ Steam\ 2} = T_{Feed\ 2} \tag{78}$$

IF $S/CO \cdot y_{CO,Feed\ 2} \cdot \dot{n}_{Feed\ 2} - y_{H_2O,Feed\ 2} \cdot \dot{n}_{Feed\ 2} > 0$ THEN

$$\dot{n}_{HP\ Steam\ 2} = S/CO \cdot y_{CO,Feed\ 2} \cdot \dot{n}_{Feed\ 2} - y_{H_2O,Feed\ 2} \cdot \dot{n}_{Feed\ 2} \tag{79}$$

ELSE
$$\dot{n}_{HP\ Steam\ 2} = 0 \tag{80}$$

END IF

This model consists of 11 equations, with 12 known variables: $y_{i,HP\ Steam\ 2}$, $\dot{n}_{Feed\ 2}$, $y_{i,Feed\ 2}$, $T_{Feed\ 2}$.

3.3.3. Mixer M3

This model assumes no direct relation between pressure p_c and the other two pressures, although they are related through an enthalpy balance. This is a necessary simplification, as the pressure in stream c is determined by the pressure at the inlet of reactor 8. Please refer to Section 3.3.5 for details. The pressure in stream c is therefore assumed to be different than the pressure in stream a and at the inlet of reactor 1. The difference is only minor, as the flow rates through reactors 1 and 8, which are in the feed step, are similar. This implies that the pressure drop is also similar. The flow rate $\dot{n}_c$ is negative.

$$\dot{n}_{inlet,1} = \dot{n}_a - \dot{n}_c \tag{81}$$

$$\dot{n}_{inlet,1} y_{i,inlet,1} = \dot{n}_a y_{i,a} - \dot{n}_c y_{i,c} \tag{82}$$

$$\dot{n}_{inlet,1} \bar{h}_{inlet,1} = \dot{n}_a \bar{h}_a - \dot{n}_c \bar{h}_c \tag{83}$$

$$p_{inlet,1} = p_a \tag{84}$$

The enthalpies $\bar{h}$ are evaluated using the gPROMS physical property interface Multiflash. This model consists of 8 equations.

3.3.4. Mixer M4

The flow rate $\dot{n}_{inlet,7}$ coming from reactor 7 is negative. This is because the reactor is in the countercurrent rinse stage, where the reactor model by definition uses negative flow rates.

$$\dot{n}_c = \frac{1}{2}\dot{n}_{inlet,7} \tag{85}$$

$$y_{i,c} = y_{i,inlet,7} \tag{86}$$

$$T_c = T_{inlet,7} \tag{87}$$

$$p_c = p_{inlet,7} \tag{88}$$

$$\dot{n}_d = \frac{1}{2}\dot{n}_{inlet,7} \tag{89}$$

$$y_{i,d} = y_{i,inlet,7} \tag{90}$$

$$T_d = T_{inlet,7} \tag{91}$$

$$p_d = p_{inlet,7} \tag{92}$$

This model consists of 16 equations.

3.3.5. Mixer M5

Modelled in almost the same way as mixer M3. However, in this model there is a direct relation between pressure p_d and the pressure at the inlet of reactor 8. The flow rate $\dot{n}_d$ is negative.

$$\dot{n}_{inlet,8} = \dot{n}_b - \dot{n}_d \tag{93}$$

$$\dot{n}_{inlet,8}y_{i,inlet,8} = \dot{n}_b y_{i,b} - \dot{n}_d y_{i,d} \tag{94}$$

$$\dot{n}_{inlet,8}\bar{h}_{inlet,8} = \dot{n}_b\bar{h}_b - \dot{n}_d\bar{h}_d \tag{95}$$

$$p_{inlet,8} = p_b \tag{96}$$

$$p_{inlet,8} = p_d \tag{97}$$

The enthalpies $\bar{h}$ are evaluated using the gPROMS physical property interface Multiflash.

This model consists of 9 equations.

3.3.6. Splitter M6

The variables in stream e are equated to the outlet variables from reactor 8.

$$\dot{n}_e = \dot{n}_{outlet,8} \tag{98}$$

$$y_{i,e} = y_{i,outlet,8} \tag{99}$$

$$T_e = T_{outlet,8} \tag{100}$$

$$p_e = p_{outlet,8} \tag{101}$$

This model consists of 8 equations.

3.3.7. Mixer M7

$$\dot{n}_{H_2 \ Product} = \dot{n}_{outlet,1} + \dot{n}_e \tag{102}$$

$$\dot{n}_{H_2 \ Product} y_{H_2 \ Product} = \dot{n}_{outlet,1} y_{i,outlet,1} + \dot{n}_e y_{i,e} \tag{103}$$

$$\dot{n}_{H_2 \ Product} \bar{h}_{H_2 \ Product} = \dot{n}_{outlet,1} \bar{h}_{outlet,1} + \dot{n}_e \bar{h}_e \tag{104}$$

$$p_{H_2 \ Product} = p_{outlet,1} \tag{105}$$

$$p_{H_2 \ Product} = p_e \tag{106}$$

The enthalpies $\bar{h}$ are evaluated using the gPROMS physical property interface Multiflash.

This model consists of 9 equations, with 1 known variable: $p_{H_2 \ Product}$. The value of $p_{H_2 \ Product}$ can be found in Table 13.

3.3.8. Reactor model equations

For each of the three reactors in this subsystem, reactors 1, 7 and 8, the reactor model provides 8 equations relating the inlet stream variables to the outlet stream variables.

The values of $\dot{n}_{outlet,7}$, $y_{i,outlet,7}$, $T_{outlet,7}$ for reactor 7, which is in the rinse stage, are equal to $-\dot{n}_{HP \ Steam \ R}$, $y_{i,HP \ Steam \ R}$, $T_{HP \ Steam \ R}$ found in Table 13. The value of the flow rate at the outlet of reactor 7, $\dot{n}_{outlet,7}$, is assumed to be equal to $-\dot{n}_{HP \ Steam \ R}$ since the reactor model assumes negative flow rates during the countercurrent rinse stage.

3.3.9. Summary

Subsystem 1 consists of 96 equations. The number of variables are equal to 16 streams · 8 stream variables = 128 stream variables. There are 32 known variables: $\dot{n}_{Feed \ 1}$, $y_{i,Feed \ 1}$, $T_{Feed \ 1}$, $\dot{n}_{Feed \ 1}$, $y_{i,Feed \ 1}$, $T_{Feed \ 1}$, $y_{i,HP \ Steam \ 1}$, $y_{i,HP \ Steam \ 2}$, $\dot{n}_{HP \ Steam \ R}$, $y_{i,HP \ Steam \ R}$,

$T_{HP\ Steam\ R}$, $p_{H_2\ Product}$. Please refer to Table 13 for values. The subsystem consists of 128 variables - 96 equations - 32 known variables = 0 degrees of freedom.

3.4. System state 1 - Subsystem 2

This subsystem consists of reactors 2 and 6 and the connecting valve V2. The boundary conditions for reactor 6 are those for the countercurrent equalization step found in Table 7, for reactor 2 the boundary conditions are those for the cocurrent re-equalization step found in Table 8.

3.4.1. Valve V2

The valve is modelled by a using simple valve characteristic to determine the flow rate through the valve as a function of the pressure difference. The following variables are defined: flow rate $\dot{n}_{valve}$, valve opening (stem position) x_{valve} and pressure difference Δp. The flow rate $\dot{n}_{inlet,6}$ is negative, because of the countercurrent flow in reactor 6. Two parameters describe the valve characteristic, a flow coefficient and a flow exponent. The flow coefficient has been determined by trial and error, which is not ideal. This is something that could be improved in later work. The valve is assumed to be isenthalpic.

$$\dot{n}_{valve} = -\dot{n}_{inlet,6} \tag{107}$$

$$\dot{n}_{valve} = \dot{n}_{inlet,2} \tag{108}$$

$$y_{i,inlet,6} = y_{i,inlet,2} \tag{109}$$

$$\bar{h}_{inlet,6} = \bar{h}_{inlet,2} \tag{110}$$

$$\Delta p = p_{inlet,6} - p_{inlet,2} \tag{111}$$

$$\dot{n}_{valve} = x_{valve} \cdot \left(Flow\ coefficient \cdot |\Delta p|\right)^{1/Flow\ exponent} \cdot SIGN(\Delta p) \tag{112}$$

This model consists of 10 equations, with 2 known parameters:

$$Flow\ coefficient = 0.001\ \text{mol}/(\text{s} \cdot \text{Pa}) \tag{113}$$

$$Flow\ exponent = 1 \tag{114}$$

3.4.2. Reactor model equations

Since the outlets of both reactor 2 and 6 are assumed closed, the stream variables $\dot{n}_{outlet,2}$ and $\dot{n}_{outlet,6}$ are known to be zero. Because the flow rate is zero, the remaining stream variables at the outlet of these reactors are not of interest. However, from a mathematical point of view, it is necessary to define these variables. Therefore, equations for these variables are included in the model, although they do not have any effect on the solution.

For reactor 6, two equations are included in the boundary conditions and stream equations given in Table 7:

$$u(z = L) = \dot{n}_{outlet,6}\bar{R}T_{outlet,6}/(p_{outlet,6}\pi(d_t/2)^2) \tag{115}$$

$$p(z = L) = p_{outlet,6} \tag{116}$$

where the 7 variables $\dot{n}_{outlet,6}$, $y_{i,outlet,6}$ and $T_{outlet,6}$ are assumed known. $y_{i,outlet,6}$ and $T_{outlet,6}$ are set to arbitrary values.

However, with the perspective of reactor 6 as a model with an inlet and an outlet, there are 8 equations relating the inlet stream variables to the outlet stream variables. This is valid although six of the stream variables at the outlet are not utilized internally in the reactor model.

For reactor 2, eight equations are included in the boundary conditions and stream equations given in Table 8:

$$u(z = L) = \dot{n}_{outlet,2}\bar{R}T_{outlet,2}/(p_{outlet,2}\pi(d_t/2)^2) \tag{117}$$

$$\bar{c}_i(z = L) = y_{i,outlet,2}p_{outlet,2}/(\bar{R}T_{outlet,2}) \tag{118}$$

$$T(z = L) = T_{outlet,2} \tag{119}$$

$$p(z = L) = p_{outlet,2} \tag{120}$$

where 1 variable $\dot{n}_{outlet,2}$ is assumed known. This means that there are 8 equations relating the inlet stream variables to the outlet stream variables.

3.4.3. Summary

Subsystem 2 consists of $10 + 8 + 8 = 26$ equations. The number of variables are equal to the stream variables 4 streams · 8 stream variables = 32 stream variables plus 3 valve variables, which gives in total 35 variables. There are 9 known variables: $\dot{n}_{outlet,6} = 0$, $y_{i,outlet,6} = 0.2$, $T_{outlet,6} = 673$, $\dot{n}_{outlet,2} = 0$, x_{valve}. The subsystem consists of 35 variables - 26 equations - 9 known variables = 0 degrees of freedom.

3.5. System state 1 - Subsystem 3

This subsystem consists of reactors 3 and 5 and the connecting valve V1. The boundary conditions for reactor 5 are those for the countercurrent equalization step found in Table 7, for reactor 3 the boundary conditions are those for the cocurrent re-equalization step found in Table 8.

The same type of equations and variables as for subsystem 2 is valid for this subsystem. This means that subsystem 3 consists of $10 + 8 + 8 = 26$ equations. The number of

variables are equal to the stream variables 4 streams · 8 stream variables = 32 stream variables plus 3 valve variables, which gives in total 35 variables. There are 9 known variables: $\dot{n}_{outlet,5} = 0$, $y_{i,outlet,5} = 0.2$, $T_{outlet,5} = 673$, $\dot{n}_{outlet,3} = 0$, x_{valve}. The subsystem consists of 35 variables - 26 equations - 9 known variables = 0 degrees of freedom.

3.6. System state 1 - Subsystem 4

This subsystem consists of only reactor 4. The boundary conditions for reactor 4, which is in the purge step, can be found in Table 6. These boundary conditions assume that the 8 stream variables $\dot{n}_{outlet,4}$, $y_{i,outlet,4}$, $T_{outlet,4}$ and $p_{inlet,4}$ are known. $\dot{n}_{outlet,4}$, $y_{i,outlet,4}$, $T_{outlet,4}$ and $p_{inlet,4}$ are assumed equal to $-\dot{n}_{LP\ Steam\ P}$, $y_{i,LP\ Steam\ P}$, $T_{LP\ Steam\ P}$ and $p_{CO_2\ Product\ 1}$ in Table 13. The 8 stream variables $p_{outlet,4}$, $\dot{n}_{inlet,4}$, $y_{i,inlet,4}$ and $T_{inlet,4}$ are unknowns. The reactor model provide 8 equations relating the inlet stream variables to the outlet stream variables.

This means that subsystem 4 consists of 8 equations. The number of variables are equal to the stream variables 2 streams · 8 stream variables = 16 stream variables. There are 8 known variables. The subsystem consists of 16 variables - 8 equations - 8 known variables = 0 degrees of freedom.

3.7. System state 1 - Summary

System state 1 consists of four subsystems. The total number of equations are 96 + 26 + 26 + 8 = 156 equations. The number of variables are equal to the stream variables 26 streams · 8 stream variables = 208 stream variables plus 6 valve variables, which gives in total 214 variables. There are 32 + 9 + 9 + 8 = 58 known variables. System state 1 consists of 214 variables - 156 equations - 58 known variables = 0 degrees of freedom.

3.8. System state 2 - Subsystem 1

This subsystem is based on subsystem 1 in system state 1, but with the addition of reactor 2 and valve V5. The extension of the system to include this extra part requires some changes in the definition and behaviour of splitter M6 and mixer M7. The remaining equations are kept unchanged.

The boundary conditions for reactor 1 and 8 is those for the cocurrent feed step found in Table 5, reactor 2 uses those for the countercurrent pressurization step found in Table 9, reactor 7 uses those for the countercurrent rinse step found in Table 6.

3.8.1. Splitter M6

With reference to the flow sheet in Figure 13, this splitter should determine the flow rate of gas going to the product stream $\dot{n}_e$ as the inlet flow rate $\dot{n}_{outlet,8}$ minus the flow rate of gas being sent to repressuarize reactor 2 $\dot{n}_f$. However, to be able to implement the equations in gPROMS, it is chosen to take a different approach.

In system state 1, splitter M6 is described by 8 equations, relating every stream variable in the stream from the outlet of reactor 8 to those in stream e going to mixer M7. In system state 2, the same is done for stream f, leaving stream e undefined:

$$\dot{n}_f = \dot{n}_{outlet,8} \tag{121}$$

$$y_{i,f} = y_{i,outlet,8} \tag{122}$$

$$T_f = T_{outlet,8} \tag{123}$$

$$p_f = p_{outlet,8} \tag{124}$$

It can be seen from Eq. 121 that all of the gas from the outlet of reactor 8 is sent to repressuarize reactor 2, which is not realistic, since this flow rate should be a function of the pressure difference. However, as it shall be seen in the modelling of valve V5 in Section 3.8.2, the value of this flow rate is not utilized.

This model consists of 8 equations.

3.8.2. Valve V5

The valve is modelled somewhat different than the other valves. The function of the valve is to allow a fraction of the gas coming from the outlet of reactor 8 to flow to the outlet of reactor 2, which is to be repressurized. The valve is assumed to function as a throttle valve. That is, the inlet pressure, equal to the pressure at splitter M6 and thus the outlet of reactor 8, is assumed to be constant. The reason for this assumption is that the flow rate through this valve should be small compared to the flow rate of gas from the outlet of reactor 8. In addition, it is necessary from a mathematical modelling perspective to assume this pressure to be known, as the boundary conditions of reactor 8 are those for the cocurrent feed step found in Table 5.

When the pressure at the inlet of the valve is assumed constant and known, all 8 stream variables in stream f and thus in the outlet stream from reactor 8 are determined. This implies that the equations describing the valve can be used to determine all 8 stream variables in the outlet stream from reactor 2.

As for the other valves, the valve is modelled using the same simple valve characteristic to determine the flow rate through the valve as a function of the pressure difference. The

following variables are defined: flow rate $\dot{n}_{valve}$, valve opening (stem position) x_{valve} and pressure difference Δp. The flow rate $\dot{n}_{outlet,2}$ is negative, because of the countercurrent flow in reactor 2. Two parameters describe the valve characteristic, a flow coefficient and a flow exponent. The valve is assumed to be isenthalpic.

However, the flow rate going to reactor 2 $\dot{n}_{valve}$ cannot be larger than the flow rate from the outlet of reactor 8 $\dot{n}_{outlet,8}$. If the flow rate implied by the pressure difference and valve characteristic is larger than what is possible, the flow rate $\dot{n}_{valve}$ is set to be equal to that coming from reactor 8 $\dot{n}_{outlet,8}$.

Using the assumptions outlined above, the model equations for the valve can formulated as follows:

$$y_{i,outlet,2} = y_{i,f} \tag{125}$$

$$\bar{h}_{outlet,2} = \bar{h}_f \tag{126}$$

$$p_f = p_{\text{H}_2 \text{ Product}} = 2689000 \text{ Pa} \tag{127}$$

$$\Delta p = p_f - p_{outlet,2} \tag{128}$$

$$\dot{n}_{valve} = -\dot{n}_{outlet,2} \tag{129}$$

IF $x_{valve} \cdot (Flow\ coefficient \cdot |\Delta p|)^{1/Flow\ exponent} \cdot SIGN(\Delta p) < \dot{n}_{outlet,8}$ THEN

$$\dot{n}_{valve} = x_{valve} \cdot (Flow\ coefficient \cdot |\Delta p|)^{1/Flow\ exponent} \cdot SIGN(\Delta p) \tag{130}$$

ELSE
$$\dot{n}_{valve} = \dot{n}_{outlet,8} \tag{131}$$

END IF

This model consists of 10 equations, with 2 known parameters:

$$Flow\ coefficient = 0.001 \text{ mol}/(\text{s} \cdot \text{Pa}) \tag{132}$$

$$Flow\ exponent = 1 \tag{133}$$

However, as will be shown through the discussion of the implementation of the model in gPROMS in Section 3.15, it is necessary to switch these equations with another set of equations during the last part of the repressurization step. These are similar, the difference

being that the flow rate through the valve is set to zero:

$$y_{i,outlet,2} = y_{i,f} \tag{134}$$

$$\bar{h}_{outlet,2} = \bar{h}_f \tag{135}$$

$$p_f = p_{H_2\ Product} = 2689000\ \text{Pa} \tag{136}$$

$$\Delta p = p_f - p_{outlet,2} \tag{137}$$

$$\dot{n}_{valve} = -\dot{n}_{outlet,2} \tag{138}$$

$$\dot{n}_{valve} = 0 \tag{139}$$

10 equations.

3.8.3. Mixer M7

As the discussion above have shown, stream e has not been determined. It will not be defined explicitly, but will be utilized implicitly in the mathematical description of mixer M7. $\dot{n}_f$ can be formulated as the flow rate $\dot{n}_{outlet,8}$ minus the absolute value of $\dot{n}_{outlet,2}$. The mole fractions $y_{i,f}$, temperature T_f and pressure p_f in stream f are assumed to be equal to the values in the outlet stream from reactor 8.

$$\dot{n}_{H_2\ Product} = \dot{n}_{outlet,1} + \left(\dot{n}_{outlet,8} + \dot{n}_{outlet,2} \right) \tag{140}$$

$$\dot{n}_{H_2\ Product} y_{H_2\ Product} = \dot{n}_{outlet,1} y_{i,outlet,1} + \left(\dot{n}_{outlet,8} + \dot{n}_{outlet,2} \right) y_{i,outlet,8} \tag{141}$$

$$\dot{n}_{H_2\ Product} \bar{h}_{H_2\ Product} = \dot{n}_{outlet,1} \bar{h}_{outlet,1} + \left(\dot{n}_{outlet,8} + \dot{n}_{outlet,2} \right) \bar{h}_{outlet,8} \tag{142}$$

$$p_{H_2\ Product} = p_{outlet,1} \tag{143}$$

The enthalpies $\bar{h}$ are evaluated using the gPROMS physical property interface MULTI-FLASH.

The following equation is not utilized

$$p_{H_2\ Product} = p_{outlet,8} \tag{144}$$

as the pressure at the outlet of reactor 8 is determined, in the mathematical description of the system, from the model equations describing valve V5. It is however, a valid relationship.

This model consists of 8 equations.

3.8.4. Reactor model equations

For each of the three reactors in this subsystem, reactors 1, 2, 7 and 8, there are 8 equations relating the inlet stream variables to the outlet stream variables.

The values of $\dot{n}_{outlet,7}$, $y_{i,outlet,7}$, $T_{outlet,7}$ for reactor 7, which is in the rinse stage, are equal to $-\dot{n}_{HP\ Steam\ R}$, $y_{i,HP\ Steam\ R}$, $T_{HP\ Steam\ R}$ found in Table 13. The value of the flow rate at the outlet of reactor 7, $\dot{n}_{outlet,7}$, is assumed to be equal to $-\dot{n}_{HP\ Steam\ R}$ since the reactor model assumes negative flow rates during the countercurrent rinse stage.

The inlet of reactor 2 is kept closed, and this means that the flow rate $\dot{n}_{inlet,2}$ is assumed known and set to zero.

3.8.5. Summary

Subsystem 1 consists of 113 equations. The number of variables are equal to the stream variables 18 streams · 8 stream variables = 144 stream variables (Stream e not included) plus 3 valve variables, which gives in total 147 variables. There are 34 known variables: $\dot{n}_{Feed\ 1}$, $y_{i,Feed\ 1}$, $T_{Feed\ 1}$, $\dot{n}_{Feed\ 2}$, $y_{i,Feed\ 2}$, $T_{Feed\ 2}$, $y_{i,HP\ Steam\ 1}$, $y_{i,HP\ Steam\ 2}$, $\dot{n}_{HP\ Steam\ R}$, $y_{i,HP\ Steam\ R}$, $T_{HP\ Steam\ R}$, $p_{H_2\ Product}$, $\dot{n}_{inlet,2} = 0$, x_{valve}. Please refer to Table 13 for values. The subsystem consists of 147 variables - 113 equations - 34 known variables = 0 degrees of freedom.

3.9. System state 2 - Subsystem 2

This subsystem consists of reactors 3 and 6 and the connecting valve V4. The boundary conditions for reactor 6 is those for the countercurrent equalization step found in Table 7, reactor 3 uses those for the cocurrent re-equalization step found in Table 8.

The same type of equations and variables as for subsystem 2 in system state 1 is valid for this subsystem, with the flow rate at the outlet of reactor 6 $\dot{n}_{outlet,6}$ set to zero. The 7 variables $\dot{n}_{outlet,6}$, $y_{i,outlet,6}$ and $T_{outlet,6}$ are assumed known. $y_{i,outlet,6}$ and $T_{outlet,6}$ are set to arbitrary values. $\dot{n}_{outlet,3}$ is set to zero.

Subsystem 2 consists of 10 + 8 + 8 = 26 equations. The number of variables are equal to the stream variables 4 streams · 8 stream variables = 32 stream variables plus 3 valve variables, which gives in total 35 variables. There are 9 known variables: $\dot{n}_{outlet,6} = 0$, $y_{i,outlet,6} = 0.2$, $T_{outlet,6} = 673$, $\dot{n}_{outlet,3} = 0$, x_{valve}. The subsystem consists of 35 variables - 26 equations - 9 known variables = 0 degrees of freedom.

3.10. System state 2 - Subsystem 3

This subsystem consists of reactor 5 and the connecting valve V3. The boundary conditions for reactor 5 is those for the countercurrent depressurization step found in Table 7, with the flow rate at the outlet of reactor 5 $\dot{n}_{outlet,5}$ set to zero. The 7 variables $\dot{n}_{outlet,5}$, $y_{i,outlet,5}$ and $T_{outlet,5}$ are assumed known. $y_{i,outlet,5}$ and $T_{outlet,5}$ are set to arbitrary values.

The equations for valve V3 is equal to those for valve V4. The pressure in the stream CO_2 Product 2 in Figure 13, $p_{CO_2\ Product\ 2}$, is assumed known and can be found in Table 13.

Subsystem 3 consists of $8 + 10 = 18$ equations. The number of variables are equal to the stream variables 3 streams $\cdot$ 8 stream variables = 24 stream variables plus 3 valve variables, which gives in total 27 variables. There are 9 known variables: $\dot{n}_{outlet,5} = 0$, $y_{i,outlet,5} = 0.2$, $T_{outlet,5} = 673$, $p_{CO_2\ Product\ 2}$, x_{valve}. The subsystem consists of 27 variables - 18 equations - 9 known variables = 0 degrees of freedom.

3.11. System state 2 - Subsystem 4

This subsystem consists of only reactor 4. The boundary conditions for reactor 4, which is in the purge stage, can be found in Table 6. These boundary conditions assume that the 8 stream variables $\dot{n}_{outlet,4}$, $y_{i,outlet,4}$, $T_{outlet,4}$ and $p_{inlet,4}$ are known. $\dot{n}_{outlet,4}$, $y_{i,outlet,4}$, $T_{outlet,4}$ and $p_{inlet,4}$ are assumed equal to $-\dot{n}_{LP\ Steam\ P}$, $y_{i,LP\ Steam\ P}$, $T_{LP\ Steam\ P}$ and $p_{CO_2\ Product\ 1}$ in Table 13. The 8 stream variables $p_{outlet,4}$, $\dot{n}_{inlet,4}$, $y_{i,inlet,4}$ and $T_{inlet,4}$ are unknowns. The reactor model provide 8 equations relating the inlet stream variables to the outlet stream variables.

Subsystem 4 consists of 8 equations. The number of variables are equal to the stream variables 2 streams $\cdot$ 8 stream variables = 16 stream variables. There are 8 known variables. The subsystem consists of 16 variables - 8 equations - 8 known variables = 0 degrees of freedom.

3.12. System state 2 - Summary

System state 2 consists of four subsystems. The total number of equations are $113 + 26 + 18 + 8 = 165$ equations. The number of variables are equal to the stream variables 27 streams $\cdot$ 8 stream variables = 216 stream variables (Stream e not included) plus 9 valve variables, which gives in total 225 variables. There are $34 + 9 + 9 + 8 = 60$ known variables. System state 2 consists of 225 variables - 165 equations - 60 known variables = 0 degrees of freedom.

3.13. Comparison of system states 1 and 2

As shown by Table 12, the number of variables, equations and known variables are different in the two system states. This has to be taken into account when the equation sets for the 16 cycle states are to be implemented in the simulation software gPROMS.

Table 12: Number of variables, equations and known variables in system states 1 and 2

	System state 1	System state 2
Number of variables	214	225
Number of equations	156	165
Number of known variables	58	60

3.14. Parameters for the system model

The pressure of the H_2 product stream is assumed to be 26.89 bar. The pressure of the CO_2 product streams is assumed to be 1.1 bar. However, as shall be seen in Section 3.15, the pressure of the stream CO_2 Product 1 was modified slightly.

To be able to reach convergence in the simulations in gPROMS, the composition of the rinse steam in stream HP Steam R and the purge steam in stream LP Steam P was assumed to not only contain steam, but very small amounts of the other four components. See Table 13 for the mole fractions of these two streams. The required rinse and purge steam flow rates were determined from the simulations. The temperature of both rinse and purge steam was assumed to be 673 K.

The cycle time of the SEWGS cycle has been determined using the following procedure: According to Table 3, the flow rate of CO_2 and CO the system of 10 SEWGS trains should be able to handle is 2222 mol CO_2 and CO/s. This means that each of the 10 trains should treat (2222 mol CO_2 and CO/s)/10 trains = 222.2 mol CO_2 and CO/s. For each train, there are 2 reactors in the feed step at each point in time during the cycle. This means that each of the 2 reactors should treat (222.2 mol CO_2 and CO/s)/2 reactors = 111.1 mol CO_2 and CO/s. According to Section 2.8.6, the maximum adsorption capacity of the adsorbent is 0.875 mol CO_2/kg adsorbent. According to Table 3, the total amount of adsorbent in each reactor is 44465 kg adsorbent. The maximum CO_2 adsorption capacity in each reactor is then 0.875 mol CO_2/kg adsorbent $\cdot$ 44465 kg adsorbent = 38906.875 mol CO_2. However, since the time period allocated for regeneration of the adsorbent is limited to a certain amount of the total cycle time of the SEWGS cycle, it is not possible to desorb and remove all of the CO_2 adsorbed. This means that the *cyclic capacity* of a reactor is lower than the maximum adsorption capacity calculated above. In general, the cyclic capacity will increase when the cycle time is increased [2]. Through single-reactor simulations, the cyclic capacity of a reactor was found to be approximately 50 %. This is to be used as a starting point for determining the cycle time. Using this assumption, the cyclic capacity of one reactor is found to be 50% $\cdot$ 38906.875 mol CO_2 = 19453.4375 mol CO_2 cyclic capacity. The time to saturate the reactor with CO_2 can then

be found as

$$Saturation\ time = \frac{19453.4375\ mol\ CO_2\ cyclic\ capacity}{111.1\ mol\ CO_2\ and\ CO/s} \approx 175.10\ s$$

The total time duration of the feed step in the SEWGS cycle should then be slightly shorter than this saturation time, to ensure that breakthrough is not reached. The feed step time is assumed to be 173.75 s. In the SEWGS cycle utilized in the present work, the feed step constitutes 25 % of the total cycle time. The cycle time can then be calculated as

$$CycleTime = 173.75\ s/0.25 = 695\ s$$

Through the simulations, this cycle time was found to be appropriate for the given system.

Table 13: System model parameters

Parameter	Value	Unit	Reference
$CycleTime$	695	s	Section 3.14
$RampTime$	2	s	Section 3.15
$ValveRampTime$	43.4375	s	Section 3.15
$SyngasFlowRatePerReactor$	210.5	mol/s	Section 3.15
$\dot{n}_{Feed\ 1}$	210.5	mol/s	1/20 of stream 2 in Table 2
$\dot{T}_{Feed\ 1}$	673	K	Stream 2 in Table 2
$y_{CO_2,Feed\ 1}$	0.0346	-	Stream 2 in Table 2
$y_{H_2,Feed\ 1}$	0.2206	-	Stream 2 in Table 2
$y_{CO,Feed\ 1}$	0.4933	-	Stream 2 in Table 2
$y_{H_2O,Feed\ 1}$	0.1817	-	Stream 2 in Table 2
$y_{N_2,Feed\ 1}$	0.0698	-	N_2 + Ar stream 2 Table 2
$\dot{n}_{Feed\ 2}$	210.5	mol/s	1/20 of stream 2 in Table 2
$\dot{T}_{Feed\ 2}$	673	K	Stream 2 in Table 2
$y_{CO_2,Feed\ 2}$	0.0346	-	Stream 2 in Table 2
$y_{H_2,Feed\ 2}$	0.2206	-	Stream 2 in Table 2
$y_{CO,Feed\ 2}$	0.4933	-	Stream 2 in Table 2
$y_{H_2O,Feed\ 2}$	0.1817	-	Stream 2 in Table 2
$y_{N_2,Feed\ 2}$	0.0698	-	N_2 + Ar stream 2 Table 2
$y_{CO_2,HP\ Steam\ 1}$	0	-	Stream 3 in Table 2
$y_{H_2,HP\ Steam\ 1}$	0	-	Stream 3 in Table 2

$y_{CO,HP\ Steam\ 1}$	0	-	Stream 3 in Table 2
$y_{H_2O,HP\ Steam\ 1}$	1	-	Stream 3 in Table 2
$y_{N_2,HP\ Steam\ 1}$	0	-	Stream 3 in Table 2
$y_{CO_2,HP\ Steam\ 2}$	0	-	Stream 3 in Table 2
$y_{H_2,HP\ Steam\ 2}$	0	-	Stream 3 in Table 2
$y_{CO,HP\ Steam\ 2}$	0	-	Stream 3 in Table 2
$y_{H_2O,HP\ Steam\ 2}$	1	-	Stream 3 in Table 2
$y_{N_2,HP\ Steam\ 2}$	0	-	Stream 3 in Table 2
S/CO	1.9139	-	Section 3.3.1
$RinseSteamFlowRate$	66.4194	mol/s	Section 3.15
$\dot{n}_{HP\ Steam\ R}$	66.4194	mol/s	Average value in simulations
$\dot{T}_{HP\ Steam\ R}$	673	K	Section 3.14
$y_{CO_2,HP\ Steam\ R}$	0.00002	-	Section 3.14
$y_{H_2,HP\ Steam\ R}$	0.00002	-	Section 3.14
$y_{CO,HP\ Steam\ R}$	0.00002	-	Section 3.14
$y_{H_2O,HP\ Steam\ R}$	0.99992	-	Section 3.14
$y_{N_2,HP\ Steam\ R}$	0.00002	-	Section 3.14
$PurgeSteamFlowRate$	132.0012	mol/s	Section 3.15
$\dot{n}_{LP\ Steam\ P}$	66.0006	mol/s	Average value in simulations
$\dot{T}_{LP\ Steam\ P}$	673	K	Section 3.14
$y_{CO_2,LP\ Steam\ P}$	0.00002	-	Section 3.14
$y_{H_2,LP\ Steam\ P}$	0.00002	-	Section 3.14
$y_{CO,LP\ Steam\ P}$	0.00002	-	Section 3.14
$y_{H_2O,LP\ Steam\ P}$	0.99992	-	Section 3.14
$y_{N_2,LP\ Steam\ P}$	0.00002	-	Section 3.14
$p_{H_2\ Product}$	2689000	Pa	Section 3.14
$p_{CO_2\ Product\ 1}$	110000	Pa	Section 3.14
$p_{CO_2\ Product\ 2}$	110000	Pa	Section 3.14
$Flow\ coefficient$	0.001	mol/(sPa)	Section 3.4.1
$Flow\ exponent$	1	-	Section 3.4.1

3.15. Implementation in gPROMS and establishment of operating schedule

As discussed in Section 3.2, the switching of the system from one cycle state to next, is carried out in a simplified way. At the end of one cycle state, some of the flow rates of the streams going into the system have been ramped down to zero. The system of equations have then been changed to those describing the system in the next cycle state. Then, the flow rates of the streams going into the system have been ramped up to their target values, and the valves controlling the internal flows of the system have been opened by ramping up the valve opening to their desired position.

It should be specified that it is only the values of the variables in each reactor that are taken as the basis for beginning the simulation of the following cycle state. The reason for this is that in the system of equations, only the reactor model contains differential variables with respect to time. Every other variable in the system is instantaneously recalculated. This is a simplification. However, it is the behaviour of the reactors which are of main interest in the present work. Therefore, as the switching of cycle state occurs, the behaviour of the mixers, splitters and valves in the system is not focused on. The influence of this on the results of the simulation is not known, and is something that should be investigated in further work with the model.

When a system model such as the present one is to be implemented in gPROMS, every possible interconnection and flow pattern between the reactors must be possible. The reason for this is that the degrees of freedom of the gPROMS model must be equal to zero at all times throughout the simulation of the cycle. That is, the number of variables minus the number of equations and number of known variables must be zero at all times.

The simulation is defined to start at $t = 0$ seconds, at which the SEWGS system of 8 reactors is in the start of cycle state 1, referred to Figure 7. The gPROMS model has therefore been developed to consist of the equations necessary to describe the system behaviour in cycle state 1.

The operating schedule, which is part of what is referred to as a *process* in gPROMS, should then give gPROMS instruction to simulate the running of the system for a time period of 1/16 of the total cycle time of the SEWGS cycle. At this point in time, cycle state 1 is completed, and the system of equations should be switched to describe the behaviour in cycle state 2. Then gPROMS should simulate the next time period of 1/16 of the total cycle time, then switch the equations to those describing cycle state 3. This operating pattern should continue until all the 16 cycle states have been simulated, which concludes the simulation of one complete SEWGS cycle.

In gPROMS, a known variable is described by an equation, equating a variable in the system to a defined, known number. This is called *assigning* a variable. At any point in time

during the simulation, it is possible to replace an assigned variable with another variable. That is, removing (*unassigning*) one equation from the system and adding (assigning) another one to replace it. In addition, it is possible to use so-called selectors to switch which equations that should govern the behaviour of each component in the model. This can be carried out as long as the number of new equations are equal to the number of old equations removed. This is called switching. Utilizing these two functions of gPROMS, it is possible to carry out the switching of the system of equations from one cycle state to those describing the next cycle state.

This has been carried out in the following way: Every necessary stream for the interconnections between all the reactors have been defined in the gPROMS model. In any given cycle state, the streams which are not used have been assigned arbitrary dummy values for the stream variables. These stream variables are not used in the equations defining the behaviour of the system in the current system state. The stream variables that are determining the behaviour are unassigned, and are given by the behaviour and equations of the system. When a switch from one cycle state to the next is to be carried out, the stream variables which were previously unused and assigned dummy values, are unassigned by replacing these by assigning dummy values to the previously unassigned stream variables. This allows the switch between cycle states to be carried out, keeping the degrees of freedom for the system of equations equal to zero before and after the switch.

This procedure of replacing known variables with unknown variable can be illustrated by the conceptual diagrams in Figures 14 and 15, showing the switch from one state to another.
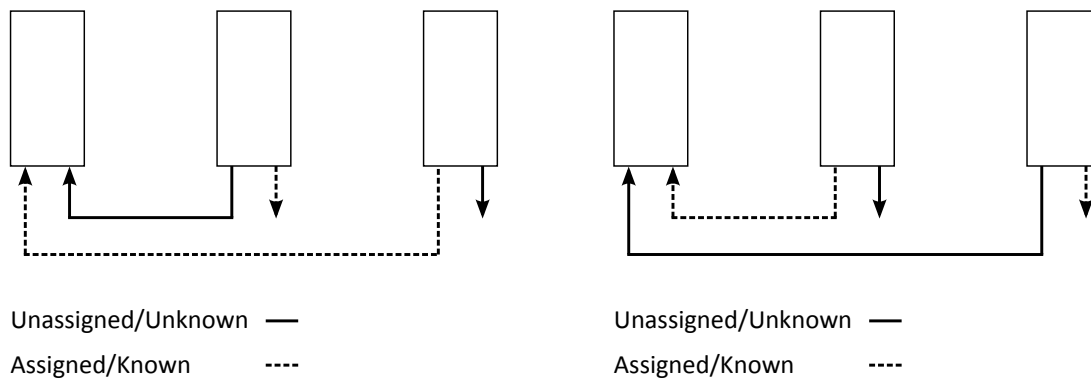

Unassigned/Unknown ——
Assigned/Known   ----

Figure 14: Example of unknowns and knowns before switch

Figure 15: Example of unknowns and knowns after switch

It is chosen to not go into further detail about this practical implementation of the model in gPROMS. However, the fundamental idea which have been conveyed in the present section is that each cycle state has its own equation system governing the behaviour, and the switch from one cycle state to the other should be possible to implement in gPROMS

using the presented methodology.

Before it is possible to describe the operating schedule utilized for the running of the simulation in gPROMS, several parameters must be defined:

- *CycleTime*: the time period it takes to complete one cycle of the SEWGS system of reactors, the SEWGS train. That is, the time it takes from the start of cycle state 1 to the end of cycle state 16. The duration of one cycle state is therefore *CycleTime*/16.

- *RampTime*: the time period it takes to ramp up or down the external flow rates of the system, such as the feed syngas stream, rinse and purge steam stream. *RampTime* is set to 2 seconds.

- *ValveRampTime*: the time period it takes to open a valve in the system. This has been chosen to be very large compared to the actual time it should take to open a valve. *ValveRampTime = CycleTime*/16. The reason for this is to be able to reach convergence in the simulations, by avoiding excessive pressure drops in the reactors.

- *SyngasFlowRatePerReactor*: the target value for the flow rate of feed syngas to one reactor in the feed step. That is, (4210 mol/s)/(10 trains · 2 reactors in feed step) = 210.5 mol/s.

- *RinseSteamFlowRate*: the target value for the flow rate of rinse steam. That is, ≈ 66.4194 mol/s.

- *PurgeSteamFlowRate*: the target value for the flow rate of purge steam. That is, ≈ 132.0012 mol/s.

In the real-world operation of the SEWGS train the flow rate of streams Feed 1 $\dot{n}_{Feed,1}$ and 2 $\dot{n}_{Feed,2}$ in Figures 12 and 13 will be approximately constant, in accordance with the assumptions in the case study in Section 1.3. However, to be able to reach convergence in the gPROMS model, some assumptions and simplifications have to be taken. These assumptions are:

- The flow rate of feed syngas delivered to a reactor which have just started the feed step, is instantaneously set to its target value, that is, *SyngasFlowRatePerReactor*.

- The flow rate of feed syngas delivered to a reactor which is close to the end of the feed step, that is, at *RampTime* seconds before the end of the feed step, is ramped down from *SyngasFlowRatePerReactor* to zero over *RampTime* seconds.

- The flow rate of rinse steam $\dot{n}_{HP\ Steam\ R}$ delivered to a reactor which have just started the rinse step, is instantaneously set to its target value, that is, *RinseSteamFlowRate*.

- The flow rate of rinse steam delivered to a reactor which are close to the end of the

rinse step, that is, at *RampTime* seconds before the end of the feed step, is ramped down from *RinseSteamFlowRate* to zero over *RampTime* seconds.

- The flow rate of purge steam $\dot{n}_{LP\ Steam\ P}$ delivered to a reactor which have just started the purge step, is ramped up from zero to *PurgeSteamFlowRate* over a time period of $(2 \cdot CycleTime/16) - RampTime$. This means that the purge steam flow rate reaches a value of *PurgeSteamFlowRate* at *RampTime* seconds before the purge step is completed. The reason for this assumption is that the velocities in the reactor will be very high due to the low pressure (1.1 bar) in the reactor during the purge step. To be able to reach convergence, the flow rate must be ramped up over a longer time period than in the other cases.

- The flow rate of purge steam delivered to a reactor which are close to the end of the purge step, that is, at *RampTime* seconds before the end of the purge step, is ramped down from *PurgeSteamFlowRate* to zero over *RampTime* seconds.

- When steps Eq3 and REq3 are started, the valve opening x_{valve} of valve V1 in Figure 12, controlling the flow rate between the reactors, is ramped up from a value of 0.0001 to 3.0 over *ValveRampTime* seconds. After *ValveRampTime*, which is equal to the duration of one cycle state, the valve opening is instantaneously set to zero. This does not pose a problem since the flow rate is very low at this point in time, due to the low pressure difference. The valve opening x_{valve} should ideally be defined to be between 0 and 1. However, due to problems with convergence, it was chosen to keep the flow coefficient of all valves in the system at a constant value, and to emulate the behaviour of valves with larger flow coefficient by ramping x_{valve} to a value above 1. In the case of valve V1, the actual flow coefficient is $3 \cdot 0.001 \text{ mol}/(\text{s} \cdot \text{Pa}) = 0.003 \text{ mol}/(\text{s} \cdot \text{Pa})$.

- When steps Eq1 and REq1 are started, the valve opening x_{valve} of valve V2 in Figure 12, controlling the flow rate between the reactors, is ramped up from a value of 0.0001 to 3.0 over *ValveRampTime* seconds. After *ValveRampTime*, which is equal to the duration of one cycle state, the valve opening is instantaneously set to zero. The actual flow coefficient for valve V2 is $3 \cdot 0.001 \text{ mol}/(\text{s} \cdot \text{Pa}) = 0.003 \text{ mol}/(\text{s} \cdot \text{Pa})$.

- When steps Eq2 and REq2 are started, the valve opening x_{valve} of valve V4 in Figure 13, controlling the flow rate between the reactors, is ramped up from a value of 0.0001 to 3.0 over *ValveRampTime* seconds. After *ValveRampTime*, which is equal to the duration of one cycle state, the valve opening is instantaneously set to zero. The actual flow coefficient for valve V4 is $3 \cdot 0.001 \text{ mol}/(\text{s} \cdot \text{Pa}) = 0.003 \text{ mol}/(\text{s} \cdot \text{Pa})$.

- When step D is started, the valve opening x_{valve} of valve V3 in Figure 13, controlling

the flow rate out from the inlet of the reactor, is ramped up from a value of 0.0001 to 4.0 over *ValveRampTime* seconds. After *ValveRampTime*, which is equal to the duration of one cycle state, the valve opening is instantaneously set to zero. The actual flow coefficient for valve V3 is $4 \cdot 0.001$ mol/(s $\cdot$ Pa) = 0.004 mol/(s $\cdot$ Pa).

- Using the current cycle time, it has not been possible to lower the pressure in the reactor in the depressurization step down to the desired pressure of $p_{CO_2 \ Product \ 2} = 1.1$ bar during the duration of the step. One of the reasons for this is that when the pressure difference over valve V3 decreases during the depressurization, the driving force for mass transfer out of the reactor descreases. However, the most important reason is that, when the pressure is decreasing in the reactor, the driving force for desorption of CO_2 increases, transferring mass of CO_2 into the gas phase in the reactor. This contributes to slowing down the pressure decrease in the reactor, since mass of gas is leaving the reactor through the inlet, leading to an increase in mass of CO_2 in the gas phase. As a result of this, the pressure at the inlet of the reactor at the end of the depressurization step is around 1.4 bar. This was found from the simulations. In the next step in the reactor cycle, the purge step, the pressure at the inlet of the reactor should ideally be set to $p_{CO_2 \ Product \ 1} = 1.1$ bar, which is the desired purge pressure. However, doing this leads to a discontinuity between the pressure in the reactor and that at the inlet, leading to very high flow rates out the inlet of the reactor, which makes the simulation not able to converge. Therefore, it has been assumed that the pressure $p_{CO_2 \ Product \ 1}$ at the start of the purge step is set to be equal to the pressure at the inlet of the reactor at the end of the depressurization step. The pressure $p_{CO_2 \ Product \ 1}$ is then ramped down to 1.1 bar over a time period *RampTime*.

- When step RP is started, the valve opening x_{valve} of valve V5 in Figure 13, controlling the repressurization flow rate, is ramped up from a value of 0.0001 to 9.539477 over *ValveRampTime − RampTime* seconds. After *ValveRampTime − RampTime*, which is equal to the duration of one cycle state minus *Ramptime* seconds, the flow rate through the valve is instantaneously set to zero by using a switch of the equations governing the behaviour of valve V5. This is done to prevent problems with the low flow rates at the outlet of the reactor which delivers gas to repressurization, which will decrease in the last *RampTime* seconds of the current cycle state. The reason for this is that the feed syngas flow rate delivered to the reactor at the last part of the feed step is ramped down during the last *RampTime* seconds of the current cycle state. Please refer to the previous discussion. This creates problems with the model equations governing the behaviour of valve V5, since the flow rate through the valve is determined by a comparison of the flow rate determined by the valve characteristic and the available flow from the out-

let of the reactor in the last part of the feed step. Please refer to the discussion of the valve model in Section 3.8.2. The actual flow coefficient for valve V5 is $9.539477 \cdot 0.001$ mol/(s · Pa) = 0.009539477 mol/(s · Pa).

- At the start of every odd-numbered cycle state, 1, 3, ... ,15, the variables in the two reactors in the feed step and the reactor in the rinse step had to be recalculated, assuming a total pressure p throughout the reactors of 26.89 bar. The gPROMS function for this is called *reinitial*, which calls for gPROMS to recalculate the equation system given a set of assumptions. The reason for this was that the reactor starting the countercurrent rinse step, previously has been in the cocurrent feed step. Therefore, when the equation system is switched to the new cycle state, gPROMS could not calculate the system, since the reactor in the rinse step was not delivering gas out through the inlet as it should, but was accepting gas from the reactors in the feed step. This is not a feasible situation within the equation system utilized, and gPROMS delivered an error. However, at the start of the cycle state, the flow rates in two of these three reactors are close to zero, that is, the reactors starting the feed step and the rinse step, as indicated by the previous assumptions. Therefore, utilizing the recalculation procedure described here should not cause large errors in the simulation results, as the pressures in the reactors before and after the switch will be close to 26.89 bar due to the low flow rates. It is not ideal to do this recalculation for the reactor which is halfway through the feed step, as this recalculation implies that the velocities in the reactor will be close to zero due to the recalculation. However, it was necessary to include this reactor in the recalculation to be able to get a convergent solution. It should also be noted that the pressure drop over the reactors in the feed step and rinse step is very small, so the error should be small.

- To be able to reach convergence in the simulations, an assumption of no WGS reaction taking place ($r = 0$) had to be made during steps Eq1, Eq2, Eq3, D, P, REq3, REq2 and REq1. The reason for this was that the reaction rate r was so small during these steps that the simulation was not able to reach convergence. This can be explained by the fact that the bulk of the forward WGS reaction takes place during the feed step. Therefore should this assumption not affect the results significantly. However, this is an aspect which could be investigated in further work.

From the previous discussion it is clear that it is necessary to control the flow rates of syngas to each reactor in the feed step separately, that is, the values of $\dot{n}_{Feed\ 1}$ and $\dot{n}_{Feed\ 2}$.

Now, it is possible to describe the operating schedule utilized for the running of the simulation in gPROMS. This can be found in Appendix A.

3.15.1. Providing initial values for the simulation - Startup cycle

The previous discussion concludes the presentation of the operating schedule of the simulation of the SEWGS train under its normal pattern of operation. However, since there are significant interaction between the reactors in the system at every point in time through the SEWGS cycle, there are some problems to be considered. When gPROMS starts the simulation, the software has to solve what is called an *initialization problem*. The reactor model consists of several time-differential variables, namely $\bar{c}_{CO_2}$, $\bar{c}_{H_2}$, $\bar{c}_{CO}$, $\bar{c}_{H_2O}$, $\bar{c}$, T and q_{CO_2}. These variables must be given initial values at $t = 0$. To be able to reach convergence in the simulation in gPROMS, it is not straightforward to give these variables arbitrary initial values and approach consistent values as the simulation carries on. By inspecting the SEWGS cycle in Figure 7, it can be seen that a $t = 0$, the eight reactors are at different steps of their individual cycles, and the initial values of the variables in each reactor will therefore be quite different from each other. To take this into account, a *startup procedure* of the reactor system needs to be established, providing initial values for the simulation of the SEWGS system defined to start at $t = 0$.

This startup procedure has been developed using several assumptions and simplifications. A simulation has been carried out on one single reactor, running it through a simplified version of the cycle starting with the feed step and concluding with a repressurization step. A flow sheet illustrating the operation of the cycle and the simplifications taken can be found in Figure 16. The objective of this simplified startup cycle is to obtain approximate initial values for the variables in the reactors in the SEWGS cycle. Very crude approximations of the interactions between this single reactor and the other reactors have been taken. Therefore, the values obtained will not be representative of a real situation, but will provide a starting point for the simulations. As the simulation of the SEWGS cycle is carried out, the behaviour of the reactors will develop gradually towards a more realistic behaviour, as the interactions between reactors take place. To be able to reach convergence in the simulations, an assumption of no WGS reaction taking place ($r = 0$) had to be made during steps Eq1, Eq2, Eq3, D, P, REq3, REq2 and REq1. Unless otherwise noted, the same parameters as in the previous discussion are utilized.
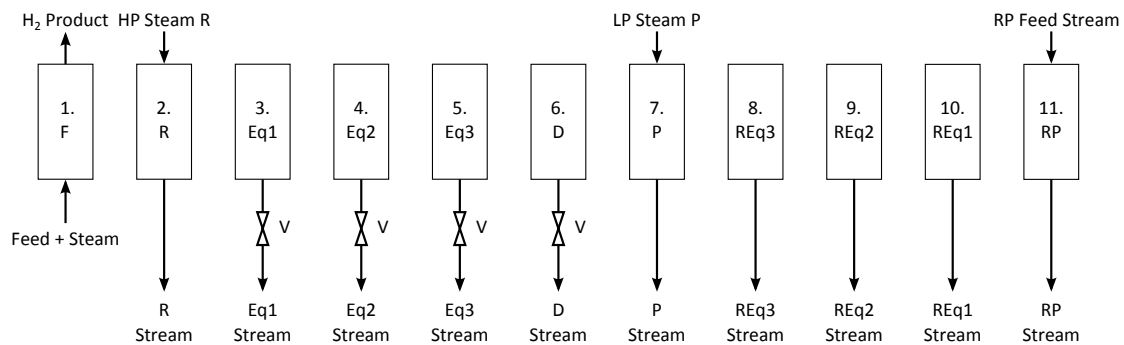

Figure 16: Single reactor operation

The procedure employed in the startup cycle can be found in Appendix B.

4. Results and discussion

The key points most important to evaluate in the present section are:

- Is the modelling of the SEWGS system appropriate?

  - Is the mass going into the system conserved? That is, is the numerical solution of the system physically consistent?

- How is the performance of the SEWGS system?

  - How constant is the flow rate and composition of the H_2 product stream?
  - Is cyclic steady state reached?
  - Does CO_2 break through into the H_2 product stream?
  - Does CO break through into the H_2 product stream?
  - Is any combustible H_2 or CO lost through the CO_2 product stream?
  - What is the CO_2 capture ratio of the system?
  - What are the rinse and purge steam requirements, and are they economically acceptable?
  - Do hot spots develop in the reactors, due to the omission of the upstream WGS reactor? If so, is the temperature increase acceptable with respect to the maximum operating temperature of the adsorbent and catalyst?
  - Is the behaviour of the system comparable to results from literature?

The simulation has been run for two complete SEWGS cycles, which means that the total time of operation simulated is $2 \cdot CycleTime = 1390$ seconds. In Section 3.2, the convention of referring to 16 different *cycle states* was established. For easy reference to the results presented in the present section, a similar convention is made. When reference is made to cycle states 1 through 16, this means the time periods of the first SEWGS cycle simulated, from $t = 0$ to $t = 695$ s. When reference is made to cycle states 17 through 32, this means the time periods of the second SEWGS cycle simulated, from $t = 695$ to $t = 1390$ s.

The results from the simulation consists of very large amounts of data, and not everything can be presented in the text of this thesis. It has been chosen to only include the most relevant data in the form of graphs and tables. In the discussion of the results to follow, there are several references to data which have not been included in the text. However, these references have only been made whenever there is need to confirm the behaviour indicated by the results presented in the text.

As the simulation has been carried out on one SEWGS train, the numerical values of the flow rates going into and out of the SEWGS train system (Figure 11) have been multiplied by 10 to give correct values for the whole SEWGS system of 10 trains.

There has been several difficulties with solving an equation system as complicated as the one utilized in the model in the present work. The simulation software gPROMS, solves the equation system numerically, and this implies that there is a possibility of errors in the values in the resulting solution. The flow through the SEWGS reactors are governed by both convection and diffusion, and one of the principal concerns is that mass will not be conserved. Since the reactor model employs distributed variables on the z-axis in the reactor, the z-axis must be discretized into a finite number of points. In most cases, as this number of points are increased, the numerical solvers utilized by gPROMS should be able to calculate the variables with decreasing errors. That is, given that the solver settings are appropriate. However, from a computational perspective, it is not desirable to use a very large number of points, as the time required to carry out the simulation will also increase. It is outside the scope of this thesis to go into detail in determining the very best configuration of number of discretization points and solver settings. Therefore, the configuration used in the simulations have been determined partly from literature, and partly by trial and error. This is something that should be considered in later work.

In the few SEWGS modelling studies found in literature, answers to these issues are scarce [44, 45, 29]. In the SEWGS modelling effort by Wright et al. [44], it is said that the model was solved using a finite-volume technique. In the one-dimensional heterogeneous PSA modelling work by Ribeiro et al. [36], gPROMS is utilized to simulate a model in some aspects similar to the one in the present work. The reactor length in this work is 1 m, with a feed velocity of ca. 0.11 m/s. The authors report that the reactor z-axis was discretized into 180 intervals using the Centered Finite Difference Method (CFDM) of second order. This means that the distributed variables in the reactor were calculated for every 0.56 cm. In the present work, the reactor length is 7.377 m, with a feed velocity of ca. 0.0735 m/s. By trial and error, gPROMS was able to reach convergence in the simulations when the reactor z-axis was discretized into 600 intervals using the Centered Finite Difference Method (CFDM) of second order. That is, calculating the distributed variables for every 1.23 cm. The standard solvers in gPROMS were utilized, with some modifications to the maximum iterations the solver should carry out before giving up. The convergence of the simulation was very slow, and the integration step size was on average $\Delta t \approx 0.0035$ seconds. The simulation took approximately 48 hours to run on a computer with an Intel Core i7-2620M 2.70 GHz CPU.

The following methodology was employed to check that mass is conserved in the SEWGS train model: A system mass balance for the SEWGS train was defined, on the form

$$\frac{\partial moles_{system}}{\partial t} = \frac{\partial moles_{in}}{\partial t} - \frac{\partial moles_{out}}{\partial t} \qquad [\text{mol/s}] \qquad (145)$$

In each reactor model, a variable was defined which accounts for the sum of the number of moles in the reactor gas phase and the number of moles of CO_2 adsorbed. This was carried out by performing an integration of

$$\frac{\partial moles_{single\ reactor}}{\partial z} = (\bar{c} \cdot \varepsilon_t + q_{CO_2} \cdot \rho_{b,ads}) \cdot \pi \cdot (d_t/2)^2 \qquad [\text{mol/m}] \qquad (146)$$

over the whole z-axis. The sum of the number of moles in all the reactors was defined to be $moles_{reactors}$. At $t = 0$, the initial value of $moles_{system}$ was set to be equal to $moles_{reactors}$. For the whole SEWGS train system, two differential variables were defined. One which accounts for the number of moles of gas being sent into the system, $moles_{in}$, starting from a value of zero at $t = 0$, and one which accounts for the same leaving the system, $moles_{out}$. With reference to Figure 11,

$$\frac{\partial moles_{in}}{\partial t} = \dot{n}_{Feed\ 1} + \dot{n}_{Feed\ 2} + \dot{n}_{HP\ Steam\ 1} + \dot{n}_{HP\ Steam\ 2} + \dot{n}_{HP\ Steam\ R} + \dot{n}_{LP\ Steam\ P} \qquad (147)$$

$$\frac{\partial moles_{out}}{\partial t} = \dot{n}_{H_2\ Product} + \dot{n}_{CO_2\ Product\ 1} + \dot{n}_{CO_2\ Product\ 2} \qquad (148)$$

From this discussion, it can be reasoned that if mass is conserved in the system, the value of $moles_{system}$, which accounts for the number of moles that should be in the system, and the value of $moles_{reactors}$, which accounts for the number of moles that are in the system, should be equal to each other. As Figure 17 shows, this is not the case. The value of $moles_{system}$ is increasingly larger than the value of $moles_{reactors}$. This implies that the some mass is disappearing within the reactor models. However, comparing this difference, the amount of moles being lost, to the amount of moles that have been sent into the system, $moles_{in}$, this ratio stabilizes at around 5 %.

What is causing the disappearance of mass within the reactors? There are several possible explanations. It might be that the number of discretization points is too low, given the utilized reactor length and velocities. It could also be explained by unknown inconsistencies in the reactor or system model. One known inconsistency in the reactor model is that the mole fractions y_i, the component concentrations $\bar{c}_i$, the total concentration $\bar{c}$, the partial pressures p_i can take negative values. Inspecting the simulation results, it can be seen that this indeed occurs at several points during the simulation. One example of this is that the mole fractions of N_2 take slightly negative values close to the outlet of reactor 1 during the rinse, depressurization and purge steps. This is shown in Figure 18.
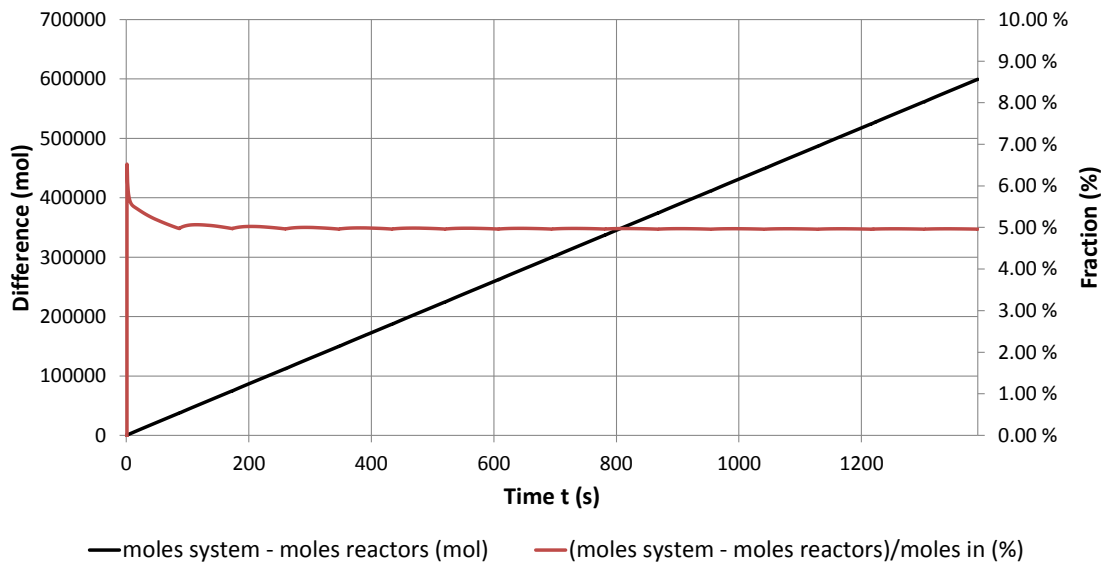
Figure 17: Difference between $moles_{system}$ and $moles_{reactors}$

Another possible explanation for this is that the equilibrium adsorption capacity of CO_2, $q^*_{CO_2}$, drops very fast close to the outlet during the rinse and purge steps, due to the counter-current flow of steam. Since the mass-transfer coefficient k_{LDF} is assumed to be constant throughout the whole cycle, the desorption of CO_2 close to the reactor outlet will be very fast. This could lead to instabilities in the simulation, requiring gPROMS to utilize very small time steps when integrating. This discussion implies that it might be necessary to increase the number of discretization points to ensure that mass is conserved in the simulations. Significant effort was made to improve this, but there was not sufficient time to reach any breakthrough. This is something that should investigated in later work.

This concludes the discussion of the overall modelling and physical consistency of the SEWGS system model. There is significant room for improvements. Some of the problems which should be worked further with, is ensuring that mass is conserved in the model. Also, a system enthalpy balance should be implemented. There was not sufficient time to incorporate this into the model as of now. The gPROMS solver settings should also be investigated further. There might be a need for increasing the solver precision, and also investigating the need for implementing the equations of the system and reactor model with variables in a dimensionless form. This was not carried out in the present work, as there was not sufficient time.

The simulation should be run for as many cycles necessary to reach cyclic steady state. That is, the point in time from which the difference between mass entering and leaving the system is on average equal to zero, and the characteristics of the streams leaving the system are following an approximately repeating pattern. However, since mass is not conserved in the system model, it has been difficult to determine if the system has reached
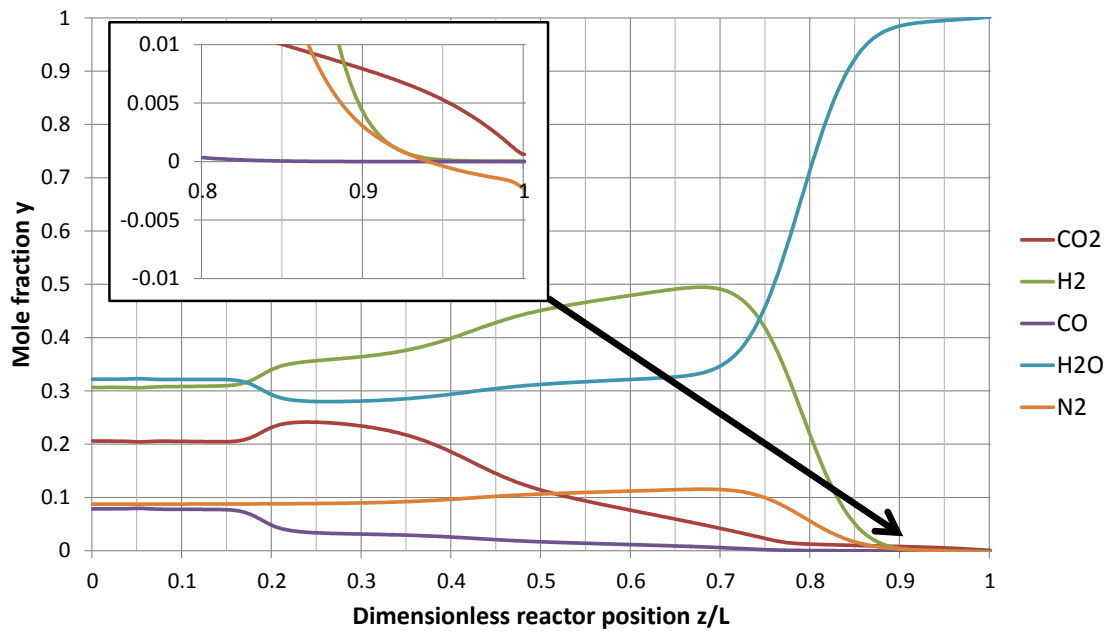
Figure 18: Reactor 1: Mole fractions at at t = 260.625 s, end of step R

cyclic steady state or not. Therefore, the discussion of the results to follow should be examined bearing this in mind.

By inspecting the flow rates of the different components in the stream H_2 product found in Figure C.1, it can be seen that the flow rates are approaching a cyclic pattern after approximately 173.75 seconds of operation. That is, when cycle state 5 in the first of the two SEWGS cycles begins. The same can be observed for the total flow rate and the mole fractions in the H_2 product stream, found in Figures C.2 and C.3. After this point in time, the flow rates and mole fractions follow approximately the same pattern, repeating itself every $2 \cdot CycleTime/16$ = 86.875 seconds. It can be seen that only very small amounts of CO_2 and CO are breaking through into the H_2 product. This is in accordance with the purpose of the SEWGS process.

The component flow rates in the stream H_2 product is both in system state 1 and 2 a sum of the component flow rates in the stream corresponding to stream outlet,1 and the stream corresponding to stream e in Figures 12 and 13. The contribution to the stream H_2 product from the reactor in the first half of the feed step is shown in Figure C.4. It can be seen that the flow rates during the first two cycle states are relatively constant. Therefore, there must be another reason that the component flow rates in the stream H_2 product in Figure C.1 drops significantly during the second cycle state. The reason can be found by inspecting the second reactor in the feed step. The contribution to the stream H_2 product from the reactor in the second half of the feed step is shown in Figure C.5. During the even-numbered cycle states, some of the outlet flow from the reactor in the second half of the feed step is used to repressurize another reactor. By inspecting Figure C.5, it can

be seen that during the first part of the repressurization, all of the outlet flow is used to repressurize the other reactor. That is, the component flow rates in Figure C.5 are zero. This is reasonable, as the pressure difference between the two reactors at the beginning of the repressurization step is approximately, 26.89 - 20.4425 bar = 6.4475 bar. A significant amount of gas must be sent to the reactor to bring increase the pressure by this amount, given the large size of the reactor. After some time, the flow rates are again increasing from zero, due to the lower pressure difference between the reactors, which should result in lower flow rates. This is confirmed by inspecting the flow rates going to the reactor which is being repressurized.

The component flow rates in the stream H_2 product are fluctuating throughout the whole time period of the two SEWGS cycles simulated. As discussed in Section 1.3, this is not very good with respect to requirements of the stream being sent to the power island and the gas turbines, which are to utilize this product stream for combustion. During the first part of the repressurization steps, the flow rate of H_2 drops from approximately 2900 mol/s to less than half, 1300 mol/s. The reasons for this drop is already discussed, but what could have been done to improve this? The core of the problem seems to be the amount of gas required to repressurize one of the reactors. One possibility for improving this is to increase the flow rate of feed syngas going into the SEWGS train. This would mean that a smaller fraction of the outlet gas of the reactor is being sent to repressurization. However, by doing this, the reactors in the feed step would reach breakthrough after a shorter time period. This would require that some action is taken to correct for this change, for example reducing the cycle time. By reducing the cycle time, the duration of the repressurization step would also be reduced, thereby requiring a larger flow rate for repressurization. This would counteract the desired effect of reducing the cycle time in the first place.

A simplified calculation can be carried out to determine the average flow rate needed for repressurization, given the defined pressure difference and the current cycle time:

Moles in reactor at lower pressure:

$$moles_{low} = \frac{2044250 \text{ Pa} \cdot 7.377 \text{ m} \cdot \pi (0.5 \cdot 3.658 \text{ m})^2}{8.314 \text{ J/(mol} \cdot \text{K)} \cdot 673 \text{ K}} \tag{149}$$
$$\approx 28325 \text{ mol}$$

Moles in reactor at higher pressure:

$$moles_{high} = \frac{2689000 \text{ Pa} \cdot 7.377 \text{ m} \cdot \pi (0.5 \cdot 3.658 \text{ m})^2}{8.314 \text{ J/(mol} \cdot \text{K)} \cdot 673 \text{ K}} \tag{150}$$
$$\approx 37258 \text{ mol}$$

Average flow rate during repressurization step:

$$\dot{moles}_{RP} = \frac{37258 \text{ mol} - 28325 \text{ mol}}{CycleTime/16}$$

$$\approx 206 \text{ mol/s}$$

(151)

According to the results, the inlet flow rate of syngas, steam and rinse gas delivered to each reactor in the feed step is ca. 405 mol/s. The outlet flow rate from the reactor will be lower, as CO_2 is adsorbed. The results confirm this, the outlet flow rates are ca. 300 mol/s. This means that, on average, $206/300 \approx 69$ % of the outlet gas from the reactor in the last fourth of the feed step needs to be sent to repressurization. As discussed in Section 3.2, the pressure at the outlet of this reactor is assumed to be constant, at 26.89 bar. If the flow taken out for repressurization is very large, this could be an incorrect assumption. This should be investigated in later work.

One possibility for lowering the average flow rate necessary for repressurization is to add additional equalization and re-equalization steps in the cycle. By doing this, and keeping the feed pressure and the purge pressure level constant, the pressure difference between two reactors undergoing pressure equalization will be lowered, thereby lowering the repressurization flow rate. However, for every step that is added, one additional reactor is required in the SEWGS train, thus increasing the capital costs of the total system [45]. As discussed, the current cycle utilizing three equalization and re-equalization pairs is reported in literature to be sufficient for this type of cycle [45].

The sudden drop in flow rates in the H_2 product stream has not been explicitly reported in literature. In the SEWGS modelling study by Wright et al. [45], which the present work bases its SEWGS cycle on, the authors state that a part of the H_2 product is sent to repressurization. However, they do not state how much this is. In the SEWGS modelling study by Wright et al. [44], the authors report constant flow rates of the H_2 product stream. The same is reported in the modelling work by Manzolini et al. [29].

This discussion raises several questions: What does this imply for the results in the present work? Are the assumptions in the reactor or system model incorrect? Is there need for a different configuration of SEWGS trains, cycle time and flow rates utilized? These questions should be investigated in further work.

The discussion will now be taken towards explaining in more detail the irregularities and the regularities observed in the component flow rates of the H_2 product stream. It is inherent in a system such as the SEWGS train that asymmetric behaviour will occur. The reason is the interactions between the reactors in the system. If the cycle time is chosen to be too short, the duration of the steps in the cycle will be to short for carrying out the purpose of each step. If for example, the duration of the purge step is too short, insuffi-

cient amounts of CO_2 will be desorbed and removed from the reactor, thus lowering the cyclic capacity of the reactor. When the reactor reaches the feed step, it might be that this causes an unacceptable level of breakthrough of CO_2 into the H_2 product stream. Another example is the steps dealing with pressure change in the reactor, the steps Eq1, Eq2, Eq3, D, REq3, REq2, REq1 and RP. If the duration of these steps are too short, the reactor will not be brought to the desired pressure level for each of these steps. The cycle time should not be too long either, as this would result in breakthrough of CO_2 into the H_2 product stream.

One irregularity in the flow rates will now be discussed. The peak in flow rate of steam H_2O in cycle states 3 and 4 in the H_2 product stream can be explained by inspecting the mole fractions in reactor 2 at the beginning of cycle steps 3 and 4, found in Figures 19 and 20. The mole fraction of H_2O is very large in parts of the reactor. The reason for this is that, at $t = 0$, reactor 2 has just completed the simplified step REq2 of the startup cycle. See Section 3.15.1. During the re-equalization steps in the startup cycle, the reactor has not received any gas from other reactors. The composition of the gas in reactor 2 at the start of the SEWGS cycle, at $t = 0$, is therefore largely steam. This is the first example of the influence of the interactions between the columns during the SEWGS cycle, or in this case, the lack of them during the startup cycle. As it shall be seen during the discussion of the results, the reactors in the SEWGS system will go towards more constant behaviour as the interactions come into effect.
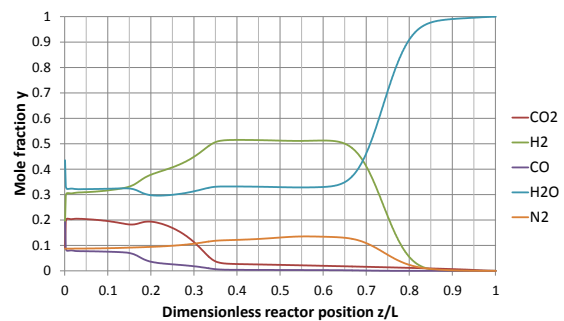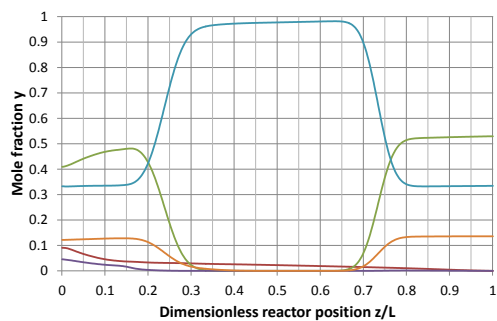

Figure 19: Reactor 2: Mole fractions at t = 86.8750 s **Figure 20:** Reactor 2: Mole fractions at t = 130.3125 s

The repeating pattern of the component flow rates in the H_2 product stream after 173.75 seconds of operation can be explained by two aspects. The first, is that the outlet flow from reactor 2, which is in the feed step during cycle states 5 and 6, now largely consists of gas which have entered the reactor from $t = 0$ and onwards. That is, the steam-rich gas have left the reactor. The second aspect is the fact that reactor 3, which is also in the feed step during cycle states 5 and 6, have during the time from $t = 0$ and up to $t = 173.75$ seconds, been re-equalized and repressurized by the other reactors in the system. This means that the interactions between the reactors in the system have finally come into action, and the

simplifications from the startup cycle have started to affect the behaviour of the system less than before. The development of the mole fractions of reactor 3 in this time period can be found in Figures E.1, E.2, E.3, E.4 and E.5. From these graphs it can be seen that the composition in the reactor at $t = 173.75$ seconds, is similar to the mole fractions near the outlet in the reactor 2 at the same time, see Figure E.6. This is desirable, as reactor 3 is to start the feed step from this point on, and by having a similar composition near the outlet, the composition of the stream H_2 product will also be close to constant. As can be seen from Figure C.1, the flow rate of H_2 is close to constant in the very first part of cycle state 5. As the variations in composition in reactor 3 observed in Figure E.5 reaches the outlet, the flow rate of the components in the stream H_2 product also starts to fluctuate. By inspecting the development of the mole fractions in the reactors throughout the two SEWGS cycles, it was confirmed that the same reasoning applies for explaining the repeating pattern for the rest of the time period of simulation. The graphs showing this behaviour will not be given in the text of this thesis.

The fluctuation of the mole fractions of H_2 and H_2O in the region $z/L \approx 0.4$ to 0.8 in Figure E.5 deserves some attention. These fluctuations leads to the variations in the component flow rate in the H_2 product stream. Inspecting Figures E.1 through E.5, the reason for these fluctuations can be explained. At the end of the purge step (Figure E.1), there is much steam in the reactor. During the cocurrent re-equalization steps (Figures E.2, E.3, E.4), this steam is being pushed towards the closed outlet end of the reactor. During the countercurrent repressurization step (Figure E.5), this steam is pushed towards the middle of the reactor, leading to the fluctuations in this region. Inspecting the component flow rates from reactor 3, found in Figure C.4 in cycle states 5 and 6, it can be seen that these fluctuations reaches the outlet of reactor 3 at $t \approx 190$ seconds. This means that, during the period from $t = 173.75$ s to 190 s, the dispersion of these two components has not been fast enough to even out the concentration differences. As discussed in Section 2.11, a constant value for the axial dispersion coefficient D_{ax} has been utilized in the model. This value was collected from a work utilizing a different setup than the one in the present work. In the SEWGS modelling effort by Wright et al. [44], the authors report constant mole fractions in the H_2 product stream. It is therefore possible that the value of D_{ax} utilized in the present work is too low, compared to the real-world behaviour of the reactors. This should be investigated in further work. After $t = 173.75$ seconds, there are some fluctuations in the mole fractions in the H_2 product stream. As can be seen from Figure C.3, these fluctuations are mainly in the mole fractions of H_2 and H_2O. The average mole fractions in the time period after $t = 173.75$ seconds can be found in Table 14.

The fluctuations in component flow rates and mole fractions in the H_2 product stream are of concern. The variations in component flow rates during the cycle states in which repressurization do no occur, are only minor. These variations could be damped by utilizing

Table 14: Average mole fractions in H_2 product stream after $t = 173.75$ s, referred to Figure 11

Mol-% CO_2	0.184
Mol-% H_2	51.4
Mol-% CO	0.0281
Mol-% H_2O	36.4
Mol-% inert Ar and N_2	12.0

a temporary storage vessel downstream of the SEWGS system, allowing mixing to occur before the gas is being sent to the gas turbines in the power island. However, the significant drop in component flow rates during the cycle states in which repressurization occur are much more concerning. Inspecting Figures C.1 and C.2, it can be seen that the flow rates in this stream is at this lower level for approximately 30 s/86.875 s $\approx$ 35 % of the time. The total flow rate drops by approximately 50 %, from ca. 6000 mol/s to 3000 mol/s. This drop cannot be handled by the downstream storage vessel. The requirement of maximum $\pm$ 5 % variation in the heating value of the H_2 stream sent to the gas turbines in the power island is difficult to fulfil under these circumstances.

Now, the focus is directed towards the CO_2 product streams of the SEWGS system, the streams CO_2 Product 1 and CO_2 Product 2 in Figure 11. The stream CO_2 Product 1 comes from the reactor in the purge step, while the stream CO_2 Product 2 is from the reactor in the depressurization step. It has been chosen to present the sum of these two streams, designated as stream CO_2 Product, in graphical form. The component flow rates of the CO_2 product stream can be found in Figure C.6. Inspecting the component flow rates, it can be seen that only very small amounts of H_2 and CO are leaving the system through the CO_2 product streams. This is in accordance with the objectives of the SEWGS process described in Section 1. However, it should be noted that these results could be affected by the assumption of no WGS reaction taking place during the equalization, depressurization, purge and re-equalization steps. The forward WGS shift reaction is favoured at lower temperatures. The temperatures of the streams CO_2 Product 1 and CO_2 Product 2 are in the range 865 - 870 K. At these high temperatures, the backwards WGS reaction is favoured, increasing the amount of CO and H_2O. However, inspecting the component mole fractions found in Figure C.8, the available amount of H_2 is very small, implying that the potential for reacting CO_2 and H_2 into CO and H_2O is small. The high temperatures of the CO_2 product streams are caused by the high temperatures near the reactor inlets, making the gas leaving the reactors during the countercurrent depressurization and purge steps take up some of the heat.

As desired, the CO_2 product stream mainly consist of CO_2 and steam H_2O. Inspecting the total flow rate found in Figure C.7, the flow rate is varying quite much. As in the H_2 product stream, the variations in the flow rate is following a repeating pattern every

$2 \cdot CycleTime/16 = 86.875$ seconds. The maximum flow rate is on average ca. 6000 mol/s, and the minimum ca. 1000 mol/s.

It is of interest to determine an average CO_2 capture ratio η_{cap} for the SEWGS system. Assuming that the system has reached steady state, this capture ratio can be expressed by the amount going out through the CO_2 product streams divided by the total amount of CO_2 and CO that have gone into the system over the simulation time:

$$\eta_{cap} = \frac{CO_2 \text{ and CO going out of the system in } CO_2 \text{ product streams 1 and 2}}{CO_2 \text{ and CO going into the system}} \quad (152)$$

The feed syngas constitutes the amount of CO_2 and CO going into the system. However, since it was necessary to assume that the rinse and purge steam stream did not only contain steam, small amounts of CO_2 and CO are going into the system through these streams. From calculations based on the simulation results, this is

$$CO_2 \text{ and CO going into the system} \approx 202479 \text{ mol } CO_2 \text{ in feed syngas}$$
$$+ 2886745 \text{ mol CO in feed syngas}$$
$$+ 3.66419 \text{ mol } CO_2 \text{ and CO in rinse steam} \quad (153)$$
$$+ 3.66350 \text{ mol } CO_2 \text{ and CO in purge steam}$$
$$\approx 3089231 \text{mol}$$

$$CO_2 \text{ and CO going out of the system in } CO_2 \text{ product streams 1 and 2}$$
$$\approx 2932293 \text{ mol } CO_2 + 208.9750 \text{ mol CO} \quad (154)$$
$$\approx 2932502 \text{ mol}$$

This gives a capture ratio of

$$\eta_{cap} \approx 94.93\%$$

This capture ratio is comparable to results from SEWGS modelling and experimental studies in the literature, such as the previously mentioned study by Wright et al. [45], which states a capture ratio of 95 %. In another work by Wright et al. [44], a capture ratio of 92.3 % is calculated. However, the capture ratio obtained in the present work should be treated with caution, considering the loss of mass in the simulation results.

The average mole fractions of the CO_2 product stream after $t = 173.75$ seconds is shown in Table 15. From this, an average dry-product CO_2 mole fraction can be calculated. That is, assuming that the steam has been removed. The average CO_2 mole fraction is then 99.32 %. According to Bolland [6], the mole fraction of CO_2 in the product stream in pre-combustion capture applications is typically larger than 95.6 % [6, p.53]. The

CO_2 purity of a stream sent to long-term storage should in most cases be larger than 95 % [6, p.54] [45]. This is satisfied given the results in the present work. In the SEWGS modelling work by Wright et al. [44], which assumes that the syngas is made through ATR of natural gas, the CO_2 product purity is set to 98 %. This is comparable to the result in the present work.

Table 15: Average mole fractions in CO_2 product stream after t = 173.75 s, referred to Figure 11

Mol-% CO_2	71.4
Mol-% H_2	0.320
Mol-% CO	0.00409
Mol-% H_2O	28.1
Mol-% inert Ar and N_2	0.163

The primary goal for the SEWGS system of trains is to convert the feed syngas into a product stream consisting of combustible H_2 which should be sent to the power island for power production. The secondary goal is to remove the CO_2 contained in the feed syngas and that which is converted from CO in the WGS reaction. To be able to achieve this secondary goal, there is a possibility that some of the combustible products, H_2 and CO, will be carried out of the system through the CO_2 product streams, thereby losing some of the available combustion energy inherent in the original feed syngas. The amount of combustible H_2 and CO leaving the system through the CO_2 product streams instead of the H_2 product stream, is primarily determined by how much of these gases that is rinsed out of the reactor during the rinse step. In general, by rinsing out more of these gases, and mixing the effluent gas into the gas going to the reactors in the feed step, less H_2 and CO is lost. In the SEWGS cycle utilized in the present work, there are three equalization steps. By having these equalization steps, it is not necessary to rinse out all of the H_2 and CO, since most of the remaining H_2 and CO will be transferred to reactors preparing for the feed step, that is, undergoing the re-equalization steps. This is in accordance with the reasoning in the work by Wright et al. [45] for not completing the rinse step until completion. However, not all of the H_2 and CO will leave the reactor before the depressurization and purge steps are initiated. As the depressurization step starts, most of the remaining H_2 and CO in the reactor will be lost through the CO_2 product streams. This is confirmed by the simulation results, see for example the mole fractions in reactor 1 at the beginning of the depressurization step in the second SEWGS cycle, found in Figure D.7. It can be seen that there is still some H_2 remaining in the reactor in the region close to the inlet. The steam flow rate for rinse, $\dot{n}_{HP\ Rinse\ R}$, should therefore be set as high as required to avoid the loss of too much H_2 and CO. However, this steam flow rate should not be too high either, as this steam is taken from the power island, thereby lowering the energy production. Please refer to the discussion in Section 1. Therefore, a trade-off between these two requirements has to be made. The rinse steam flow rate is also determining

for the CO_2 product stream purity. In the work by Wright et al. [44], the purity of 98 % was set to determine the required amounts of rinse and purge steam. According to Wright et al. [45], the CO_2 product purity is increased when the rinse steam flow rate is increased, since more of the H_2 , CO and N_2 have left the reactor before the depressurization starts. This is confirmed by the results in the present work. The rinse steam flow rate utilized in the simulations have been determined by trial and error.

Assuming that the system has reached steady state, the H_2 and CO recovery factor can be defined as

$$\eta_{Recovery} = \frac{H_2 \text{ and } CO \text{ going out of the system in } H_2 \text{ product stream}}{H_2 \text{ and } CO \text{ going into the system}}$$

(155)

$$\approx \frac{3619034.411 \text{ mol } H_2 \text{ and } CO}{4177678.738 \text{ mol } H_2 \text{ and } CO} \approx 86.63\%$$

This is not a very good recovery factor. Only 86.63 % of the total combustible components in the feed syngas reaches the H_2 product stream. There could be several explanations for this low value. As discussed earlier, the mass going into the system is not conserved. This could one part of the explanation. It could also be that the system has not reached cyclic steady state. The SEWGS modelling work by Wright et al. [44], does not explicitly state the recovery factor obtained. However, given the stream data in their work, a value of 100 % is calculated. This is a remarkably high value, and it might be that their stream data does not work as a valid basis for this calculation. However, the value obtained in the present work is very low compared to this one.

The cycle time determined in Section 3.14, of 695 seconds, has been found to be appropriate for the SEWGS system configuration utilized in the present work. Given this cycle time, only small amounts of CO_2 and CO breaks through into the H_2 product stream. The amount of H_2 and CO breaking through into the CO_2 product streams is also very small. There are few reported values for the cycle time utilized in similar SEWGS systems. The SEWGS modelling work by Allam et al. [2], reports a value of 280.2 seconds [2, p.244]. This work utilizes a similar SEWGS cycle as the one in the present work, the difference being that CO_2 is used in a cocurrent rinse step, with the cycle configured for 7 reactors per train. The reactor dimensions and feed flow rates are comparable to those in the present work.

In the few SEWGS modelling studies available in open literature, the results given are not very detailed. In most cases, only key numbers such as capture ratio, CO_2 product purity and rinse and purge steam requirements, are given. However, in the work by Wright et al. [44], a few graphs are given, showing the cumulative partial pressures in one of the reactors at a few key points in time during the cycle. It is of interest to see how the results

generated in the present work compares to these. In Figure 21, the cumulative partial pressures in reactor 1 at the end of the feed step in the second SEWGS cycle is shown. As the feed syngas in the study by Wright et al. [44] is made from natural gas, there should be less CO_2 and CO in the reactor. In the data given for the feed syngas by Wright et al. [44], the sum of the mole fractions of CO_2 and CO is 0.117 + 0.026 = 0.143. In the present work, the same sum is $0.0196 + 0.2799 = 0.2995$, referring to stream 4 in Table 2. There is approximately twice the amount of CO_2 and CO in the present work. Another difference is that the feed syngas pressure in the work by Wright et al. [44] is 28 bar, compared to 26.89 bar in the present work. The purge pressure is the same, 1.1 bar.
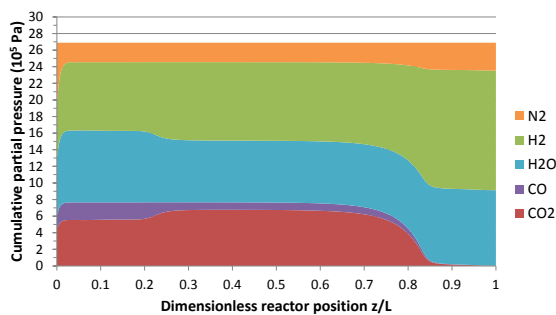

Figure 21: Cumulative partial pressures (10^5 Pa) in reactor 1 at $t = 868.75$ s, after step F

Comparing Figure 21 to its equivalent in the work by Wright et al. [44], there are several differences to be noted. One is the significant larger partial pressure of CO_2 . At its maximum, this partial pressure in the present work is approximately twice that of Wright et al. [44]. This is reasonable, given the previous discussion. The same seems to be valid for the CO, but it is difficult to be sure from the limited detail given in the figure by Wright et al. [44]. The CO_2 adsorption front in the present work is much sharper than the one in Wright et al. [44]. That is, the degree of more or less S-shape of the CO_2 partial pressure front near the outlet of the reactor. This could be due to two different aspects of the reactor model. It could be that the adsorption rate is much faster in the present work. For a given flow rate, the sharpness of the adsorption front increase when the adsorption rate increase. With reference to Table 3, it is known that the feed syngas flow rate going to each reactor in the feed step in the present work is 42 % of that used in the work by Wright et al. [44]. For a given adsorption rate, the sharpness of the adsorption front will decrease when the flow rate is increased. This could be the second explanation for the difference in the sharpness in the adsorption fronts. In the work by Wright et al. [44], it looks like the feed step has been run until after there is breakthrough of CO_2 at the outlet. Based on the information in the graph, the outlet mole fraction of CO_2 is approximately 4 %. In the present work, there are almost no breakthrough of CO_2 into the H_2 product stream. The maximum value of the mole fraction of CO_2 in this stream is ca. 0.8 %, at $t = 519.25$ s. This is a very low value, and can be explained by inspecting the mole fractions in the reactors at the end of the feed step. The mole fractions in reactor 1 at the end of the feed step in the second SEWGS cycle is shown in Figure D.3. It can be seen that the adsorption front is some distance from the outlet. The same is valid for the other reactors.

This discussion raises an important question: Is the SEWGS system over-dimensioned with respect to the number of SEWGS trains utilized? Given the syngas flow rate to be treated, stream 4 in Table 2, if one were to lower the number of SEWGS trains, the syngas flow rate being sent to each reactor in the feed step is increased. This implies that the CO_2 adsorption front will be less sharp. This will cause the mole fraction of CO_2 at the outlet to increase faster than before. Allowing for a higher breakthrough CO_2 mole fraction, and reducing the cycle time according to this specification, it should be possible to achieve a SEWGS system which goes towards cyclic steady state. By reducing the number of SEWGS trains, the capital costs will decrease. This is in accordance with the discussion in Section 1.3, and should be considered in further work.
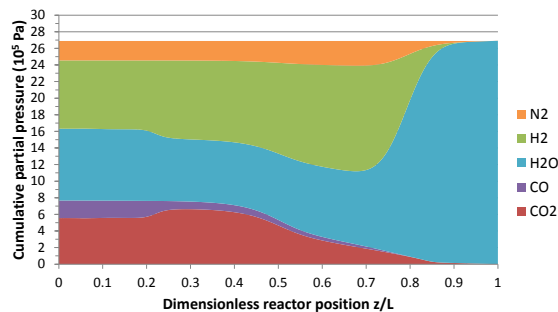

Figure 22: Cumulative partial pressures (10^5 Pa) in reactor 1 at $t = 955.625$ s, after step R

Figure 22 shows the cumulative partial pressures in reactor 1 after the rinse step in the second SEWGS cycle. Comparing this to its equivalent presented in the work by Wright et al. [44], it can be seen that the rinse steam has travelled approximately the same length into the reactor. This implies that approximately the same portion of the residual gases in the reactor at the end of the feed step, has been rinsed out of the column.

The cumulative partial pressures in reactor 1 after the third equalization step Eq3 in the second SEWGS cycle is shown in Figure 23. It is very similar to the equivalent figure in the work by Wright et al. [44], and differences are not easy to identify. This implies that approximately the same amount of H_2 and CO remains in the gas-phase in the reactor before the depressurization step starts. This H_2 and CO will be lost into the CO_2 product streams.

It is of interest to compare the rinse and purge steam requirements obtained in the present work to reported values from literature. Table 16 compares the values obtained in the present work to those found in the SEWGS modelling work on a natural gas-fed IRCC power plant by Wright et al. [44], and to the SEWGS modelling work on a coal-fed IGCC power plant by Wright et al. [45]. Key indicators are the rinse and purge
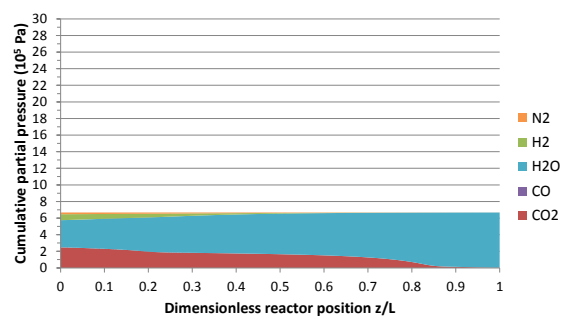

Figure 23: Cumulative partial pressures (10^5 Pa) in reactor 1 at $t = 1085.9375$ s, after step Eq3

to feed flow ratios, the rinse and purge to feed carbon flow ratios and the total steam-to-carbon ratio. The total steam-to-carbon ratio does only account for the steam added in the rinse and purge steps, not the steam in stream 3 in Table 2. It can be seen that the key indicators obtained in the present work are significantly lower than those reported by Wright et al. [45]. The most notable difference is the significantly lower purge to feed flow and purge to feed carbon flow. In the reactor model utilized in the present work, it is assumed that the mass transfer coefficient k_{LDF} is constant for both adsorption and desorption of CO_2. As discussed in Section 2.8.8, there is significant debate regarding the adsorption and desorption kinetics of the K-HTC adsorbent. In the literature presented in Section 2.8.8, some authors state that the desorption is much slower than the adsorption, which means that k_{LDF} should be lower for desorption than adsorption. The significantly lower required purge steam flow rates obtained in the present work is therefore affected by the assumption of a constant k_{LDF}. If a lower value of k_{LDF} had been utilized during the desorption, the purge steam requirement would have been increased. Since there is so much uncertainty about the correct values of k_{LDF}, the purge steam requirements obtained in the present work should be treated with caution.

Table 16: Comparison of rinse and purge steam requirements

	Unit	Present case 400 MW IGCC	Wright et al. [44] 330 MW IRCC	Wright et al. [45] IGCC
Syngas mol-% CO_2	-	1.96	11.7	24
Syngas mol-% H_2	-	12.52	32.2	35
Syngas mol-% CO	-	27.99	2.6	6
Syngas mol-% H_2O	-	53.57	15.2	31
Syngas mol-% Inert	-	3.96	38.2	4
Rinse to feed flow	mol/mol	0.0895	0.1270	0.15
Purge to feed flow	mol/mol	0.0890	0.1905	0.40
Rinse to feed carbon flow	mol/mol	0.2989	0.8880	0.57
Purge to feed carbon flow	mol/mol	0.2970	1.3320	1.33
Total steam-to-carbon ratio	mol/mol	0.5959	2.22	1.90

The total steam-to-carbon ratio obtained for the present work is very low. As discussed in Section 1, Wright et al. [45] states that the total steam-to-carbon ratio from rinse and purge should not exceed a value of 2.0, to be able to be economically competitive with other pre-combustion capture technologies. A value of 0.5959 is certainly below this limit, but should for the reasons discussed above be interpreted with some scepticism.

One of the differences between the case studied in the present work and others are the omission of the upstream WGS reactor, as discussed in Section 1.3. A significant temperature increase is to be expected in the reactors due to the exothermic forward WGS reaction. The temperature profiles in the 8 reactors in the SEWGS train are found to be

very similar, both qualitatively and quantitatively. The temperature profile for reactor 1 will therefore be used as an example in the discussion to follow. Figure 24 shows the temperatures in reactor 1 as a function of time and axial position. It can be seen that the temperature in the region $z = 0$ to $z \approx 2$ m is quite high. The maximum temperature in this region is ca. 882 K at $z/L \approx 0.0615$ m/7.377 m ≈ 0.00833, $t = 31$ s. This corresponds to a temperature increase of 209 K compared to the feed syngas temperature of 673 K. As discussed in Section 1, the maximum operating temperature of the FeCr-based catalyst is 773 K. With a temperature spike of 882 K the catalyst might be destroyed. The maximum temperature K-HTC can endure is around 800 K, as discussed in Section 1. If the hot spot temperature is in fact as high as this, the adsorbent might be destroyed. The heat generated at this hot spot spreads through the first part of the reactor from $z = 0$ to $z \approx 2$ m, and is partly absorbed in the gas phase and in the solid catalyst, while some of the heat is transferred out through the reactor wall.
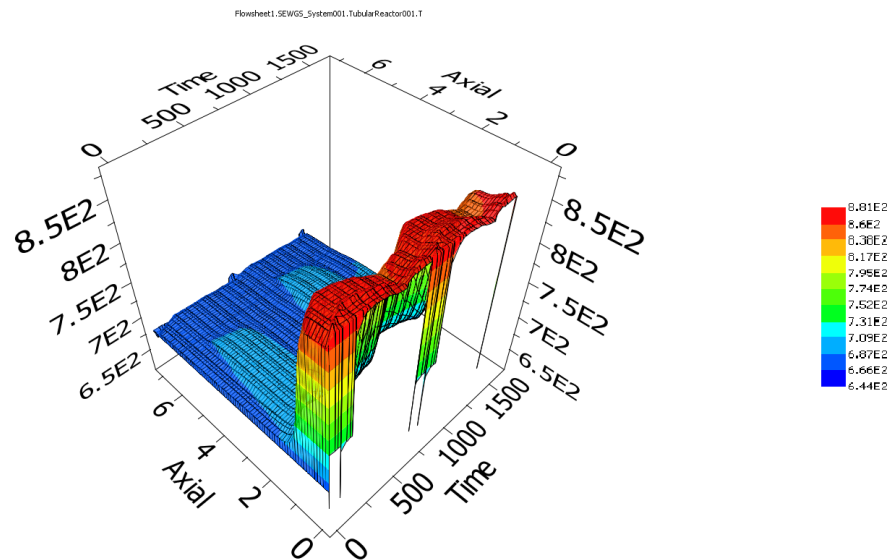

Figure 24: Reactor 1: Temperature T (K) as a function of time t (s) and axial position z (m)
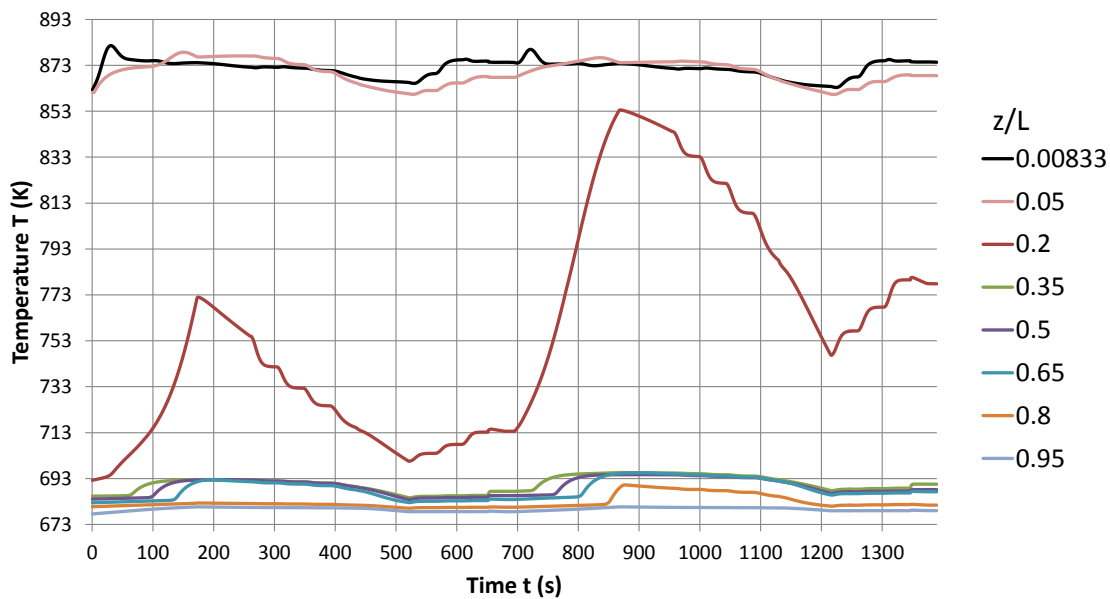
Figure 25: Reactor 1: Temperature profiles T (K) for different points z/L in the reactor as a function of time t (s)

There could be several reasons for this temperature spike. Since the mole fraction of CO in the feed syngas is very high, the heat generated through the conversion of CO and H_2O to CO_2 and H_2 will be significantly higher than for a feed with less CO. A single-reactor simulation using the feed mole fractions after the high-temperature WGS reactor from the DECARBit test case was conducted to verify this (CO mol-% of 6.31) [16]. As expected the temperature increase was much lower, spiking at ca. 705 K. This corresponds to a temperature increase of 32 K compared to the temperature of the feed syngas.

The SEWGS experimental work by Van Selow et al. [42] provides data which can be used for comparison with the results for the temperature in the present work. Van Selow et al. [42] uses the same adsorbent and catalyst setup as in the present work. The single-reactor experiments were performed using a reactor column 2 m long with an internal diameter of 38 mm. The column was fed a gas mixture consisting of 16 % CO_2, 58 % H_2, 10 % CO, 16 % H_2O at 400 °C and 28 bar, with an inlet velocity of ca. 0.01 m/s. The feed composition in the present work is different, which is due to that the bulk of the CO conversion through the WGS reaction is assumed to take place in the SEWGS reactor. In contrast to the work by Van Selow et al. [42], which assumes that a WGS reactor is used before the SEWGS reactor. The curves in Figure 25 are comparable to the temperature profiles for sorption-enhanced reaction experiments found in Figure 13 in the work by Van Selow et al. [42], showing similar shapes although quite different relative scales. Please note that, in contrast to Figure 25, the figure provided by Van Selow et al. [42] shows the temperature profiles for the feed step only. The most remarkable difference is the spike in temperature close to reactor inlet, at z/L = 0.05, at 807 K, compared to 718 K in the work by Van Selow

et al. [42]. The reasons for this are related to the mole fraction of CO, as discussed in the previous paragraph. The temperature spike of 718 K in the work by Van Selow et al. [42], with the feed containing 10 % CO, is comparable to the single-reactor simulations in the present work, with a temperature spike of 705 K, with the feed containing 6.31 % CO.

Inspecting Figure 25, it can be seen that reactor 1 has not reached steady state with respect to the distribution of temperatures within the reactor. The temperature at the point $z/L =$ 0.2 is increasing from the first to the second SEWGS cycle. This is also confirmed by inspection of Figure 24. It can be seen that the heat developed from the forward WGS reaction near the inlet spreads through the reactor as time passes. If the simulation had been run for additional cycles, it is reasonable to assume that the temperatures within the reactor will increase for each additional cycle. There was not sufficient time to investigate this in detail.

This discussion suggests that the omission of an upstream WGS reactor might lead to unacceptable high temperatures in the SEWGS reactors. The temperatures within the reactor will quite possibly destroy the catalyst and adsorbent. However, these results should be treated with care, as some of the reactor model assumptions might be unreasonable. As discussed in Section 2.11, there are several uncertainties related to the parameters and correlations utilized by the model. The value for the overall heat transfer coefficient U was chosen to be set to a constant value. It is possible that this constant value is too low, making the heat transferred out through the reactor wall too low. It might be necessary to obtain a correlation for the value of U that is valid for the reactor dimensions and setup utilized in the model. This should be investigated in later work. The heat capacity of the catalyst was chosen to be equal to that of the adsorbent, and this might affect the results. Also, it might be that the catalyst efficiency is too high, making the forward WGS reaction to take place in a very limited part of the reactor, close to the inlet. The reactor wall temperature T_{wall} was chosen to be equal to 673 K over the whole length of the reactor. Since the bulk of the forward WGS reaction takes place near the inlet of the reactor, it might be possible to lower the temperature in this region by applying some form of additional cooling on the reactor wall in this region. This should be investigated in later work.

The objective of this work is to simulate the SEWGS system. The discussion so far has therefore considered the behaviour and characteristics of the streams going into and out of the SEWGS system (Figure 11). However, a discussion of the behaviour of the individual reactors leading to the system behaviour is appropriate. This discussion will be based on the behaviour of reactor 1 in the second SEWGS cycle simulated, when the assumptions of the startup cycle are not affecting the behaviour any more. The behaviour of the other reactors in the system are similar. Figures D.1 through D.13 shows the mole fractions in this reactor at the start and end of every step in the second SEWGS cycle, from $t = 695$ to $t = 1390$ seconds. Upon starting the feed step, the adsorbent in the region close to the inlet

is saturated with CO_2 which has been received from other reactors during the cocurrent re-equalization steps (Figure 26). This explains the CO_2 and CO in the gas-phase near the reactor inlet (Figure D.1). It can be seen from Figure 26 that the available adsorption capacity in the reactor increases further away from the inlet. Halfway through the feed step, the adsorption front has travelled more than halfway through the reactor (Figure D.2). With reference to Figures 24 and 25, it can be seen that due to the high temperatures in the region $z/L = 0$ to 0.2, the forward WGS reaction only take place to some extent, converting CO and H_2O into CO_2 and H_2 . In the region $z/L \approx 0.2$ to 0.4, the lower temperature favours the forward WGS reaction, allowing even more CO and H_2O to be converted.

In the region from the adsorption front and up to the reactor outlet, $z/L \approx 0.6$ to 1.0, it can be seen that the adsorption of CO_2 shifts the equilibrium of the WGS reaction towards the products, allowing the conversion of CO to approach completion. This illustrates the advantage of combining the WGS reaction with adsorption of CO_2 in a single reactor vessel. At the end of the feed step, the adsorption front has not reached the out-

Figure 26: Reactor 1: Adsorbent loading q_{CO_2} (mol CO_2/kg adsorbent) at $t = 695$ s, as a function of dimensionless axial position z/L

let, ensuring that very small amounts of CO_2 and CO break through into the H_2 product stream (Figure D.3). At the end of the rinse step, some of the gas in the reactor at the end of the feed step has been pushed out of the reactor (Figure D.4). Figures D.5, D.6 and D.7 shows how most of the residual gases in the reactor at the end of the rinse step is being transferred to the reactors in the re-equalization steps. These figures also show how some of the adsorbed CO_2 is being desorbed as the pressure in the reactor decreases. During the depressurization step, the pressure is lowered, and even more CO_2 is desorbed and is being transferred out through the reactor inlet, going to the CO_2 product streams (Figure D.8).

At the end of the purge step. there is still some CO_2 left in the gas-phase in the reactor (Figure D.9). Figures D.10, D.11 and D.12 shows how the reactor under the re-equalization steps receives gas cocurrently from the reactors undergoing the equalization steps. As gas is received, the pressure in the reactor increases, and CO_2 is being adsorbed as the increase in pressure also increases the equilibrium adsorption capacity. During the repressurization step, the reactor receives product gas from the reactor in the last fourth of the feed step (Figure D.13).

Figure 29 shows the total pressure profile for reactor 1 as a function of time and axial position. During the feed step, the outlet pressure is assumed to be at 26.89 bar = 2689000
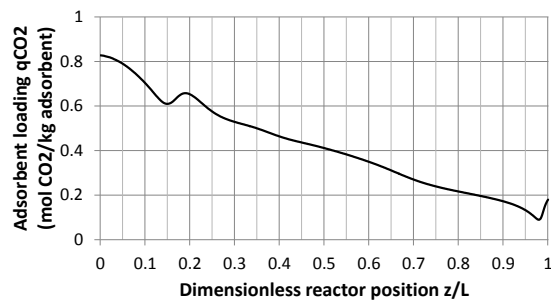
Pa. The simulation results shows that the pressure drop over the reactor during this step is at its maximum ca. 277 Pa. That is, an inlet pressure of 2689277.2 Pa at $t = 866.75$ s. It has not been possible to find data from literature on SEWGS reactors for comparison. However, the pressure drop over the high-temperature WGS reactor from DECARBit is stated as 1 bar [16]. Compared to this, the pressure drop obtained in the results in the present work is very low. This should be investigated in further work. Figure 27 shows the total pressure p at $z = 0$ as a function of time. It can be seen that the operating pattern of the valves controlling the flow between the reactors during the equalization, depressurization, re-equalization and repressurization steps are appropriate for allowing the necessary pressure changes to take place in the time duration allocated for these steps.
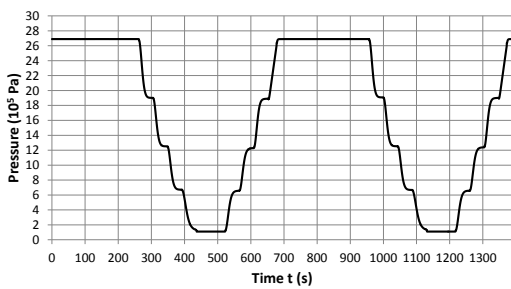
Figure 27: Reactor 1: Total pressure $p(z = 0)$ (10^5 Pa) as a function of time t (s)
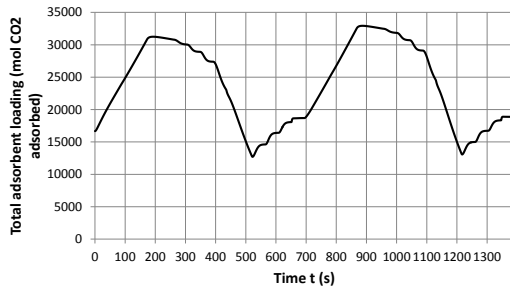
Figure 28: Reactor 1: Total adsorbent loading $moles_{single\ reactor}$ (mol CO_2 adsorbed) as a function of time t (s)
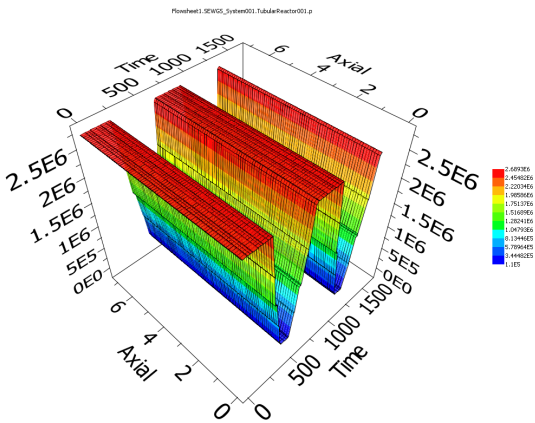
Figure 29: Reactor 1: Total pressure p (Pa) as a function of time t (s) and axial position z (m)
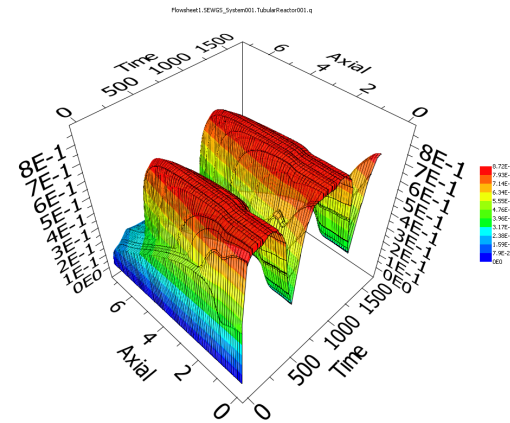
Figure 30: Reactor 1: Adsorbent loading q_{CO_2} (mol CO_2/kg adsorbent) as a function of time t (s) and axial position z (m)

Figure 30 shows the adsorbent loading of CO_2 in reactor 1 as a function of time and axial position. Figure 28 shows the total amount of adsorbed CO_2 in reactor 1 as a function of time. The cyclic capacity of the reactor is determined by the difference between the total adsorbent loading in the reactor at the end of the feed step and at the start of the feed step. Table 17 sums up the total adsorbent loading at these points in time. It can be seen

that the total adsorbent loading at the start of the feed step is increasing slightly for each cycle. However, inspecting the total adsorbent loading for the other reactors, it can be seen that for some of the reactors the total adsorbent loading at the start of the feed step is decreasing slightly. This is another example of the asymmetric behaviour of the SEWGS system of reactors. As no breakthrough of CO_2 into the H_2 product streams is observed, it can be concluded that the total cyclic capacity of the SEWGS system is high enough to handle the flow of CO_2 and CO going into the system.

Table 17: Reactor 1: Total adsorbent loading $moles_{single\ reactor}$ (mol CO_2 adsorbed) and cyclic capacity

$moles_{single\ reactor}(t = 0)$	16679
$moles_{single\ reactor}(t = 173.75)$	30911
Capacity	14232
$moles_{single\ reactor}(t = 695)$	18693
$moles_{single\ reactor}(t = 868.75)$	32604
Capacity	13911
$moles_{single\ reactor}(t = 1390)$	18891

The behaviour of reactor 1 which has now been presented, is qualitatively in accordance with what is expected. This is also valid for the other reactors, which have not been described in this text. However, as the previous discussion suggests, the quantitative results from the simulations, are to some extent questionable. There is significant improvement potential for the model with respect to the parameters and correlations utilized in both the reactor and system model. The framework for the simulation of such a system of reactors has been established, and the necessary modifications to the reactor model and the system model should therefore be fairly uncomplicated to carry out.

5. Conclusions and further work

5.1. Conclusions

The simulation of the SEWGS system has given results that are quantitatively infeasible in several aspects. Several of the reasons for this have been discussed. There is a significant need for a thorough evaluation of the reactor model assumptions and the implementation of the system model in gPROMS, to ensure that the model gives quantitatively consistent results. As there are several aspects which could contribute to the errors observed in the results, it is difficult to draw any conclusions about the quantitative behaviour of the SEWGS system. However, the results confirm the physical mechanisms and qualitative trends expected for a SEWGS system. The system is operating as it is intended, fulfilling its primary objective of converting carbon-rich syngas into a hydrogen-rich combustible gas mixture. The secondary objective is also fulfilled, capturing CO_2 and bringing this out of the system in a gas stream containing mostly CO_2 and steam, with essentially no nitrogen. After removal of the steam, this stream is highly suitable for being sent to CO_2 storage, as the stream consists of mostly CO_2, ensuring that the storage volume required is minimized.

However, there are significant variations in the flow rate of the H_2 product stream. When some of the product gas from the reactors in the feed step is being sent to repressurize another reactor in the SEWGS train, the flow rate of the H_2 product stream is reduced by approximately 50 %. This behaviour has not been reported in available literature on the performance of SEWGS systems. The requirement of maximum ± 5 % variation in the heating value of the H_2 stream sent to the gas turbines in the power island is difficult to fulfil under these circumstances. The reasons for this should be investigated in later work.

The temperatures in the reactors of the system reaches an unacceptable high level, which could destroy the catalyst and adsorbent materials. The reason for this is most likely the omission of the upstream WGS reactor, which gives very a very high content of CO in the feed syngas being sent into the system. As a consequence of this, significant heat being developed close to the reactor inlets as the conversion of CO takes place in the exothermic forward WGS reaction. It might be possible to correct for this by introducing extra cooling at the reactor wall in the region close to the inlet. There is also a possibility that some of the model assumptions are incorrect, giving too high temperatures in the results than would have been in the real-world operation of the reactors. As there are several uncertainties about the quantitative reliability of the results, it is difficult to draw any conclusions regarding this matter.

The number of SEWGS trains utilized was chosen to be very large. This assumption should be investigated in detail, as this implies significantly higher costs than which might

be necessary. Therefore, the configuration of the SEWGS system developed in the present work should be taken as a basis for optimization work, with considerable focus on the economical viability in terms of capital costs.

A fully customizable modelling framework for the simulation of the SEWGS system utilizing the chosen type of cycle has been developed in the simulation software gPROMS. Although there are significant improvements to be made with respect to reactor model assumptions, this framework should make it fairly uncomplicated to be used as a basis for optimization, and further on as a fully functioning dynamic model which could be integrated into a larger system model for the operation of an IGCC power plant within gPROMS.

5.2. Further work

As discussed in Section 2, several problems with the reactor model was discovered late during the work process. In Section 2, it was assumed that it was possible to utilize mass balances for all components except one, and include a total mass balance and a relationship equating the sum of the component concentrations $\bar{c}_i$ to the total concentration $\bar{c}$. A better solution strategy would be to replace the relationship equating the sum of the component concentrations $\bar{c}_i$ to the total concentration $\bar{c}$, Eq. (22), with a component mass balance for the last component and corresponding boundary conditions. The component mass balance for the last component should be on the same form as for the other components, Eq. (10). In addition, it is necessary to redefine the partial derivatives with respect to the reactor z-axis, to be on a dimensionless form. That is, substitute all occurrences of z with $z \cdot L$. There is also a need for reconfiguring the upper and lower bounds for the variables in gPROMS.

There are several other aspects of the reactor model which should be investigated. To summarize:

- Expanding the energy balance and momentum balance to account for non-instantaneous pressure change.
- Substitution of the adsorption isotherm with one that better describes the properties of the new types of K-HTC under development.
- Determining more consistent void fractions.
- Determining the specific heat capacity of the catalyst.
- Determining values for β_1, γ, Φ, e, k_g, k_s, a_{k_z} consistent with K-HTC and FeCr-based catalyst.
- Investigate the need for a correlation or utilizing another constant for the bed-to-wall heat transfer coefficient U, which is valid for the reactor dimensions and setup utilized.

- It is possible to calculate values of μ using the Multiflash physical property package in gPROMS, and implement μ as a variable in gPROMS, instead of a constant value.
- Investigate the effect of assuming no WGS reaction during the steps Eq1, Eq2, Eq3, D, P, REq3, REq2 and REq1.
- Investigate the need for additional cooling on the wall near the reactor inlets, to lower the temperature in this region to acceptable levels for the catalyst and adsorbent.
- Investigate the realism of the very small pressure drops obtained in the results, and the reasons for this.
- Investigate the realism of the rinse and purge requirements obtained in the results. This is closely linked to the constant value of the linear driving force model mass-transfer coefficient k_{LDF} utilized. Is there a need for implementing a correlation for k_{LDF} instead of using a constant value?
- Implement an energy balance check for the boundary of the reactors, to ensure that energy is conserved.
- Determine the molecular diffusion coefficient D_m, to be able to use the correlation for the axial dispersion coefficient D_{ax}.

Also, there are several aspects of the system model that should be investigated. These can be summarized as:

- Since the system had not reached cyclic steady state, it is necessary to simulate additional cycles.
- Investigate the possibility of reducing the steam-to-carbon ratio in a stream sent to a SEWGS system compared to a case where the stream is to be sent to a ordinary WGS reactor.
- Investigate the choice of the valve flow coefficients, and the necessity of changing the valve model equations.
- Investigate the need of reconfiguring the gPROMS solver configuration and the number of discretization points utilized in the reactor model, to ensure conservation of mass.
- Investigate the possibility for decreasing the number of SEWGS trains utilized, to lower the capital costs of the SEWGS system. This will lead to increased flow rates and shorter cycle time, implying that the number of discretization points in the reactor models should be increased, to ensure that mass is conserved in the reactors.
- Investigate the reasons for the large variations in flow rates in the H_2 product stream. Is there a need for substituting the current cycle with another type?
- Investigate the effects of the simplifications utilized in the implementation of the system model in gPROMS, especially with focus on the switching between each state in the SEWGS cycle.

References

[1] T.A. Adams II and P.I. Barton. A dynamic two-dimensional heterogeneous model for water gas shift reactors. *International Journal of Hydrogen Energy*, 34(21):8877–8891, 2009.

[2] R.J. Allam, R. Chiang, J.R. Hufton, P. Middleton, E.L. Weist, and V. White. Development of the sorption enhanced water gas shift process. *Carbon Dioxide Capture for Storage in Deep Geologic Formations*, 1:227–256, 2005.

[3] E. Alpay, C.N. Kenney, and D.M. Scott. Simulation of rapid pressure swing adsorption and reaction processes. *Chemical Engineering Science*, 48(18):3173–3186, 1993.

[4] K. Atwood, M.R. Arnold, and E.G. Appel. Water-gas shift reaction. Effect of pressure on rate over an iron-oxide-chromium oxide catalyst. *Industrial & Engineering Chemistry*, 42(8):1600–1602, 1950.

[5] E. Bakken, P.D. Cobden, P.P. Henriksen, S.F. Håkonsen, A.I. Spjelkavik, M. Stange, R.E. Stensrød, Ø. Vistad, and R. Blom. Development of CO_2 sorbents for the SEWGS process using high throughput techniques. *Energy Procedia*, 4:1104–1109, 2011.

[6] O. Bolland. Power generation: CO_2 capture and storage. 2011.

[7] O. Bolland. Personal communication, 2012.

[8] S. Choi, J.H. Drese, and C.W. Jones. Adsorbent materials for carbon dioxide capture from large anthropogenic point sources. *ChemSusChem*, 2(9):796–854, 2009.

[9] P.D. Cobden, P. van Beurden, H.T.J. Reijers, G.D. Elzinga, S.C.A. Kluiters, J.W. Dijkstra, D. Jansen, and R.W. Van Den Brink. Sorption-enhanced hydrogen production for pre-combustion CO_2 capture: Thermodynamic analysis and experimental results. *International Journal of Greenhouse Gas Control*, 1(2):170–179, 2007.

[10] P.V. Danckwerts. Continuous flow systems: Distribution of residence times. *Chemical Engineering Science*, 2(1):1–13, 1953.

[11] A.P. De Wasch and G.F. Froment. Heat transfer in packed beds. *Chemical Engineering Science*, 27 (3):567–576, 1972.

[12] Y. Ding and E. Alpay. Equilibria and kinetics of CO_2 adsorption on hydrotalcite adsorbent. *Chemical Engineering Science*, 55(17):3461–3474, 2000.

[13] Y. Ding and E. Alpay. Adsorption-enhanced steam-methane reforming. *Chemical Engineering Science*, 55(18):3929–3940, 2000.

[14] M.F. Edwards and J.F. Richardson. Gas dispersion in packed beds. *Chemical Engineering Science*, 23 (2):109–123, 1968.

[15] S. Ergun. Fluid flow through packed columns. *Chemical Engineering Progress*, 48:89–94, 1952.

[16] F. (Editor) Franco, R. Anantharaman, O. Bolland, N. Booth, E. van Dorst, C. Ekstrom, E. Sanchez Fernandes, E. Macchi, G. Manzolini, D. Nikolic, A. Pfeffer, M. Prins, S. Rezvani, and L. Robinson. Enabling advanced pre-combustion capture techniques and plants. Technical report, Alstom UK, 2011.

[17] M. Gazzani, E. Macchi, and G. Manzolini. CAESAR: SEWGS integration into an IGCC plant. *Energy Procedia*, 4:1096–1103, 2011.

[18] C.J. Geankoplis. *Transport processes and separation process principles: (includes unit operations).* Prentice Hall Professional technical reference. Prentice Hall Professional Technical Reference, 2003. ISBN 013101367X.

[19] M.H. Halabi, M. De Croon, J. Van Der Schaaf, P.D. Cobden, and J.C. Schouten. Reactor modeling of sorption-enhanced autothermal reforming of methane. Part I: Performance study of hydrotalcite and lithium zirconate-based processes. *Chemical Engineering Journal*, 168:872–882, 2011.

[20] D.P. Harrison. Sorption-enhanced hydrogen production: A review. *Industrial & Engineering Chemistry Research*, 47(17):6486–6501, 2008.

[21] S.S. Hla, D. Park, G.J. Duffy, J.H. Edwards, D.G. Roberts, A. Ilyushechkin, L.D. Morpeth, and

T. Nguyen. Kinetics of high-temperature water-gas shift reaction over two iron-based commercial catalysts using simulated coal-derived syngases. *Chemical Engineering Journal*, 146(1):148–154, 2009.

[22] J. Hoogschagen. Diffusion in porous catalysts and adsorbents. *Industrial & Engineering Chemistry*, 47(5):906–912, 1955.

[23] J.R. Hufton, R.J. Allam, R. Chiang, P. Middleton, E.L. Weist, and V. White. Development of a process for CO_2 capture from gas turbines using a sorption enhanced water gas shift reactor system. In *Proceedings of 7th International Conference on Greenhouse Gas Control Technologies*, volume 1, pages 253–262, 2005.

[24] D. Kunii and J.M. Smith. Heat transfer characteristics of porous rocks. *AIChE Journal*, 6(1):71–78, 1960.

[25] K.B. Lee, A. Verdooren, H.S. Caram, and S. Sircar. Chemisorption of carbon dioxide on potassium-carbonate-promoted hydrotalcite. *Journal of colloid and interface science*, 308(1):30–39, 2007.

[26] K.B. Lee, M.G. Beaver, H.S. Caram, and S. Sircar. Reversible chemisorbents for carbon dioxide and their potential applications. *Industrial & Engineering Chemistry Research*, 47(21):8048–8062, 2008.

[27] C.H. Li and B.A. Finlayson. Heat transfer in packed beds–a reevaluation. *Chemical Engineering Science*, 32(9):1055–1066, 1977.

[28] Z. Liu, C.A. Grande, P. Li, J. Yu, and A.E. Rodrigues. Multi-bed vacuum pressure swing adsorption for carbon dioxide capture from flue gas. *Separation and Purification Technology*, 81(3):307–317, 2011.

[29] G. Manzolini, E. Macchi, M. Binotti, and M. Gazzani. Integration of SEWGS for carbon capture in natural gas combined cycle. Part A: Thermodynamic performances. *International Journal of Greenhouse Gas Control*, 5(2):200–213, 2011.

[30] M.J. Moran and H.N. Shapiro. *Fundamentals of engineering thermodynamics*. John Wiley & Sons, 2006. ISBN 9780470030370.

[31] D. Nikolic, A. Giovanoglou, M.C. Georgiadis, and E.S. Kikkinides. Generic modeling framework for gas separations using multibed pressure swing adsorption processes. *Industrial & Engineering Chemistry Research*, 47(9):3156–3169, 2008.

[32] R.H. Perry and D.W. Green. *Perry's chemical engineers' handbook*. Chemical Engineers Handbook. McGraw-Hill, 2008. ISBN 9780071422949.

[33] H.F. Rase. *Chemical reactor design for process plants*, volume 2. John Wiley & Sons New York, 1977.

[34] H.T.J. Reijers, S.E.A. Valster-Schiermeier, P.D. Cobden, and R.W. van den Brink. Hydrotalcite as CO_2 sorbent for sorption-enhanced steam reforming of methane. *Industrial & engineering chemistry research*, 45(8):2522–2530, 2006.

[35] H.T.J. Reijers, J. Boon, G.D. Elzinga, P.D. Cobden, W.G. Haije, and R.W. van den Brink. Modeling study of the sorption-enhanced reaction process for CO_2 capture. I. model development and validation. *Industrial & Engineering Chemistry Research*, 48(15):6966–6974, 2009.

[36] A.M. Ribeiro, C.A. Grande, F.V.S. Lopes, J.M. Loureiro, and A.E. Rodrigues. A parametric study of layered bed PSA for hydrogen purification. *Chemical Engineering Science*, 63(21):5258–5273, 2008.

[37] C.P.P. Singh and D.N. Saraf. Simulation of high-temperature water-gas shift reactors. *Industrial & Engineering Chemistry Process Design and Development*, 16(3):313–319, 1977.

[38] R. Singh, M.K. Ram Reddy, S. Wilson, K. Joshi, J.C. Diniz da Costa, and P. Webley. High temperature materials for CO_2 capture. *Energy Procedia*, 1(1):623–630, 2009.

[39] R.V. Siriwardane, C. Robinson, M. Shen, and T. Simonyi. Novel regenerable sodium-based sorbents for CO_2 capture at warm gas temperatures. *Energy & fuels*, 21(4):2088–2097, 2007.

[40] R.J. Smith, M. Loganathan, and M.S. Shantha. A review of the water gas shift reaction kinetics.

International Journal of Chemical Reactor Engineering, 8(8):4, 2010.

[41] R.W. Stevens Jr., A. Shamsi, S. Carpenter, and R. Siriwardane. Sorption-enhanced water gas shift reaction by sodium-promoted calcium oxides. *Fuel*, 89(6):1280–1286, 2010.

[42] E.R. Van Selow, P.D. Cobden, P.A. Verbraeken, J.R. Hufton, and R.W. Van Den Brink. Carbon capture by sorption-enhanced water-gas shift reaction process using hydrotalcite-based material. *Industrial & Engineering Chemistry Research*, 48(9):4184–4193, 2009.

[43] E.R. Van Selow, P.D. Cobden, A.D. Wright, R.W. Van Den Brink, and D. Jansen. Improved sorbent for the sorption-enhanced water-gas shift process. *Energy Procedia*, 4:1090–1095, 2011.

[44] A. Wright, V. White, J. Hufton, E. Selow, and P. Hinderink. Reduction in the cost of pre-combustion CO_2 capture through advancements in sorption-enhanced water-gas-shift. *Energy Procedia*, 1(1):707–714, 2009.

[45] A.D. Wright, V. White, J.R. Hufton, R. Quinn, P.D. Cobden, and E.R. Van Selow. CAESAR: Development of a SEWGS model for IGCC. *Energy Procedia*, 4:1147–1154, 2011.

[46] G. Xiu, P. Li, and A.E. Rodrigues. Sorption-enhanced reaction process with reactive regeneration. *Chemical engineering science*, 57(18):3893–3908, 2002.

[47] S. Yagi and D. Kunii. Studies on effective thermal conductivities in packed beds. *AIChE Journal*, 3 (3):373–381, 1957.

A. Operating schedule SEWGS cycle

The notation t denotes seconds of simulation time, with $t = 0$ as the start of the simulation.

To be able to reach convergence, some modifications to the previously discussed driving patterns for the flow rates and valve openings were necessary in the first part of the operating schedule.

Table A.1: Operating schedule

Cycle state 1 starts at $t = 0$:
Set $\dot{n}_{Feed\ 1} = SyngasFlowRatePerReactor$ $\dot{n}_{Feed\ 2} = SyngasFlowRatePerReactor$ $\dot{n}_{HP\ Steam\ R} = 0 + \dfrac{1}{RampTime} \cdot (t - 0) \cdot (RinseSteamFlowRate - 0)$ $\dot{n}_{LP\ Steam\ P} = 0$ $\quad + \dfrac{1}{(2 \cdot CycleTime/16) - RampTime} \cdot (t - 0) \cdot (PurgeSteamFlowRate - 0)$ For valve V1 in Figure 12: $x_{valve} = 0 + \dfrac{1}{ValveRampTime} \cdot (t - 0) \cdot (3.0 - 0)$ For valve V2 in Figure 12: $x_{valve} = 0 + \dfrac{1}{ValveRampTime} \cdot (t - 0) \cdot (3.0 - 0)$
Simulate for $RampTime$.
Current time $t = 2$ s.
Set $\dot{n}_{HP\ Steam\ R} = RinseSteamFlowRate$
Simulate for $CycleTime/16 - RampTime$.
Current time $t = CycleTime/16 = 43.4375$ s.
Switch system of equations to governing equations for cycle state 2.
Set   For valve V1 in Figure 12: $x_{valve} = 0$ For valve V2 in Figure 12: $x_{valve} = 0$ For valve V3 in Figure 13: $x_{valve} = 0.0001$ $\quad + \dfrac{1}{ValveRampTime} \cdot (t - CycleTime/16) \cdot (4.0 - 0.0001)$ For valve V4 in Figure 13: $x_{valve} = 0.0001$ $\quad + \dfrac{1}{ValveRampTime} \cdot (t - CycleTime/16) \cdot (3.0 - 0.0001)$ For valve V5 in Figure 13: $x_{valve} = 0.0001$

$$+\frac{1}{ValveRampTime} \cdot (t - CycleTime/16) \cdot (10.0 - 0.0001)$$

Simulate for $CycleTime/16 - RampTime$.

Current time $t = 2 \cdot CycleTime/16 - RampTime = 84.8750$ s.

Set

$\dot{n}_{Feed\ 2} = SyngasFlowRatePerReactor$
$$+\frac{1}{RampTime} \cdot (t - 2 \cdot CycleTime/16 - RampTime)$$
$$\cdot (0 - SyngasFlowRatePerReactor)$$

$\dot{n}_{HP\ Steam\ R} = RinseSteamFlowRate$
$$+\frac{1}{RampTime} \cdot (t - 2 \cdot CycleTime/16 - RampTime)$$
$$\cdot (0 - RinseSteamFlowRate)$$

$\dot{n}_{LP\ Steam\ P} = PurgeSteamFlowRate$
$$+\frac{1}{RampTime} \cdot (t - 2 \cdot CycleTime/16 - RampTime)$$
$$\cdot (0 - PurgeSteamFlowRate)$$

Switch equations for valve V5 in Figure 13 to equations setting flow rate $\dot{n}_{valve} = 0$.

Simulate for $RampTime$.

Current time $t = 2 \cdot CycleTime/16 = 86.8750$ s.

Switch system of equations to governing equations for cycle state 3.

Please note that this set of equations is not given explicitly in the text

of the present work. They are, as discussed in Section 3.2,

based on the equations for system state 1, adapted for cycle state 3.

Set

For valve V3 in Figure 13: $x_{valve} = 0$

For valve V4 in Figure 13: $x_{valve} = 0$

For valve V5 in Figure 13: $x_{valve} = 0$

For valve V1: $x_{valve} = 0.0001$
$$+\frac{1}{ValveRampTime} \cdot (t - 2 \cdot CycleTime/16) \cdot (3.0 - 0.0001)$$

For valve V2: $x_{valve} = 0.0001$
$$+\frac{1}{ValveRampTime} \cdot (t - 2 \cdot CycleTime/16) \cdot (3.0 - 0.0001)$$

$\dot{n}_{Feed\ 1} = SyngasFlowRatePerReactor$

$\dot{n}_{Feed\ 2} = SyngasFlowRatePerReactor$

$\dot{n}_{HP\ Steam\ R} = RinseSteamFlowRate$

$$\dot{n}_{LP\ Steam\ P} = 0 + \frac{1}{(2 \cdot CycleTime/16) - RampTime} \cdot (t - 2 \cdot CycleTime/16)$$
$$\cdot (PurgeSteamFlowRate - 0)$$

$$p_{CO_2\ Product\ 1} = \text{OLD}(p_{inlet,5})$$
$$+ \frac{1}{RampTime} \cdot (t - 2 \cdot CycleTime/16) \cdot (110000 - \text{OLD}(p_{inlet,5}))$$

where OLD denotes the values of the variables before the switch.

That is, the values at $t = 86.8750^-$.

Reinitial the time-differential variables in reactor 1, 2 and 8

using the following relationships:

$$\bar{c}_{CO_2} = \text{OLD}(y_{CO_2}) \cdot p/(\bar{R} \cdot \text{OLD}(T))$$

$$\bar{c}_{H_2} = \text{OLD}(y_{H_2}) \cdot p/(\bar{R} \cdot \text{OLD}(T))$$

$$\bar{c}_{CO} = \text{OLD}(y_{CO}) \cdot p/(\bar{R} \cdot \text{OLD}(T))$$

$$\bar{c}_{H_2O} = \text{OLD}(y_{H_2O}) \cdot p/(\bar{R} \cdot \text{OLD}(T))$$

$$T = \text{OLD}(T)$$

$$q_{CO_2} = \text{OLD}(q_{CO_2})$$

$$p = p_{H_2\ Product} = 2689000 \text{ Pa}$$

Simulate for $RampTime$.

Current time $t = 2 \cdot CycleTime/16 + RampTime = 88.8750$ s.

Set

$p_{CO_2\ Product\ 1} = 110000$ Pa.

Simulate for $CycleTime/16 - RampTime$.

Current time $t = 3 \cdot CycleTime/16 = 130.3125$ s.

Switch system of equations to governing equations for cycle state 4.

Please note that this set of equations is not given explicitly in the text

of the present work. They are, as discussed in Section 3.2,

based on the equations for system state 2, adapted for cycle state 4.

Set

For valve V1: $x_{valve} = 0$

For valve V2: $x_{valve} = 0$

For valve V3: $x_{valve} = 0.0001$
$$+ \frac{1}{ValveRampTime} \cdot (t - 3 \cdot CycleTime/16) \cdot (4.0 - 0.0001)$$

For valve V4: $x_{valve} = 0.0001$

$$+\frac{1}{ValveRampTime} \cdot (t - 3 \cdot CycleTime/16) \cdot (3.0 - 0.0001)$$

For valve V5: $x_{valve} = 0.0001$

$$+\frac{1}{ValveRampTime} \cdot (t - 3 \cdot CycleTime/16) \cdot (10.0 - 0.0001)$$

Simulate for $CycleTime/16 - RampTime$.

Current time $t = 4 \cdot CycleTime/16 - RampTime = 171.7500$ s.

Set

$$\dot{n}_{Feed\ 2} = SyngasFlowRatePerReactor$$
$$+\frac{1}{RampTime} \cdot (t - 4 \cdot CycleTime/16 - RampTime)$$
$$\cdot (0 - SyngasFlowRatePerReactor)$$

$$\dot{n}_{HP\ Steam\ R} = RinseSteamFlowRate$$
$$+\frac{1}{RampTime} \cdot (t - 4 \cdot CycleTime/16 - RampTime)$$
$$\cdot (0 - RinseSteamFlowRate)$$

$$\dot{n}_{LP\ Steam\ P} = PurgeSteamFlowRate$$
$$+\frac{1}{RampTime} \cdot (t - 4 \cdot CycleTime/16 - RampTime)$$
$$\cdot (0 - PurgeSteamFlowRate)$$

Switch equations for valve V5 to equations setting flow rate $\dot{n}_{valve} = 0$.

Simulate for $RampTime$.

Current time $t = 4 \cdot CycleTime/16 = 173.7500$ s.

From this point on, the operating schedule follows a repeating pattern, carrying out the equivalent operations for every set of system states 1 and 2. That is, the operation of cycle states 5, 7, 9, 11, 13, 15 and 1 is the same as that for cycle state 3. The operation of cycle states 6, 8, 10, 12, 14, 16 and 2 is the same as that for cycle state 4.

Therefore, continue in same pattern of operation until cycle state 16 completed at $t = CycleTime = 695$ s.

Switch system of equations to governing equations for cycle state 1.

Since the operating pattern for cycle state 1 should be the same as cycle state 3, the following is carried out:

Set

For valve V3 in Figure 13: $x_{valve} = 0$

For valve V4 in Figure 13: $x_{valve} = 0$

For valve V5 in Figure 13: $x_{valve} = 0$

For valve V1 in Figure 12: $x_{valve} = 0.0001$
$$+\frac{1}{ValveRampTime} \cdot (t - 16 \cdot CycleTime/16) \cdot (3.0 - 0.0001)$$

For valve V2 in Figure 12: $x_{valve} = 0.0001$
$$+\frac{1}{ValveRampTime} \cdot (t - 16 \cdot CycleTime/16) \cdot (3.0 - 0.0001)$$

$\dot{n}_{Feed\ 1} = SyngasFlowRatePerReactor$

$\dot{n}_{Feed\ 2} = SyngasFlowRatePerReactor$

$\dot{n}_{HP\ Steam\ R} = RinseSteamFlowRate$

$$\dot{n}_{LP\ Steam\ P} = 0 + \frac{1}{(2 \cdot CycleTime/16) - RampTime} \cdot (t - 16 \cdot CycleTime/16)$$
$$\cdot (PurgeSteamFlowRate - 0)$$

$$p_{CO_2\ Product\ 1} = \text{OLD}(p_{inlet,4})$$
$$+\frac{1}{RampTime} \cdot (t - 16 \cdot CycleTime/16) \cdot (110000 - \text{OLD}(p_{inlet,4}))$$

where OLD denotes the values of the variables before the switch.

That is, the values at $t = 695^-$.

Reinitial the time-differential variables in reactor 1, 7 and 8

using the following relationships:

$\bar{c}_{CO_2} = \text{OLD}(y_{CO_2}) \cdot p/(\bar{R} \cdot \text{OLD}(T))$

$\bar{c}_{H_2} = \text{OLD}(y_{H_2}) \cdot p/(\bar{R} \cdot \text{OLD}(T))$

$\bar{c}_{CO} = \text{OLD}(y_{CO}) \cdot p/(\bar{R} \cdot \text{OLD}(T))$

$\bar{c}_{H_2O} = \text{OLD}(y_{H_2O}) \cdot p/(\bar{R} \cdot \text{OLD}(T))$

$T = \text{OLD}(T)$

$q_{CO_2} = \text{OLD}(q_{CO_2})$

$p = p_{H_2\ Product} = 2689000$ Pa

The system is now ready to carry out the simulation of the second SEWGS cycle.

B. Operating schedule for the startup cycle

The feed step (step 1.F in Figure 16) was run using reactor inlet feed gas composition and temperature equal to that of stream 4 in Table 2. The flow rate was set to be 7420 mol/s/(10 trains · 2 reactors in feed step per train) = 371 mol/s. The reactor outlet pressure was set to 26.89 bar.

The initial values of the variables in the reactor at the start of the simulation were set to be:

$y_{CO_2}(z, t = 0) = 0.00002 \qquad z \in (0, L)$

$y_{H_2}(z, t = 0) = 0.00002 \qquad z \in (0, L)$

$y_{CO}(z, t = 0) = 0.00002 \qquad z \in (0, L)$

$y_{H_2O}(z, t = 0) = 0.00002 \qquad z \in (0, L)$

$T(z, t = 0) = 673 \text{ K} \qquad z \in (0, L)$

$p(z, t = 0) = 2689000 \text{ Pa} \qquad z \in (0, L)$

$q_{CO_2}(z, t = 0) = 0 \text{ mol } CO_2 \text{ adsorbed/kg adsorbent} \qquad z \in [0, L]$

These initial values were chosen to describe a clean, isothermal and isobaric reactor filled with 99.992 % inert nitrogen. It was not possible to set the mole fractions of the other components to zero, giving 100 % nitrogen in the reactor. The simulation did not converge when this was tried. However, the effects of this assumption on the results should be negligible.

The feed step was run for 660.25 seconds, which is longer than necessary to reach breakthrough of CO_2. This was done to saturate the adsorbent with CO_2, to ensure convergence in subsequent steps.

Halfway into this feed step time period of 660.25 s, at $t = 330.125$ s, the reactor variables were saved, providing initial values for reactor 8, which should be halfway through the feed step in the start of the SEWGS cycle.

At the end of the cycle, the reactor should be repressurized with product gas from another reactor. Therefore, at $t = 330$ s, the mole fractions at the outlet end of the reactor, at $z = 7.377$ m, were collected and used to set a value for the mole fractions of the repressurization feed gas.

$y_{CO_2, RP \, Feed \, Stream} = y_{CO_2}(z = 7.377 \text{ m}, t = 330 \text{ s}) = 9.8274676 \times 10^{-8}$

$y_{H_2, RP \, Feed \, Stream} = y_{H_2}(z = 7.377 \text{ m}, t = 330 \text{ s}) = 0.52929956$

$y_{CO, RP \, Feed \, Stream} = y_{CO}(z = 7.377 \text{ m}, t = 330 \text{ s}) = 1.3134734 \times 10^{-8}$

$y_{H_2O,RP\ Feed\ Stream} = y_{H_2O}(z = 7.377\ \text{m}, t = 330\ \text{s}) = 0.33428416$

$y_{N_2,RP\ Feed\ Stream} = y_{N_2}(z = 7.377\ \text{m}, t = 330\ \text{s}) = 0.1364162$

After the cocurrent feed step was completed, at $t = 660.25$ s, the reactor variables were then saved, providing initial values for reactor 7, which should be finished with the feed step and ready for the rinse step in the start of the SEWGS cycle.

At this point the countercurrent rinse step was started. The time-differential variables in the reactor were reinitialized, using the following relationships:

$\bar{c}_{CO_2} = \text{OLD}(y_{CO_2}) \cdot p/(\bar{R} \cdot \text{OLD}(T))$

$\bar{c}_{H_2} = \text{OLD}(y_{H_2}) \cdot p/(\bar{R} \cdot \text{OLD}(T))$

$\bar{c}_{CO} = \text{OLD}(y_{CO}) \cdot p/(\bar{R} \cdot \text{OLD}(T))$

$\bar{c}_{H_2O} = \text{OLD}(y_{H_2O}) \cdot p/(\bar{R} \cdot \text{OLD}(T))$

$T = \text{OLD}(T)$

$q_{CO_2} = \text{OLD}(q_{CO_2})$

$p = p_{H_2\ Product} = 2689000\ \text{Pa}$

The rinse steam flow rate was ramped over *RampTime* seconds to the value of *RinseSteamFlowRate*. At $t = 745.1250$ s, the rinse steam flow rate was ramped down to zero over *RampTime* seconds. At $t = 747.1250$ s, the rinse step was completed. The reactor variables were then saved, providing initial values for reactor 6, which should be finished with the rinse step and ready for step Eq1 in the start of the SEWGS cycle.

In a single-reactor simulation of the equalization steps, some simplifications had to be made. The inlet of the reactor in steps Eq1, Eq2 and Eq3 is not connected to another reactor through a valve. Instead, the inlet of the reactor is connected to a valve, utilizing the same valve model as in Section 3.8.2, with a stream with a known pressure on the other side of the valve.

At the start of step Eq1, the time-differential variables in the reactor were reinitialized, using the following relationships:

$\bar{c}_{CO_2} = \text{OLD}(y_{CO_2}) \cdot p/(\bar{R} \cdot \text{OLD}(T))$

$\bar{c}_{H_2} = \text{OLD}(y_{H_2}) \cdot p/(\bar{R} \cdot \text{OLD}(T))$

$\bar{c}_{CO} = \text{OLD}(y_{CO}) \cdot p/(\bar{R} \cdot \text{OLD}(T))$

$\bar{c}_{H_2O} = \text{OLD}(y_{H_2O}) \cdot p/(\bar{R} \cdot \text{OLD}(T))$

$T = \text{OLD}(T)$

$q_{CO_2} = \text{OLD}(q_{CO_2})$

$p = p_{H_2 \, Product} = 2689000$ Pa

The pressure $p_{Eq1 \, Stream}$ was set to 2044250 Pa.

The valve opening x_{valve} was then controlled in the following way over the duration of step Eq1:

Set

$$x_{valve} = 0.0001 + \frac{1}{0.5 \cdot ValveRampTime} \cdot (t - 747.1250) \cdot (4.0 - 0.0001)$$

Simulate for $0.5 \cdot ValveRampTime$. Current time $t = 768.8438$ s.

Set

$$x_{valve} = 4.0$$

Simulate for $CycleTime/16 - 0.5 \cdot ValveRampTime - RampTime$. Current time $t = 788.5625$ s.

Set

$$x_{valve} = 4.0 + \frac{1}{RampTime} \cdot (t - 788.5625) \cdot (0 - 4.0)$$

Simulate for $RampTime$. Current time $t = 790.5625$ s.

This concludes step Eq1, and step Eq2 starts.

The pressure $p_{Eq2 \, Stream}$ was then set to 1399500 Pa, and the valve opening x_{valve} was controlled in the same way as in step Eq1.

After simulating $CycleTime/16$, at $t = 834$ s, step Eq2 is completed. The reactor variables were then saved, providing initial values for reactor 5, which should be finished with step Eq2 and ready for step Eq3 in the start of the SEWGS cycle.

Step Eq3 starts with setting the pressure $p_{Eq3 \, Stream}$ to 754750 Pa. The valve opening x_{valve} was controlled in the same way as in step Eq1.

After simulating $CycleTime/16$, at $t = 877.4375$ s, step Eq3 is completed.

The pressure $p_{D \, Stream}$ was then set to 110000 Pa, and the valve opening x_{valve} was controlled in a slightly different way over the duration of step D:

Set

$$x_{valve} = 0.0001 + \frac{1}{0.5 \cdot ValveRampTime} \cdot (t - 877.4375) \cdot (6.0 - 0.0001)$$

Simulate for $0.5 \cdot ValveRampTime$. Current time $t = 899.1563$ s.

Set

$$x_{valve} = 6.0$$

Simulate for $CycleTime/16 - 0.5 \cdot ValveRampTime - RampTime$. Current time $t = 918.8750$ s.

Set

$$x_{valve} = 6.0 + \frac{1}{RampTime} \cdot (t - 918.8750) \cdot (0 - 6.0)$$

Simulate for $RampTime$. Current time $t = 920.8750$ s.

This concludes step D. The reactor variables were then saved, providing initial values for reactor 4, which should be finished with step D and ready for step P in the start of the SEWGS cycle.

The purge step in the startup cycle is different than in the SEWGS cycle described previously. The purge steam flow rate $\dot{n}_{LP\ Steam\ P}$ is different, and the pressure $p_{P\ Stream}$ is ramped down to 1.1 bar in over time period of $2 \cdot CycleTime/16$ seconds. This was done to be able to reach convergence.

Set

$$\dot{n}_{LP\ Steam\ P} = 0 + \frac{1}{RampTime} \cdot (t - 920.8750) \cdot (-120.00106 - 0)$$

$$p_{P\ Stream} = \text{OLD}(p_{inlet}) + \frac{1}{2 \cdot CycleTime/16} \cdot (t - 920.8750) \cdot (110000 - \text{OLD}(p_{inlet}))$$

Simulate for $RampTime$. Current time $t = 922.8750$ s.

Set

$$\dot{n}_{LP\ Steam\ P} = -120.00106 \text{ mol/s}$$

Simulate for $2 \cdot CycleTime/16 - 2 \cdot RampTime$. Current time $t = 1005.7500$ s.

Set

$$\dot{n}_{LP\ Steam\ P} = -120.00106 + \frac{1}{RampTime} \cdot (t - 1005.7500) \cdot (0 - (-120.00106))$$

Simulate for $RampTime$. Current time $t = 1007.7500$ s.

This concludes the purge step. The reactor variables were then saved, providing initial values for reactor 3, which should be finished with step P and ready for step REq3 in the start of the SEWGS cycle.

The re-equalization steps REq3, REq2 and REq1 are simulated in a very simplified way. The pressure in the column is stepwise increased for each re-equalization step, reinitializ-

ing the variables in the reactor at the start of each step. This is best explained by showing how the procedure is carried out.

Step REq3 starts:

Set

$p_{REq3\ Stream} = 754750$ Pa

The time-differential variables in the reactor were reinitialized, using the following relationships:

$\bar{c}_{CO_2} = \text{OLD}(y_{CO_2}) \cdot p/(\bar{R} \cdot \text{OLD}(T))$

$\bar{c}_{H_2} = \text{OLD}(y_{H_2}) \cdot p/(\bar{R} \cdot \text{OLD}(T))$

$\bar{c}_{CO} = \text{OLD}(y_{CO}) \cdot p/(\bar{R} \cdot \text{OLD}(T))$

$\bar{c}_{H_2O} = \text{OLD}(y_{H_2O}) \cdot p/(\bar{R} \cdot \text{OLD}(T))$

$T = \text{OLD}(T)$

$q_{CO_2} = \text{OLD}(q_{CO_2})$

$p = 754750$ Pa

Simulate for $CycleTime/16$. Current time $t = 1051.1875$ s.

By reinitializing the variables in the reactor, assuming that the total pressure p is increased in a stepwise manner, while the mole fractions, temperature and amount of CO_2 adsorbed is kept the same, the total amount of moles of gas in the reactor increases in a stepwise manner. This is equivalent to creating mass from nothing, and is not realistic. However, this is a necessary simplification which is only utilized in the startup cycle.

Step REq2 starts:

Set

$p_{REq2\ Stream} = 1399500$ Pa

The time-differential variables in the reactor were reinitialized, using the following relationships:

$\bar{c}_{CO_2} = \text{OLD}(y_{CO_2}) \cdot p/(\bar{R} \cdot \text{OLD}(T))$

$\bar{c}_{H_2} = \text{OLD}(y_{H_2}) \cdot p/(\bar{R} \cdot \text{OLD}(T))$

$\bar{c}_{CO} = \text{OLD}(y_{CO}) \cdot p/(\bar{R} \cdot \text{OLD}(T))$

$\bar{c}_{H_2O} = \text{OLD}(y_{H_2O}) \cdot p/(\bar{R} \cdot \text{OLD}(T))$

$T = \text{OLD}(T)$

$q_{CO_2} = OLD(q_{CO_2})$

$p = 1399500$ Pa

Simulate for $CycleTime/16$. Current time $t = 1094.6250$ s.

This concludes step REq2. The reactor variables were then saved, providing initial values for reactor 2, which should be finished with step REq2 and ready for step REq1 in the start of the SEWGS cycle.

Step REq1 starts:

Set

$p_{REq2\ Stream} = 2044250$ Pa

The time-differential variables in the reactor were reinitialized, using the following relationships:

$\bar{c}_{CO_2} = OLD(y_{CO_2}) \cdot p/(\bar{R} \cdot OLD(T))$

$\bar{c}_{H_2} = OLD(y_{H_2}) \cdot p/(\bar{R} \cdot OLD(T))$

$\bar{c}_{CO} = OLD(y_{CO}) \cdot p/(\bar{R} \cdot OLD(T))$

$\bar{c}_{H_2O} = OLD(y_{H_2O}) \cdot p/(\bar{R} \cdot OLD(T))$

$T = OLD(T)$

$q_{CO_2} = OLD(q_{CO_2})$

$p = 2044250$ Pa

Simulate for $CycleTime/16$. Current time $t = 1138.0625$ s.

This concludes step REq1, and the reactor should undergo the repressurization step RP. This is modelled in a very simplified way, by countercurrently feeding the column gas with a temperature of 673 K and a composition equal to $y_{i,RP\ Feed\ Stream}$ described earlier. The flow rate of repressurization gas is set to a relatively high value, determined such that the gas reaches the inlet during the time length of the step.

Set

$\dot{n}_{RP\ Feed\ Stream} = 0 + \dfrac{1}{RampTime} \cdot (t - 1138.0625) \cdot (-691.86896 - 0)$

$p_{RP\ Stream} = 2689000$ Pa

The time-differential variables in the reactor were reinitialized, using the following relationships:

$\bar{c}_{CO_2} = OLD(y_{CO_2}) \cdot p/(\bar{R} \cdot OLD(T))$

$\bar{c}_{H_2} = \text{OLD}(y_{H_2}) \cdot p/(\bar{R} \cdot \text{OLD}(T))$

$\bar{c}_{CO} = \text{OLD}(y_{CO}) \cdot p/(\bar{R} \cdot \text{OLD}(T))$

$\bar{c}_{H_2O} = \text{OLD}(y_{H_2O}) \cdot p/(\bar{R} \cdot \text{OLD}(T))$

$T = \text{OLD}(T)$

$q_{CO_2} = \text{OLD}(q_{CO_2})$

$p = p_{H_2\ Product} = 2689000$ Pa

Simulate for *RampTime*. Current time $t = 1140.0625$ s.

Set

$\dot{n}_{RP\ Feed\ Stream} = -691.86896$ mol/s

Simulate for $CycleTime/16 - 2 \cdot RampTime$. Current time $t = 1179.5000$ s.

Set

$\dot{n}_{RP\ Feed\ Stream} = -691.86896 + \dfrac{1}{RampTime} \cdot (t - 1179.5000) \cdot (0 - (-691.86896))$

Simulate for *RampTime*. Current time $t = 1181.5$ s.

This concludes step RP and the simulation of the startup cycle. The reactor variables were then saved, providing initial values for reactor 1, which should be finished with step RP and ready for the feed step in the start of the SEWGS cycle.

The saved variable sets providing initial values for each of the eight reactors in the SEWGS system were then collected and used as initial values at the start of the SEWGS cycle at $t = 0$. However, to be able to reach convergence, the variables in the eight reactors had to be reinitialized before the simulation of the SEWGS cycle could commence. The SEWGS system model at $t = 0$ was reinitialized using the following relationships for each reactor:

$\bar{c}_{CO_2} = \text{OLD}(y_{CO_2}) \cdot p/(\bar{R} \cdot \text{OLD}(T))$

$\bar{c}_{H_2} = \text{OLD}(y_{H_2}) \cdot p/(\bar{R} \cdot \text{OLD}(T))$

$\bar{c}_{CO} = \text{OLD}(y_{CO}) \cdot p/(\bar{R} \cdot \text{OLD}(T))$

$\bar{c}_{H_2O} = \text{OLD}(y_{H_2O}) \cdot p/(\bar{R} \cdot \text{OLD}(T))$

$T = \text{OLD}(T)$

$q_{CO_2} = \text{OLD}(q_{CO_2})$

$p = InitialPressure$

where the value of *InitialPressure* was different for each reactor. The values can be found in Table B.1.

Table B.1: Initial pressure at $t = 0$ for the reactors in the system

Reactor	1	2	3	4	5	6	7	8
InitialPressure (Pa)	2689000	1399500	110000	110000	1399500	2689000	2689000	2689000

C. System streams

Figure C.1: Component flow rates (mol/s) in stream H$_2$ product, referred to Figure 11

Time (s)	0	43.4375	86.875	130.3125	173.75	217.1875	260.625	304.0625	347.5	390.9375	434.375	477.8125	521.25	564.6875	608.125	651.5625
System state	1	2	1	2	1	2	1	2	1	2	1	2	1	2	1	2
Cycle state	1	2	3	4	5	6	7	8	9	10	11	12	13	14	15	16

SEWGS reactor 1	F			R	Eq1	Eq2	Eq3	D	P		REq3	REq2	REq1	RP
SEWGS reactor 2	REq1	RP	F		R			Eq1	Eq2	Eq3	D	P		REq3	REq2
SEWGS reactor 3	REq3	REq2	REq1	RP	F		R		Eq1	Eq2	Eq3	D	P
SEWGS reactor 4	P		REq3	REq2	REq1	RP	F		R		Eq1	Eq2	Eq3	D
SEWGS reactor 5	Eq3	D	P		REq3	REq2	REq1	RP	F		R		Eq1	Eq2
SEWGS reactor 6	Eq1	Eq2	Eq3	D	P		REq3	REq2	REq1		F		R
SEWGS reactor 7	R		Eq1	Eq2	Eq3	D	P		REq3	REq2	REq1	RP	F
SEWGS reactor 8	F		R		Eq1	Eq2	Eq3	D	P		REq3	REq2	REq1	RP	F

695	738.4375	781.875	825.3125	868.75	912.1875	955.625	999.0625	1042.5	1085.938	1129.375	1172.813	1216.25	1259.688	1303.125	1346.563	1390
1	2	1	2	1	2	1	2	1	2	1	2	1	2	1	2	
17	18	19	20	21	22	23	24	25	26	27	28	29	30	31	32	

F			R	Eq1	Eq2	Eq3	D	P		REq3	REq2	REq1	RP
REq1	RP	F		R			Eq1	Eq2	Eq3	D	P		REq3	REq2
REq3	REq2	REq1	RP	F		R		Eq1	Eq2	Eq3	D	P
P		REq3	REq2	REq1	RP	F		R		Eq1	Eq2	Eq3	D
Eq3	D	P		REq3	REq2	REq1	RP	F		R		Eq1	Eq2
Eq1	Eq2	Eq3	D	P		REq3	REq2	REq1	RP		F		R
R		Eq1	Eq2	Eq3	D	P		REq3	REq2	REq1	RP	F
	R		Eq1	Eq2	Eq3	D	P		REq3	REq2	REq1	RP	F

Figure C.2: Total flow rate (mol/s) of stream H_2 product, referred to Figure 11

Time (s)	0	43.4375	86.875	130.3125	173.75	217.1875	260.625	304.0625	347.5	390.9375	434.375	477.8125	521.25	564.6875	608.125	651.5625
System state	1	2	1	2	1	2	1	2	1	2	1	2	1	2	1	2
Cycle state	1	2	3	4	5	6	7	8	9	10	11	12	13	14	15	16

	Time (s)	695	738.4375	781.875	825.3125	868.75	912.1875	955.625	999.0625	1042.5	1085.938	1129.375	1172.813	1216.25	1259.688	1303.125	1346.563	1390
	System state	1	2	1	2	1	2	1	2	1	2	1	2	1	2	1	2	
	Cycle state	17	18	19	20	21	22	23	24	25	26	27	28	29	30	31	32	

Figure C.3: Mole fractions in stream H_2 product, referred to Figure 11

Figure C.4: Outlet component flow rates (mol/s) of reactor in first half of feed step

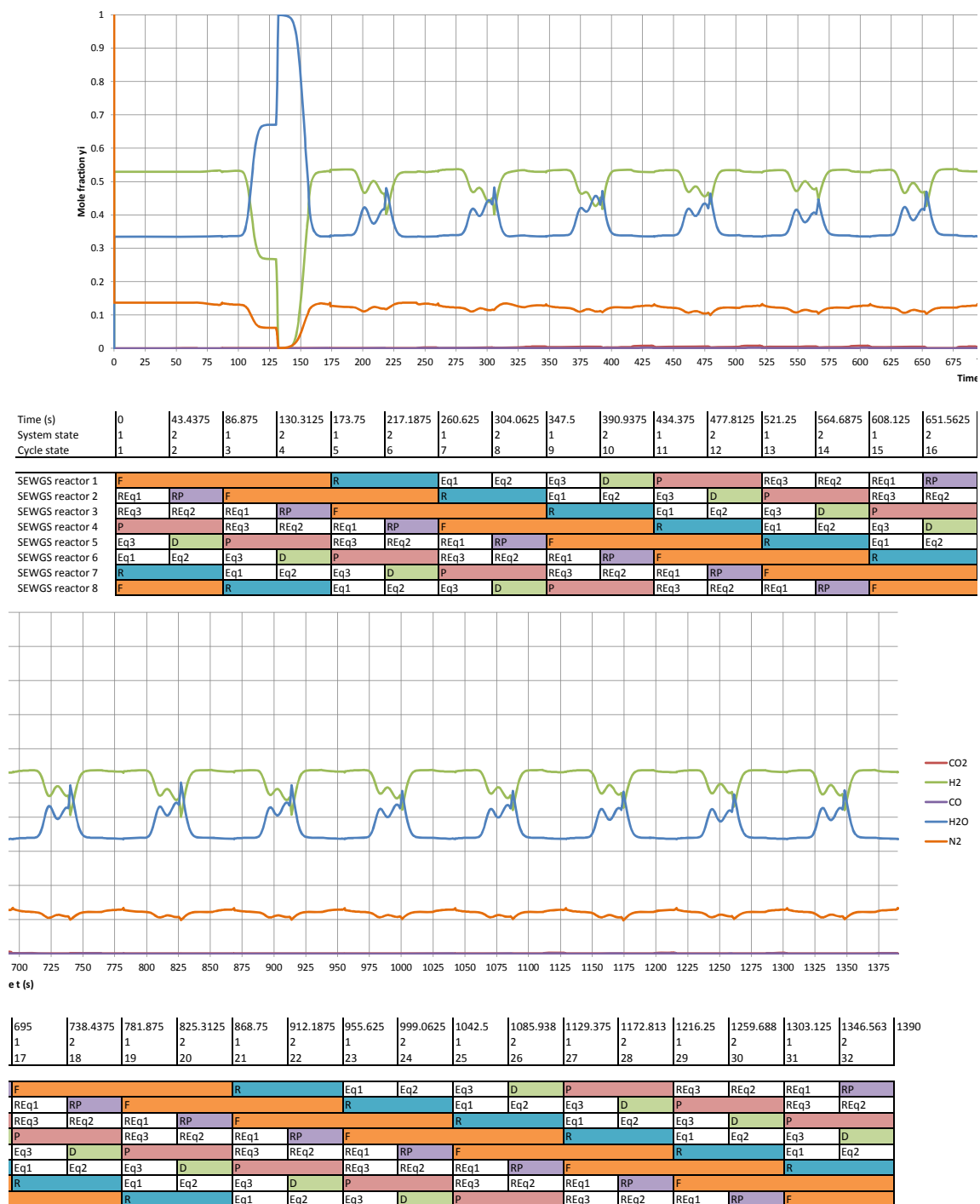| Time (s)	0	43.4375	86.875	130.3125	173.75	217.1875	260.625	304.0625	347.5	390.9375	434.375	477.8125	521.25	564.6875	608.125	651.5625
System state	1	2	1	2	1	2	1	2	1	2	1	2	1	2	1	2
Cycle state	1	2	3	4	5	6	7	8	9	10	11	12	13	14	15	16

SEWGS reactor 1	F				R		Eq1	Eq2	Eq3	D	P		REq3	REq2	REq1	RP
SEWGS reactor 2	REq1	RP	F			R		Eq1	Eq2	Eq3	D	P		REq3	REq2	
SEWGS reactor 3	REq3	REq2	REq1	RP	F			R		Eq1	Eq2	Eq3	D	P		
SEWGS reactor 4	P		REq3	REq2	REq1	RP	F			R		Eq1	Eq2	Eq3	D	
SEWGS reactor 5	Eq3	D	P		REq3	REq2	REq1	RP	F			R		Eq1	Eq2	
SEWGS reactor 6	Eq1	Eq2	Eq3	D	P		REq3	REq2	REq1	RP	F			R		
SEWGS reactor 7	R		Eq1	Eq2	Eq3	D	P		REq3	REq2	REq1	RP	F			
SEWGS reactor 8	F		R		Eq1	Eq2	Eq3	D	P		REq3	REq2	REq1	RP	F	

Graph shows contribution to H2 product from reactors marked with brown color

695	738.4375	781.875	825.3125	868.75	912.1875	955.625	999.0625	1042.5	1085.938	1129.375	1172.813	1216.25	1259.688	1303.125	1346.563	1390
1	2	1	2	1	2	1	2	1	2	1	2	1	2	1	2	
17	18	19	20	21	22	23	24	25	26	27	28	29	30	31	32	

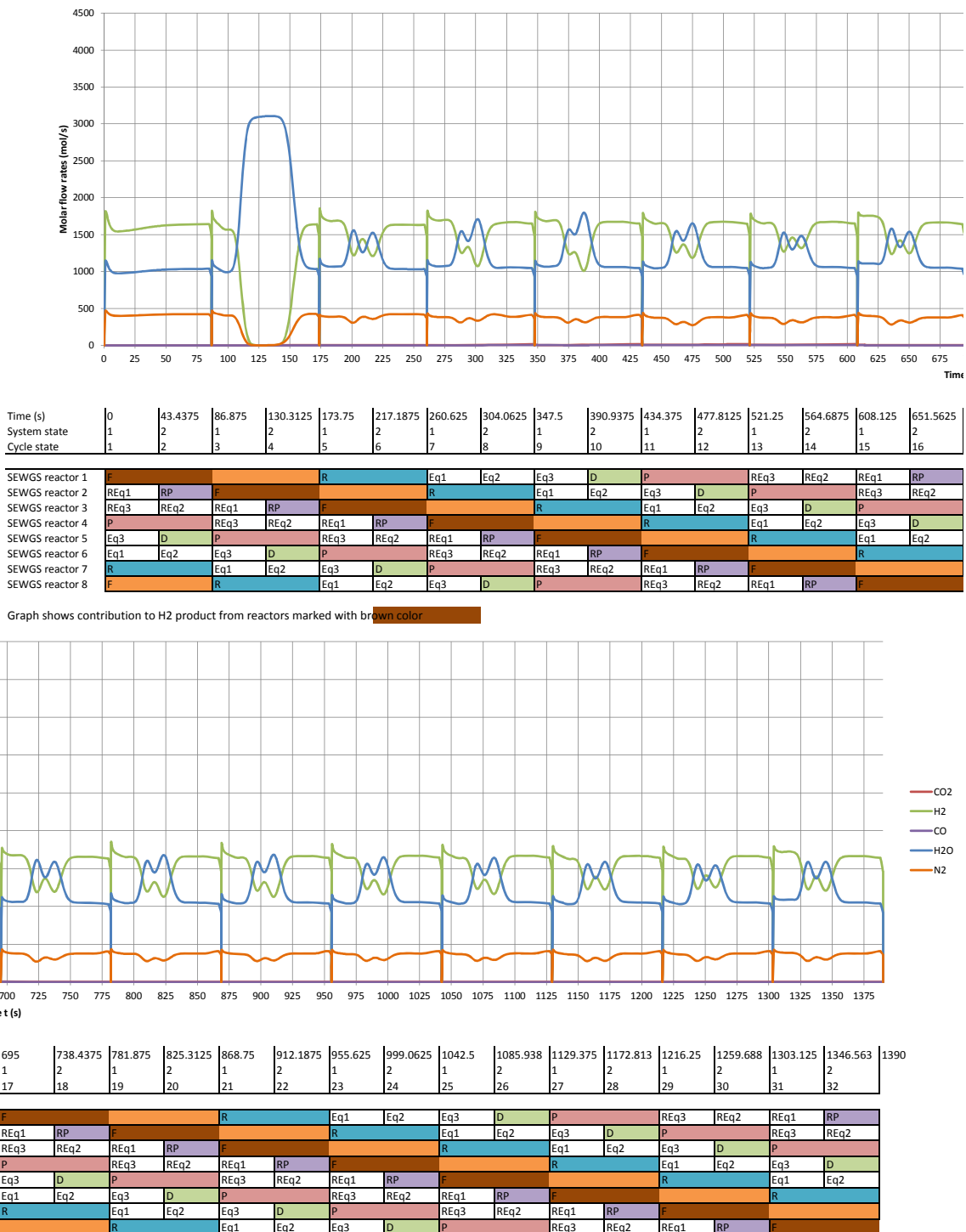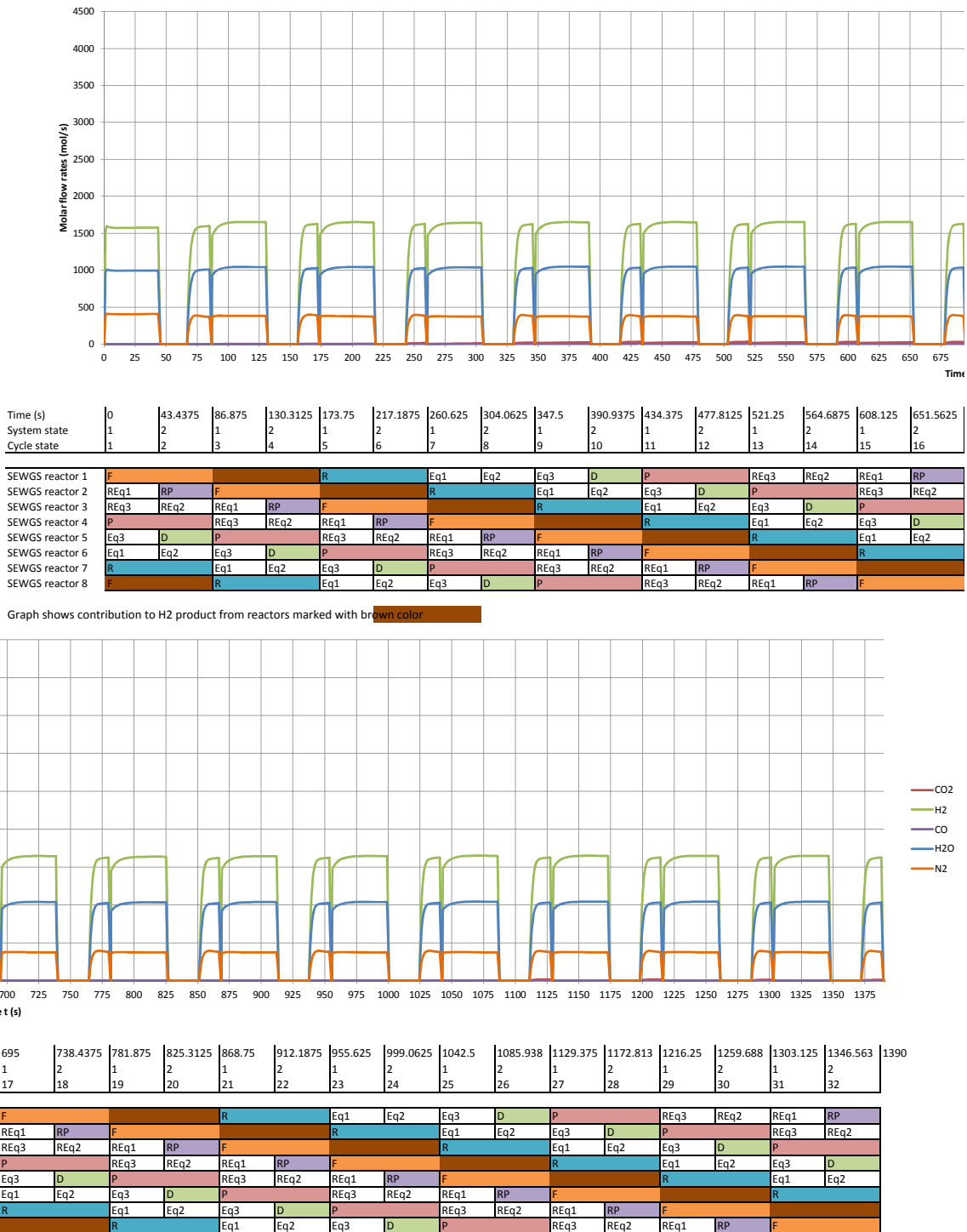|																
F				R		Eq1	Eq2	Eq3	D	P		REq3	REq2	REq1	RP	
REq1	RP	F			R		Eq1	Eq2	Eq3	D	P		REq3	REq2		
REq3	REq2	REq1	RP	F			R		Eq1	Eq2	Eq3	D	P			
P		REq3	REq2	REq1	RP	F			R		Eq1	Eq2	Eq3	D		
Eq3	D	P		REq3	REq2	REq1	RP	F			R		Eq1	Eq2		
Eq1	Eq2	Eq3	D	P		REq3	REq2	REq1	RP	F			R			
R		Eq1	Eq2	Eq3	D	P		REq3	REq2	REq1	RP	F				
	R		Eq1	Eq2	Eq3	D	P		REq3	REq2	REq1	RP	F			

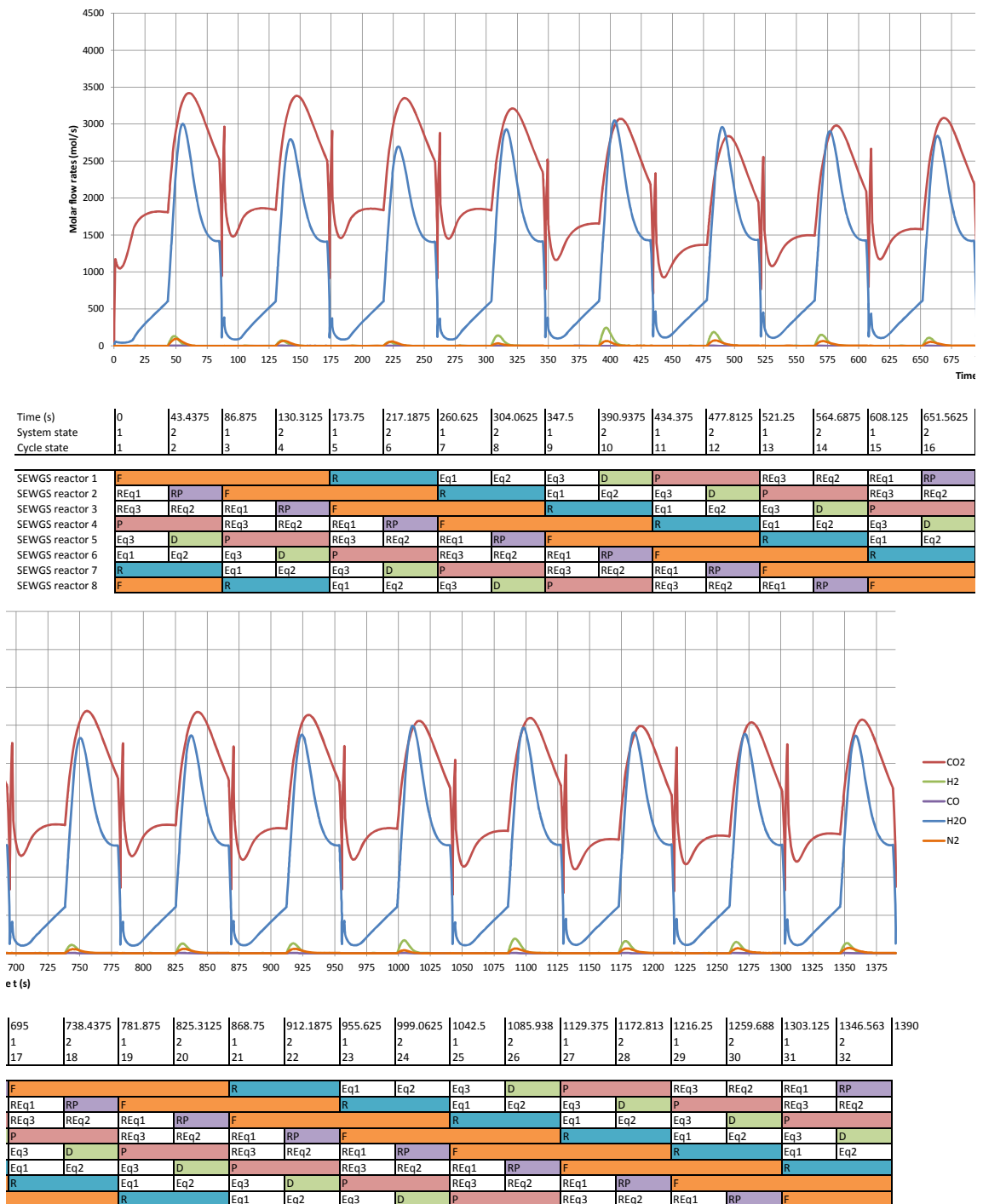**Figure C.5:** Outlet component flow rates (mol/s) of reactor in second half of feed step

Figure C.6: Component flow rates (mol/s) in the CO_2 product, i.e. the sum of the two streams CO_2 product 1 and CO_2 product 2, referred to Figure 11
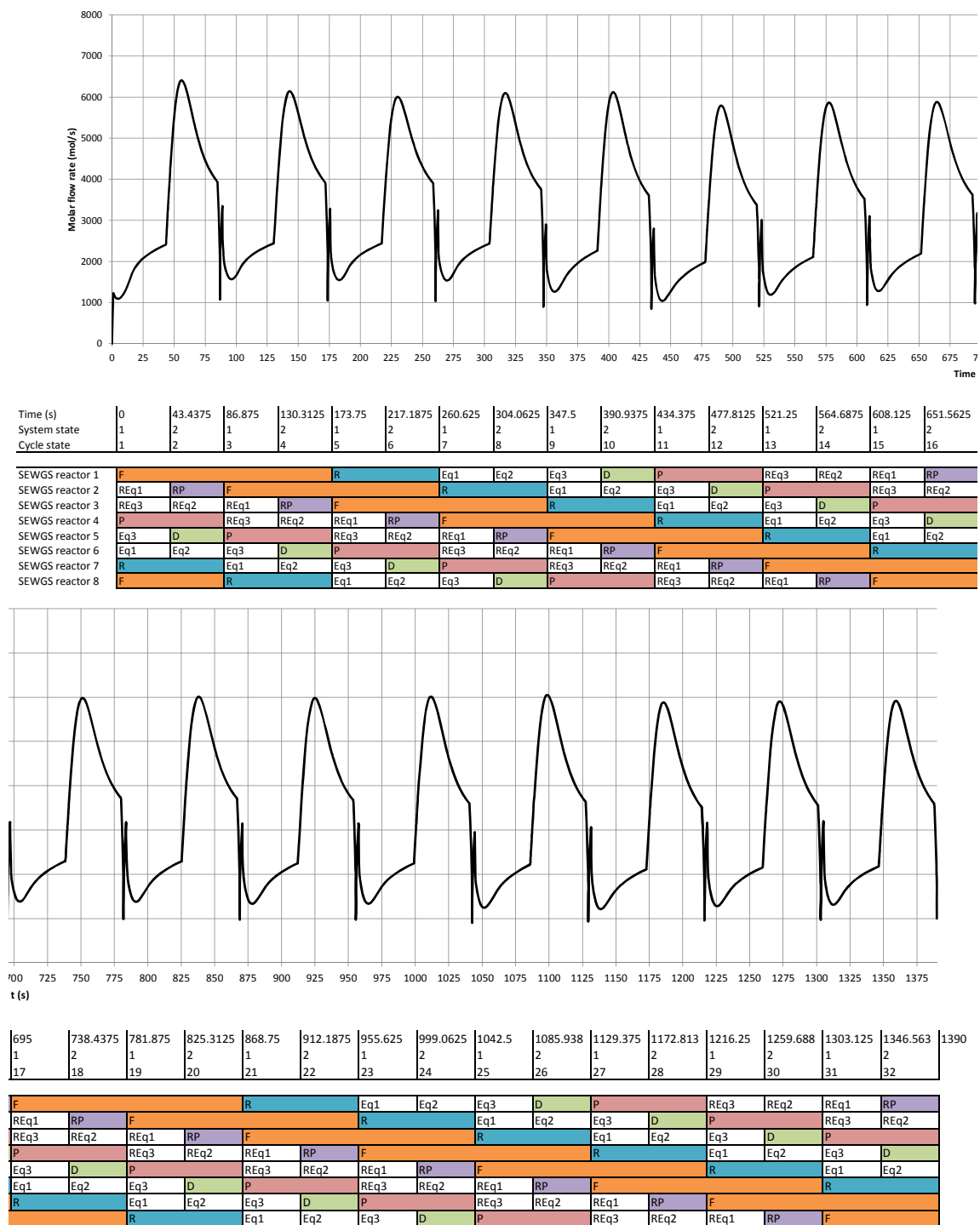
Time (s)	0	43.4375	86.875	130.3125	173.75	217.1875	260.625	304.0625	347.5	390.9375	434.375	477.8125	521.25	564.6875	608.125	651.5625
System state	1	2	1	2	1	2	1	2	1	2	1	2	1	2	1	2
Cycle state	1	2	3	4	5	6	7	8	9	10	11	12	13	14	15	16

SEWGS reactor 1	F			R		Eq1	Eq2	Eq3	D	P		REq3	REq2	REq1	RP	
SEWGS reactor 2	REq1	RP	F		R			Eq1	Eq2	Eq3	D	P		REq3	REq2	
SEWGS reactor 3	REq3	REq2	REq1	RP	F		R		Eq1	Eq2	Eq3	D	P			
SEWGS reactor 4	P		REq3	REq2	REq1	RP	F		R		Eq1	Eq2	Eq3	D		
SEWGS reactor 5	Eq3	D	P		REq3	REq2	REq1	RP	F		R		Eq1	Eq2		
SEWGS reactor 6	Eq1	Eq2	Eq3	D	P		REq3	REq2	REq1	RP	F		R			
SEWGS reactor 7	R		Eq1	Eq2	Eq3	D	P		REq3	REq2	REq1	RP	F			
SEWGS reactor 8	F		R		Eq1	Eq2	Eq3	D	P		REq3	REq2	REq1	RP	F	

695	738.4375	781.875	825.3125	868.75	912.1875	955.625	999.0625	1042.5	1085.938	1129.375	1172.813	1216.25	1259.688	1303.125	1346.563	1390
1	2	1	2	1	2	1	2	1	2	1	2	1	2	1	2	
17	18	19	20	21	22	23	24	25	26	27	28	29	30	31	32	

F			R		Eq1	Eq2	Eq3	D	P		REq3	REq2	REq1	RP		
REq1	RP	F		R			Eq1	Eq2	Eq3	D	P		REq3	REq2		
REq3	REq2	REq1	RP	F		R		Eq1	Eq2	Eq3	D	P				
P		REq3	REq2	REq1	RP	F		R		Eq1	Eq2	Eq3	D			
Eq3	D	P		REq3	REq2	REq1	RP	F		R		Eq1	Eq2			
Eq1	Eq2	Eq3	D	P		REq3	REq2	REq1	RP	F		R				
R		Eq1	Eq2	Eq3	D	P		REq3	REq2	REq1	RP	F				
		R		Eq1	Eq2	Eq3	D	P		REq3	REq2	REq1	RP	F		

Figure C.7: Total flow rate (mol/s) in the CO_2 product, i.e. the sum of the two streams CO_2 product 1 and CO_2 product 2, referred to Figure 11
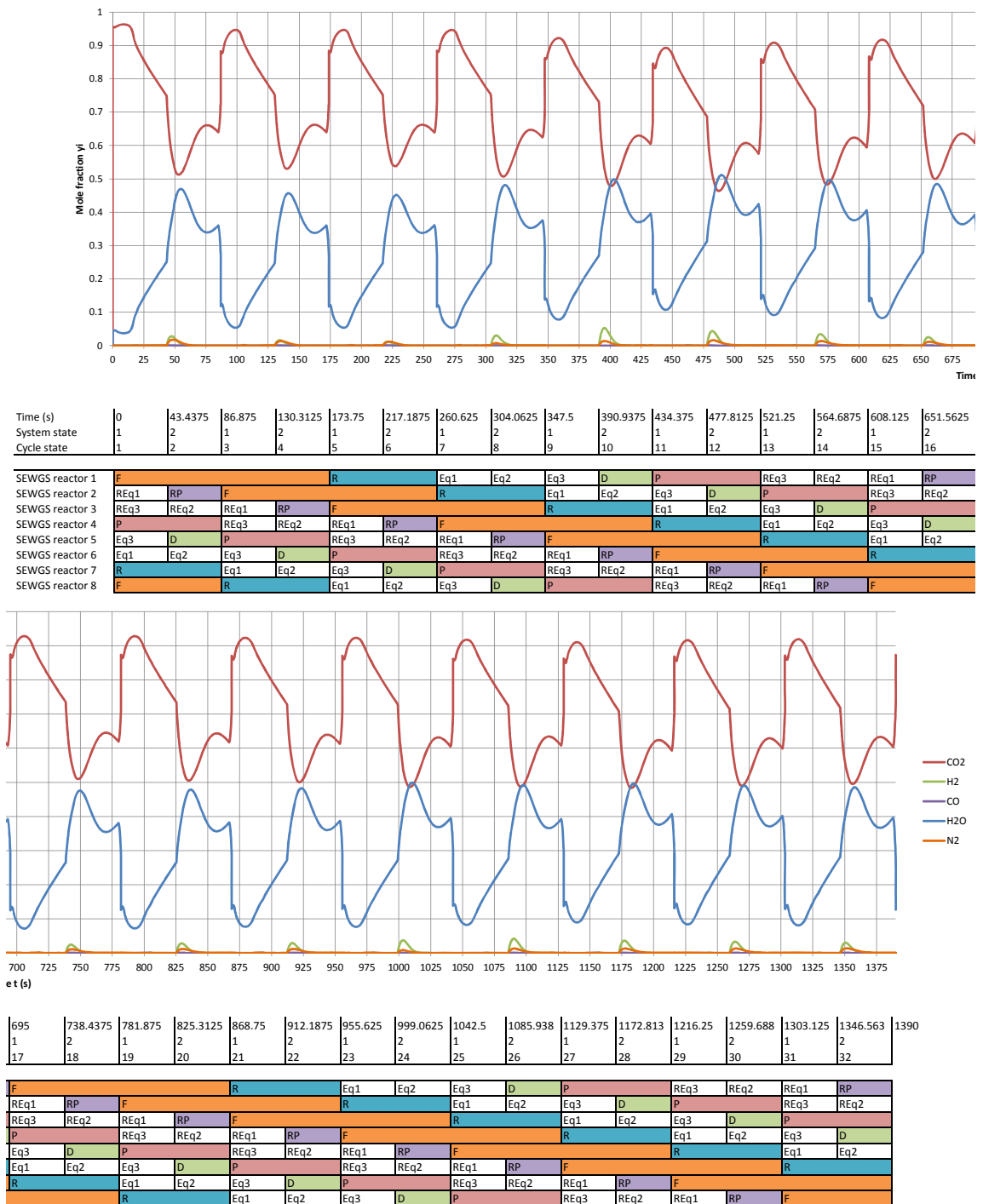
Figure C.8: Component mole fractions of in the CO_2 product, i.e. the sum of the two streams CO_2 product 1 and CO_2 product 2, referred to Figure 11

D. Mole fractions in reactor 1
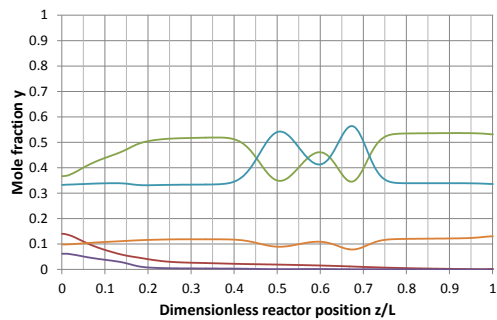
Figure D.1: Reactor 1: Mole fractions at t = 695 s. Start of step F.
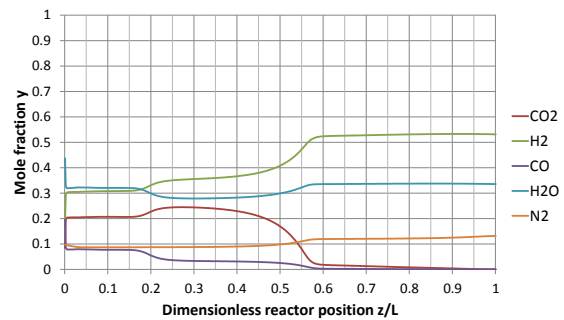
Figure D.2: Reactor 1: Mole fractions at t = 781.8750 s. Middle of step F.
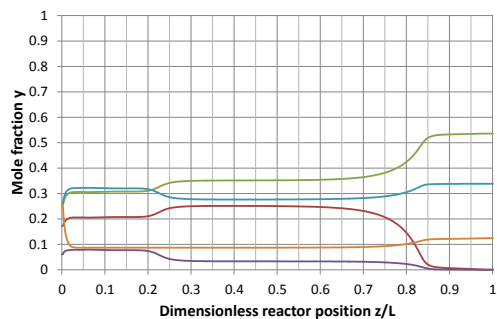
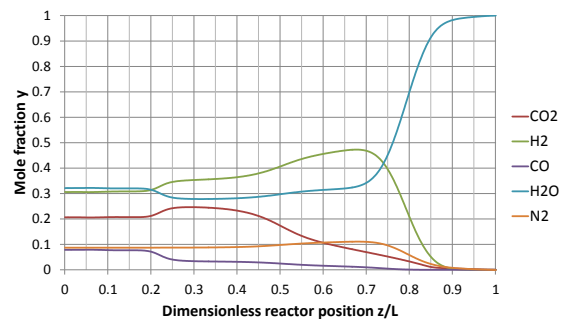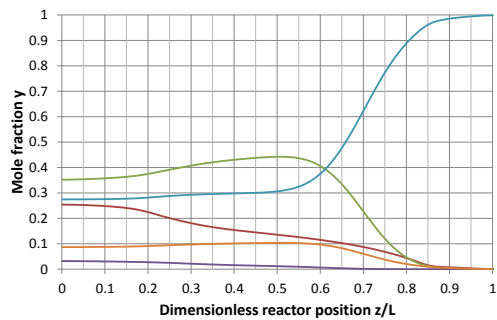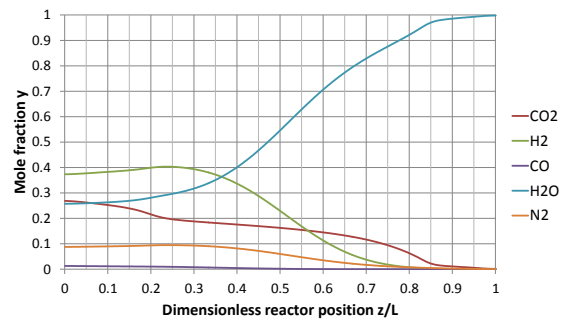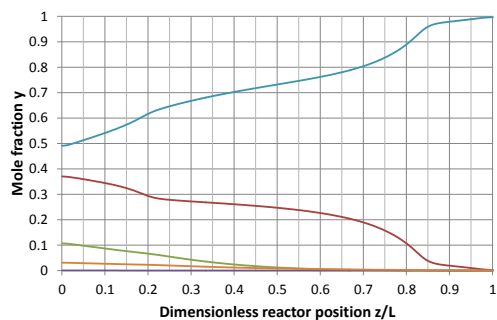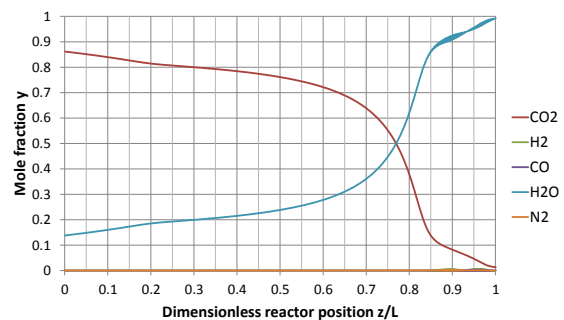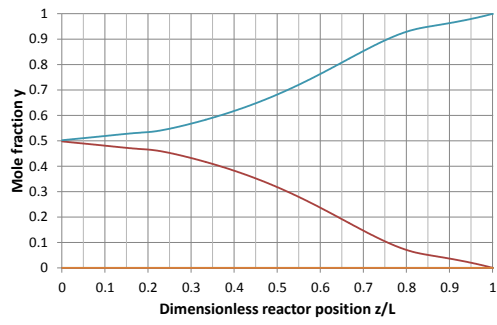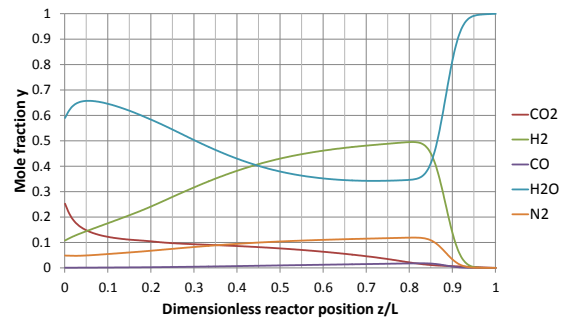**Figure D.3:** Reactor 1: Mole fractions at t = 868.7500 s. End of step F.

Figure D.4: Reactor 1: Mole fractions at t = 955.6250 s. End of step R.

Figure D.5: Reactor 1: Mole fractions at t = 999.0625 s. End of step Eq1.

Figure D.6: Reactor 1: Mole fractions at t = 1042.5000 s. End of step Eq2.

Figure D.7: Reactor 1: Mole fractions at t = 1085.9375 s. End of step Eq3.

Figure D.8: Reactor 1: Mole fractions at t = 1129.3750 s. End of step D.

Figure D.9: Reactor 1: Mole fractions at t = 1216.2500 s. End of step P.

Figure D.10: Reactor 1: Mole fractions at t = 1259.6875 s. End of step REq3.
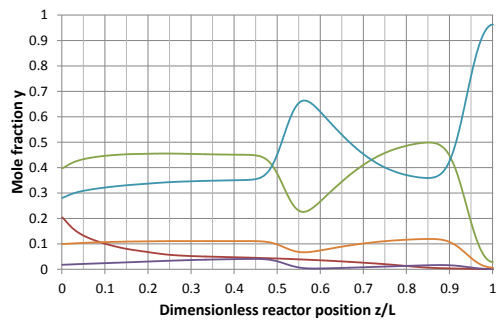
Figure D.11: Reactor 1: Mole fractions at t = 1303.1250 s. End of step REq2.
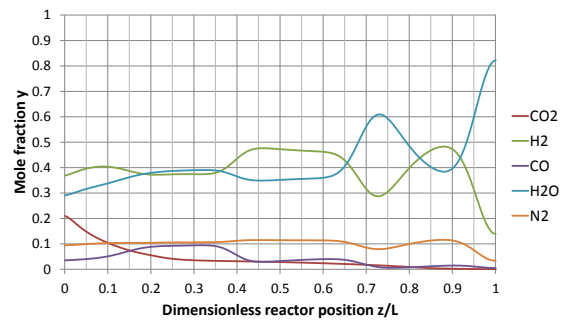
Figure D.12: Reactor 1: Mole fractions at t = 1346.5625 s. End of step REq1.
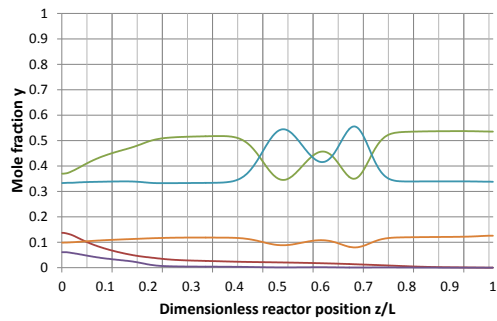
Figure D.13: Reactor 1: Mole fractions at t = 1390 s. End of step RP.
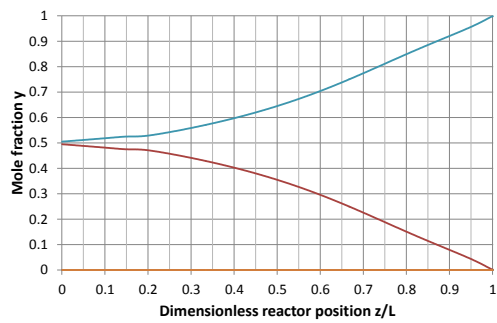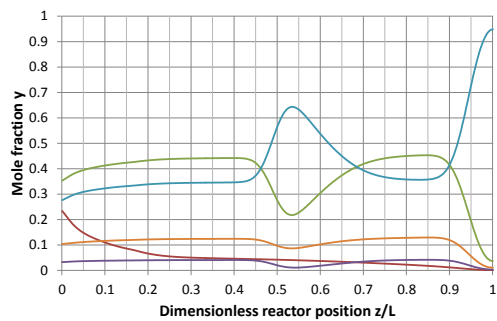
E. Mole fractions in reactors 2 and 3

Figure E.1: Reactor 3: Mole fractions at t = 0 s. End of step P.
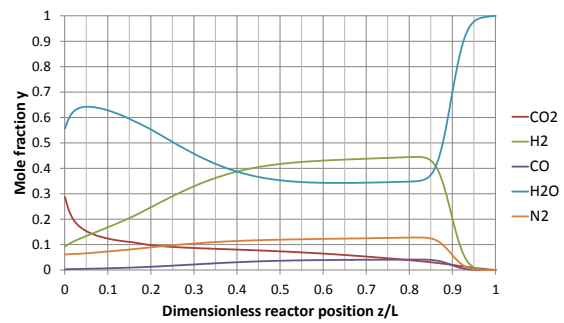
Figure E.2: Reactor 3: Mole fractions at t = 43.4750 s. End of step REq3.

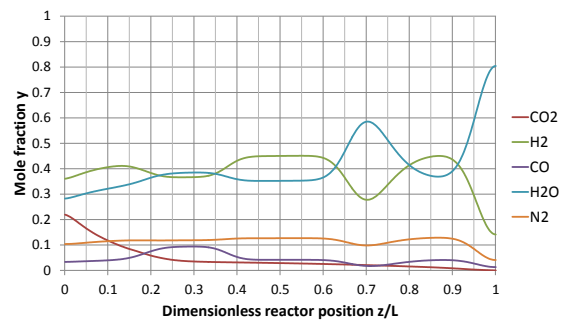**Figure E.3:** Reactor 3: Mole fractions at t = 86.8750 s. End of step REq2.

Figure E.4: Reactor 3: Mole fractions at t = 130.3125 s. End of step REq1.
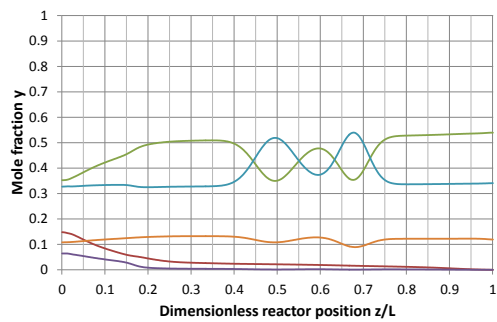

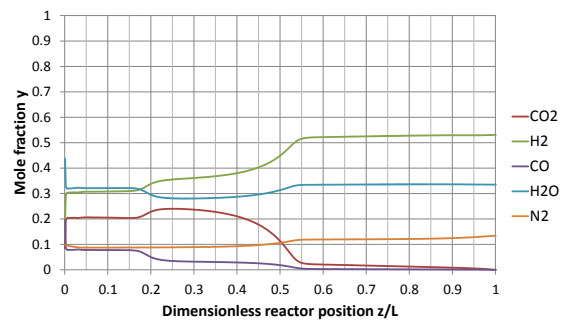**Figure E.5:** Reactor 3: Mole fractions at t = 173.75 s. End of step RP.

Figure E.6: Reactor 2: Mole fractions at t = 173.75 s. Halfway through step F.